UNIVERSITY OF CALIFORNIA MERCED

Zebrafish-on-a-Chip: Milli Fluidic Systems for Zebrafish Studies

A dissertation submitted in partial satisfaction of the

requirements for the degree of

Doctor of Philosophy

in

Quantitative and Systems Biology

by

Songtao Ye

Committee in charge:

Professor Kara McCloskey, Chair

Professor Nguyen Son

Professor Wei-Chun Chin, Co-adviser

Dr. Chih-Wen Ni, Co-adviser

Summer 2023

The dissertation of Songtao Ye is approved, and it is acceptable in quality and form for publication on microfilm and electronically:

_____

Professor Kara McCloskey, Chair

_____

Professor Nguyen Son

_____

Professor Wei-Chun Chin

_____

Dr. Chih-Wen Ni

University of California, Merced

Summer 2023

Table of Contents

List of Figures

List of Tables

Acknowledgements

First, I would like to give my deepest gratitude to my P.I., Dr. Chih-Wen Ni, for giving me the opportunity to complete the PhD degree and guiding me through the journey. I would also like to thank my committee, Dr. Kara McCloskey, Dr. Nguyen Son, and Dr. Wei-Chun Chin, for their valuable advice and unconditional help for my projects. Without them, the works presented in this dissertation are not possible to be completed. Next, I want to thank Pin, Po-Shu, Yue, and all the other friends. My time in UC Merced will be very gray without them. Finally, I deeply appreciate my family, who gave me endless support during my academic pursuit. They are the safe harbor that I can rely on.

Abstract

Zebrafish-on-a-Chip: Milli Fluidic Systems for Zebrafish Studies

by

Songtao Ye

Doctor of Philosophy in Quantitative and Systems Biology

University of California, Merced

Dr. Chih-Wen Ni, Principal Investigator

Lab-on-a-chip (LOC) technologies have revolutionized the fields of quantitative biology, tissue engineering, diagnostics, etc. However, the LOC implementations in the studies of small model organisms remain relatively low and are constrained in a small research community due to the complexity and high cost in the device development. For zebrafish research in particular, similar zebrafish-on-a-chip (ZOC) designs have been repeatedly used and some of the needs in zebrafish studies are far from fulfilled. The goal for this dissertation is to develop novel ZOCs and an overall zebrafish testing system to assist and accelerate zebrafish studies.

In this dissertation, I reported the development of novel ZOC systems for automated zebrafish embryo positioning and flowthrough assays. The ZOCs are fabricated by a rapid and inexpensive 3D LCD stereolithography assisted prototyping method which is suitable for the labs with limited budgets. A simple computational fluid dynamic based analytical model was developed and validated to estimate ZOC's embryo trapping potential as well as to guide future ZOC designs. Moreover, the operational conditions in the ZOC were evaluated and optimized via both simulations and experiments. To examine the ZOC's feasibility in zebrafish studies, I showed the zebrafish embryo can be cultured in ZOC's flowthrough environment and the embryonic development as well as embryo behavior can be affected by alternating the fluidic conditions. To fill the gap for the ZOC-based whole mount zebrafish immunohistochemistry, the whole mount zebrafish Caspase-3 antibody staining procedure was streamlined and accelerated using the ZOC. At last, the versatile ZOC design can be easily modified into a concentration gradient generator and was used for high resolution embryo caffeine dose-response screening.

I foresee the developments, and applications of ZOCs will be accelerated in zebrafish research due to the growing needs for the laboratory automation as well as the increasing accessibility of LOC and 3D printing technologies. In addition, the continued input efforts from both academia and industry will facilitate the emergence of highly integrated zebrafish testing systems for fully automated zebrafish procedures.

Chapter 1
Introduction

1.1 Lab-on-a-chip

Background

In life science labs, procedures often require extensive manual handling of tools, chemicals, and equipment by research staff and students. While the reasons for the lack of automation in life science lab are complex, this has become a significant obstacle to the progress of biotechnology and can negatively impact the reproducibility of science research.[1] Tools that can liberate the researchers from the tedious manual procedures will be crucial for future biology research and discovery.[1] For this, automated and miniaturized technologies have been developed to improve automation in laboratory research. Among them, lab-on-a-chip (LOC) is one of the most promising and rapidly growing technologies. LOC is a class of miniaturized devices that integrate manual laboratory procedures on a single chip. The integration and miniaturization of manual procedures allow for faster, cheaper, more efficient, and higher-throughput experimentation and analysis. Major applications of LOC technology are showcased here and are grouped into cell and subcellular analysis, tissue engineering, and small animal studies.

1.1.1 Cell and Subcellular Analysis

One of primitive driving forces for the advancement of LOC technology was the growing needs for fast and high-throughput cell and subcellular analysis.[2] The LOC used for cell and molecular analysis is usually called microfluidic which indicates its ability to manipulate and control the subjects in microscale fluidic environments. This controllable high surface-to-volume ratio environment gives the microfluidic device advantages in conducting rapid, high throughput, high content and cost-effective cell and subcellular analysis with exceptional sensitivity and specificity. Importantly, the fine control over the particle's motions in a fluidic environment allows the analysis to be conducted at a single cell level which was not possible for the conventional bulk methods. These advantages make microfluidic a highly sought-after tool for cell and subcellular analysis and have driven people from both academia and industry to continuously improve and innovate the LOCs' capability for this application. The cell and subcellular analysis include cell imaging, quantification, classification, and the analysis of "omics" viz. geonomics, proteomic, metabolomic, transcriptomic, epigenomic.[2] To perform these analyses at a single cell level, three key steps: 1) cell sorting, 2) cell isolation, and 3) cell/subcellular analysis need to be achieved in microfluidic.

For cell sorting, mechanisms including "intrinsic" force (i.e., hydrodynamic force), "extrinsic" external force (e.g., magnetic, electric, or dielectric field, etc.), as well as exploiting the properties (e.g., size, shape, density, or deformability etc.) of cells are commonly used in microfluidic (Figure 1.1).[3,4] Despite each mechanism having its own

pros and cons, the goal is always to sort specific cell type from a heterogeneous population. In my opinion, the "intrinsic" force, or the physical property-dependent mechanisms (i.e., size, shape, etc.) will be ideal for cell sorting because no foreign force fields are involved so that the cells can be sorted without being labeled. Hence, it minimizes cell damage and the adverse effects on these cells.

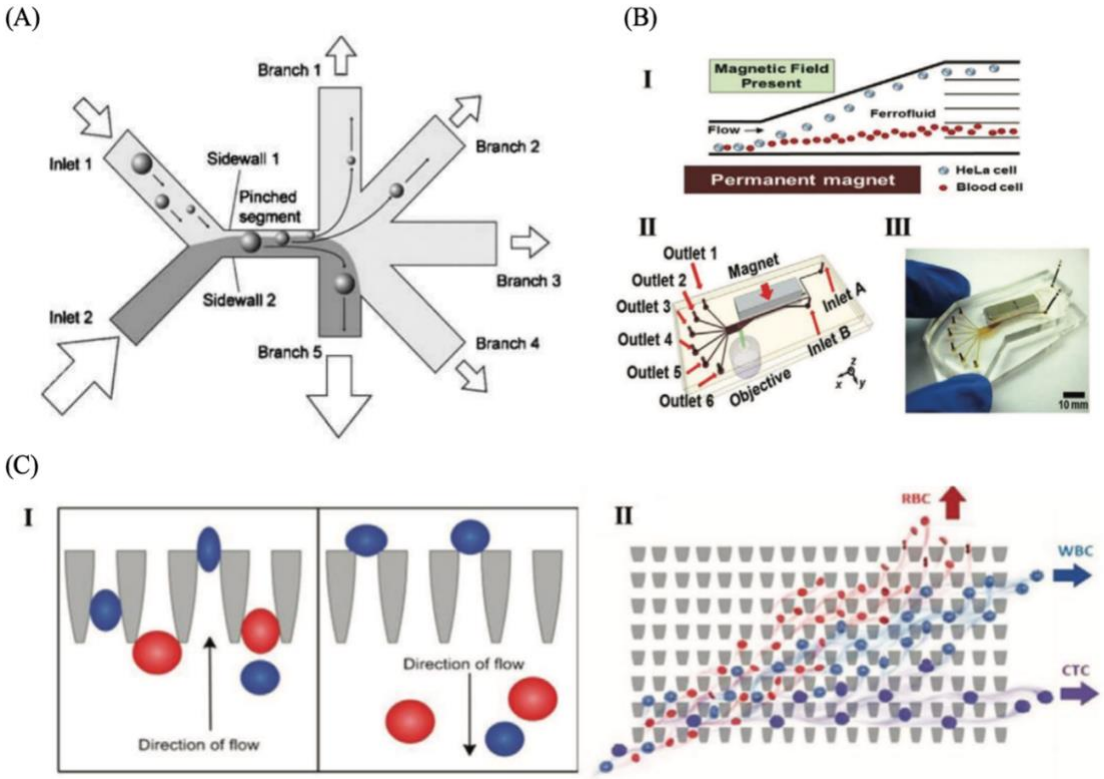

Figure 1.1. Different cell separation mechanisms for microfluidic-based cell and subcellular analysis. A) Cell separation using microfluidic pinched flow fractionation (i.e., hydrodynamic force).[5] B) Cell separation using magnetic field. I) Cell sorting mechanism of the magnetic field-based microfluidic. II) overall microfluidic configuration. III) Representative image for the fabricated device.[6] C) Cell separation using size-dependent ratchets. I) the mechanism of microfluidic ratchet cell sorting. II) the matrix of the ratchets used to separate circulating tumor cells (CTC) from the WBCs and RBCs. [4,7]

After cell sorting, the cell isolation from homogenous cells is the next step to reach single cell resolution in microfluidic. One signature of the cell isolation technologies is the droplet microfluidic (Figure 1.2).[8] Droplet microfluidic isolates cells by encapsulating cells in individual micro droplets. These droplets are the carrying vessels for multiple or single cell allowing for multiplexed, high-throughput, and high-content cell analysis. Furthermore, within the droplets, the procedures such cell lysis, protein or DNA extractions can be carried on at a single cell level which was previously challenging for other methods.[9] The most recent successful story for the application of droplet microfluidic in single cell analysis is perhaps the rising of 10× Genomics. Other cell isolation techniques including hydrodynamic trap, pneumatic membrane valving, optical traps, acoustic traps etc. are also

used in cell isolation.[10] However, these methods usually have limited throughputs and are prone to the defects.[10,11]

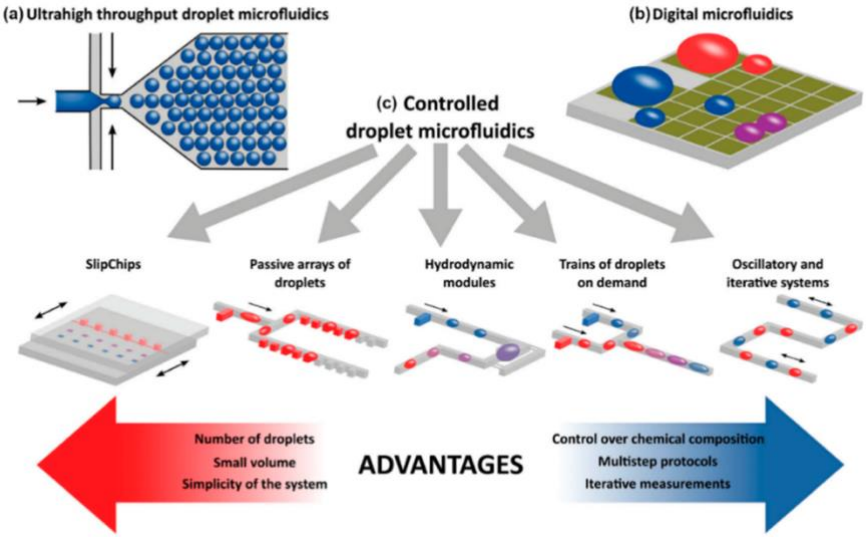

Figure 1.2. Droplet microfluidic for cell isolation. [8]

The single cell-based cell and subcellular analysis can be conducted during or after the cell sorting and/or isolation processes. One of the aiming directions for microfluidic-based cell/subcellular analysis is to achieve multiplexed analysis. As mentioned above, the droplet microfluidic can perform different types of cell/subcellular analyses by adjusting the droplet contents and analyzing the signal in sequence (Figure 1.3.A).[12] Other microfluidics achieve the multiplexed cell analysis by splitting or interconnecting the channels into different reaction chambers for parallel or sequential analysis (Figure 1.3.B).[13]

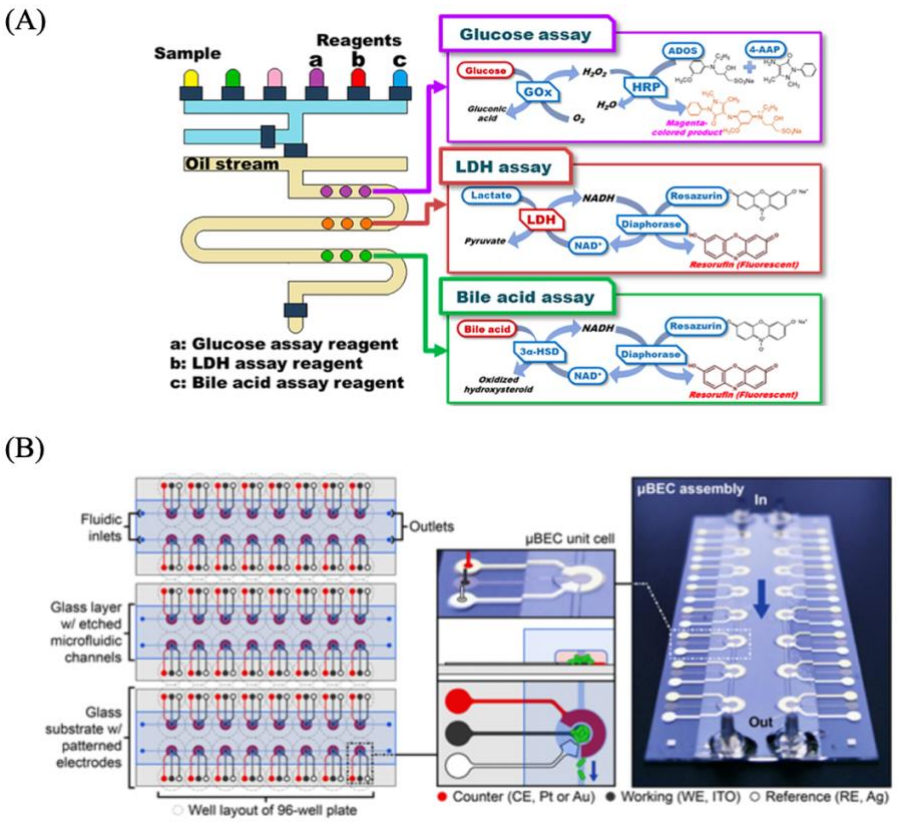

Figure 1.3. Multiplexed cell analysis using microfluidic. A) Multiplexed cell analysis by adjusting droplet contents.[12] B) Multiplexed cell analysis by splitting the main channel into individual reaction chambers.[13]

To achieve a better readout, an additional step of signal amplification is necessary. Polymerase chain reaction (PCR) is one of the basic signal amplification techniques for genomics analysis. The DNA and RNA are amplified through PCR via 3-steps thermal cycles, denaturation (≈95℃), annealing (≈56℃), and extension (≈72℃). Microfluidic offer a high surface-to-volume ratio environment for rapid heat transfer which can significantly reduce the procedure time of the PCR amplification. Generally, space domain and time domain are the two types of microfluidic designs for PCR.[14] The space domain or flowthrough PCR requires the sample to move along the channels with preset temperatures. Hence, the duration of each thermal step is dependent on the length of the channel and traveling speed of the sample (Figure 1.4.A.). The major advantage for the space domain microfluidic PCR is it can be easily integrated into the upstream sample preparation steps to ensure a high-throughput analysis.[14] Nevertheless, the space domain microfluidic PCR requires delicate channel design and holistic system coordination. The time domain microfluidic PCR, on the other hand, does not require sample movements and the heating and cooling steps are realized by an active temperature controller (Figure 1.4.B). The time domain microfluidic PCR is more flexible in channel design and can be combined with cell sorting or isolation devices such as cell traps and droplet microfluidic. However, the throughput of the time domain PCR is limited as no continuous sample feeding from the upstream.

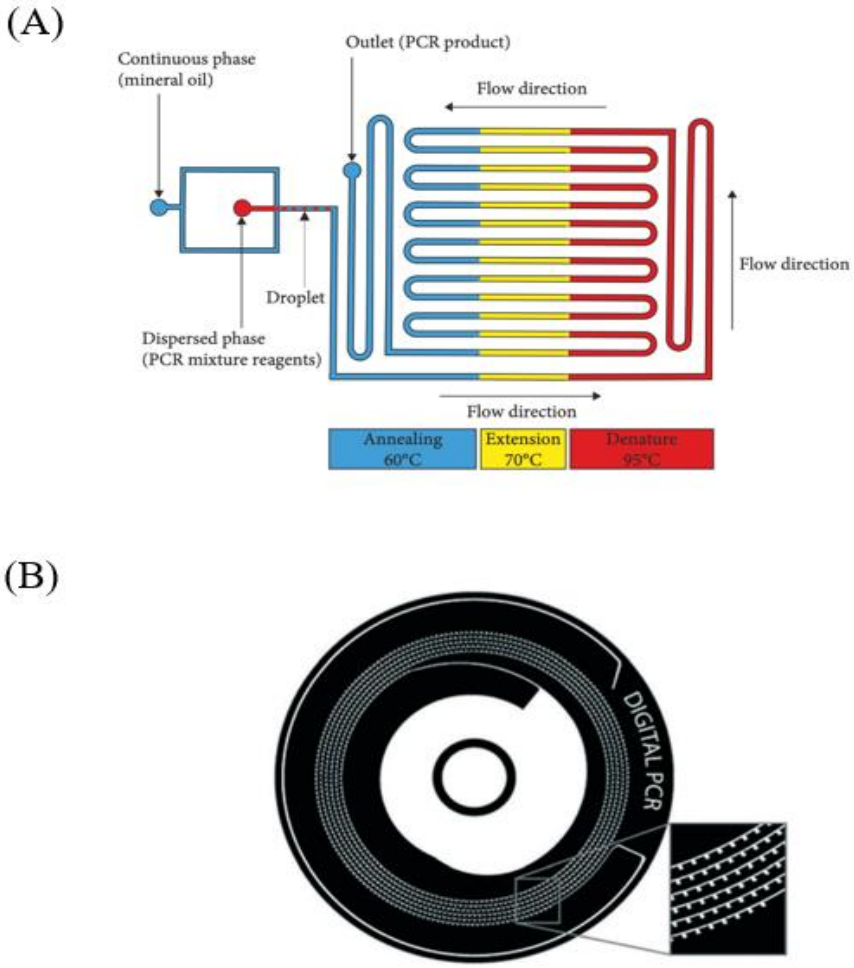

Figure 1.4. Microfluidic PCR. A) The space domain PCR microfluidic.[15] B) The time domain PCR microfluidic.[16]

Overall, LOC technology has enabled the researchers to study complex biological processes with a level of detail and precision that was previously unattainable using conventional techniques and has opened a new avenue of research in cellular biology and related fields.

1.1.2 Tissue Engineering

Tissue engineering is another big sector for LOC. The most well-known name for tissue engineering LOC is organ-on-a-chip (OOC). The OOC are microfluidic devices that aim to recreate *in vitro* organs by mimicking the structural and functional characteristics of human organs *in vivo*.[17] To simulate the complex intercellular interactions and physiological responses that occur *in vivo*, parameters such as concentration gradient, shear force, cell patterning, and other mechanical or chemical cues are regulated in the OOCs.[18]

One of the representative OOCs is the lung-on-a-chip. In 2010, Huh et al. reported a lung-on-a-chip device (Figure 1.5). [19] The device is made of polydimethylsiloxane (PDMS), an

elastic material, and used to simulate the alveoli expansion/contraction during respiration by deforming the PDMS membrane accordingly. Also, the alveolar epithelial cells and endothelial cells are seeded at the top and bottom surfaces of extracellular matrix (ECM) membrane to mimic the alveolar-capillary barrier. This simple yet robust model has proven to be valid in recreating *in vivo* lung responses under various pathological stimuli and has become an *in vitro* alternative for the studies of pulmonary diseases such as pneumonia, asthma, and cystic fibrosis, etc..[17,19]

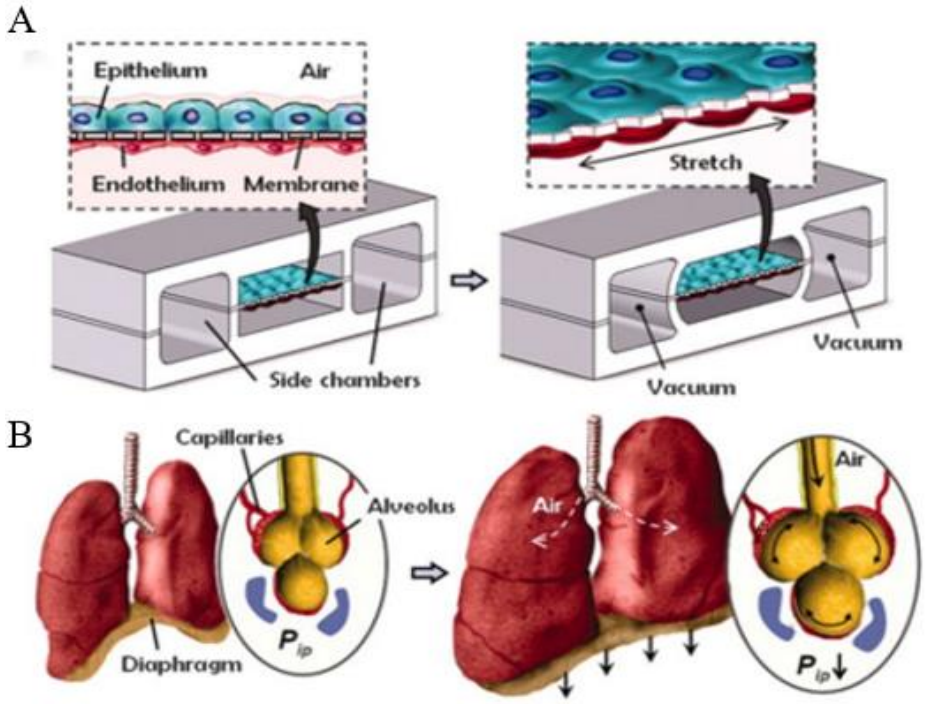

Figure 1.5. Lung-on-a-chip. A) The lung-on-a-chip schematic in mimicking the breathing movement of the alveolus-capillary barrier. B) The alveolus distension and alveolus-capillary barrier stretching during inhalation.[19]

Other OOCs such as liver-on-a-chip, [20] heart-on-a-chip,[21] intestine-on-a-chip,[22] etc. also take the advantages of microfluidic's controllable 3D microenvironment (e.g., flow and concentration), material elasticity, and porosity to increase the physiological relevance in the studies of organ function, cell behaviors and tissue formations (Figure 1.6).

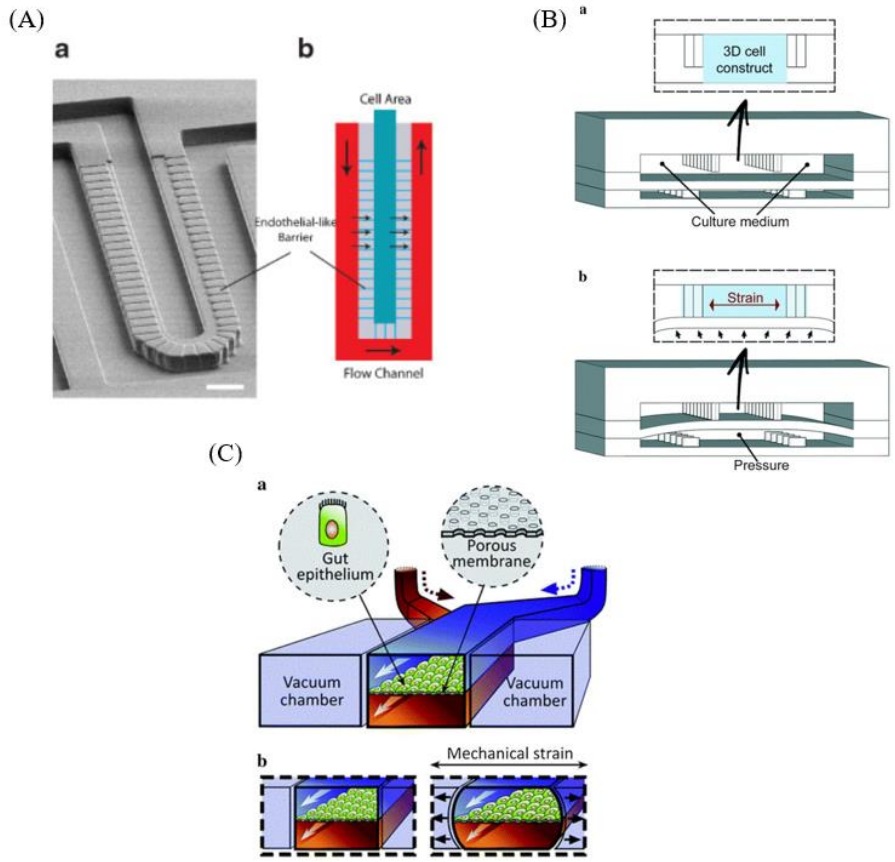

Figure 1.6. Other OOCs. A) liver-on-a-chip.[20] B). heart-on-a-chip.[21] C) intestine-on-a-chip.[22]

Incorporating stem cell engineering with microfluidic is another key direction for the OOC development. Stem cells, by definition, are self-renewing pluripotent cells that have the potential to differentiate into a wide range of cell types.[17] In contrast to the other cell types, stem cells can be more easily obtained without biopsy and the self-renewing nature makes them ideal cell sources for the OOCs.[17] Also, from tissue regeneration perspective, utilizing stem cells as the building blocks to produce various organs *in vitro* will have more clinical potential (e.g., patient-specific organ or tissue regenerations).[17,23] In 2018, Musah et al. developed a protocol to guide the differentiation of induced pluripotent stem cells (iPSCs) into mature kidney glomerular podocytes (Figure 1.7. A.).[24] The protocol was then applied in microfluidic for 3D iPSCs culture and was able to generate a functional *in vitro* human kidney glomerulus (i.e., kidney-on-a-chip) (Figure 1.7.B&C).[24] This chip has been used to investigate the effects of mechanical forces on glomerular development which is not possible with the conventional cell culture methods.[24] The combination of stem cell engineering with OOCs models allows the establishment of more physiologically relevant *in vitro* organ models and facilitates the studies of tissue and organ machanisms.[23]

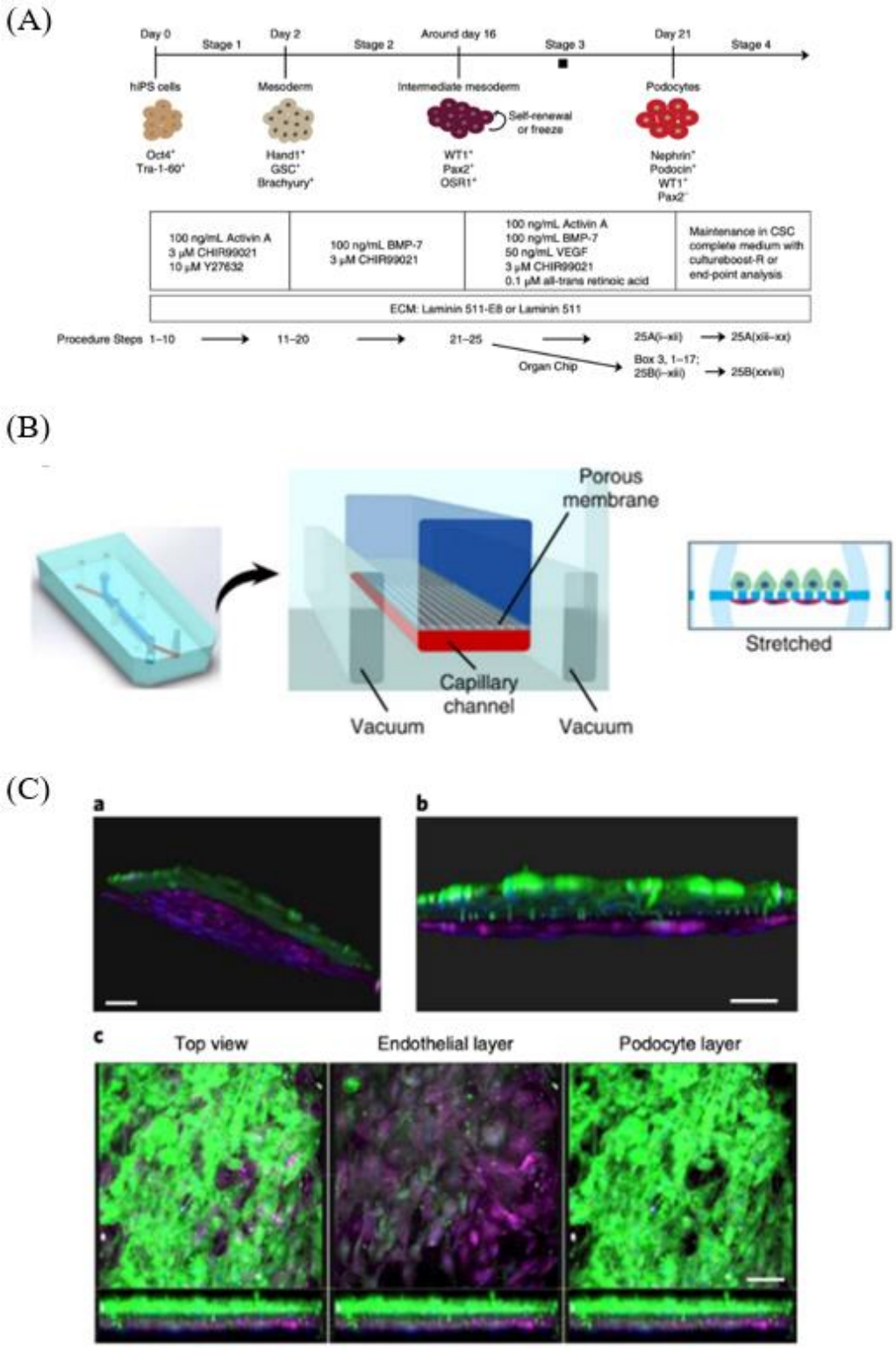

Figure 1.7. Kidney-on-a-chip. A) The protocol for iPSC differentiation into mature podocytes. B) The schematic of kidney-on-a-chip. C) Fluorescence microscopy images for the glomerulus developed in the microfluidic device.[24]

While individual OOC has proven to be useful in mimicking certain aspects of organ function, the integrated organ function cannot be fully realized by a single OOC due to the missing of physiological fluidic connections (e.g., blood flow, lymph fluid, etc.) or organ-to-organ interactions. As a result, "human-on-a-chip" or "multiorgan-on-a-chip", the more comprehensive *in vitro* human organ systems have gained increasing research attention and has become one of the leading directions for the OOC development (Figure 1.8.).[25]

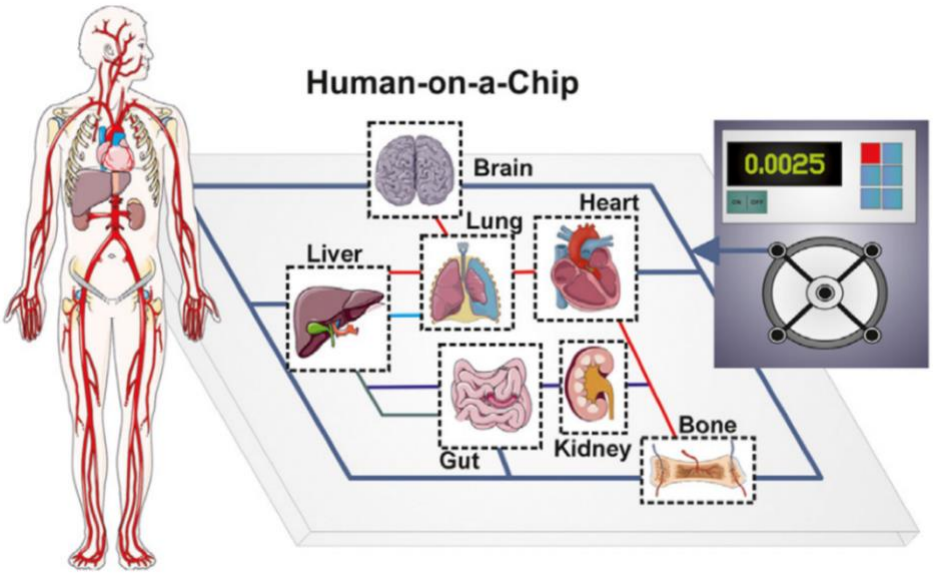

Figure 1.8. Human-on-a-chip. [25]

Despite the rapid development of OOC technology in the last decades, it is still at its infancy and is distanced from the goal of recreating the entire human organ systems in vitro. The continuous advancement of OOCs will renew our understanding about human physiology as well as revolutionize disease mechanism studies and drug discovery.

1.1.3 Small Animal Studies

While cell and tissue studies can provide valuable insights into cellular and multicellular mechanisms, small model organisms such as *Caenorhabditis elegans* (nematode), *Drosophila melanogaster* (fruit fly), and *Danio rerio* (zebrafish) offer a more complete biological context in the studies of physiological and biological processes. Like most of the cell and tissue procedures, the conventional small model organism handling procedures usually lack automation and are highly skill dependent. The researchers are usually swamped in these manual routine procedures with less time for thinking and planning. Moreover, the manual procedures and the lack of experimental conditions control can introduce considerable variability in the experimental results and the throughput is usually low.[26,27] To address these limitations, small animal LOC technologies have emerged as one of the solutions.

The very first problem to tackle in the small animal LOC development is the fabrication methods. The conventional micro- or nano- fluidics took advantage of the development of the semiconductor industry in which the cleanroom microfabrication techniques such as SU-8 photolithography, or ion etching are usually employed to prototype, or mass produce the molds and devices. For small animal LOCs, sometimes the traditional microfabrication methods are too costly to use because the dimension of these small animal models (e.g., zebrafish embryo) are in millimeter scale, which are much larger than micro- or nano-meter particles. Therefore, non-cleanroom fabrication methods such as laser micromachining, micro-milling, and 3D printing are typically used for making small animal LOCs that have millimeter scaled channels (i.e., milli fluidic).[28,29] For the zebrafish-on-a-chip (ZOC) in particular, the trend for the fabrication methods has shifted from laser micromachining and micro-milling towards the 3D stereolithography (SLA) in the recent decade thanks to the advancements in 3D printing technologies (Figure 1.9).[29–31]

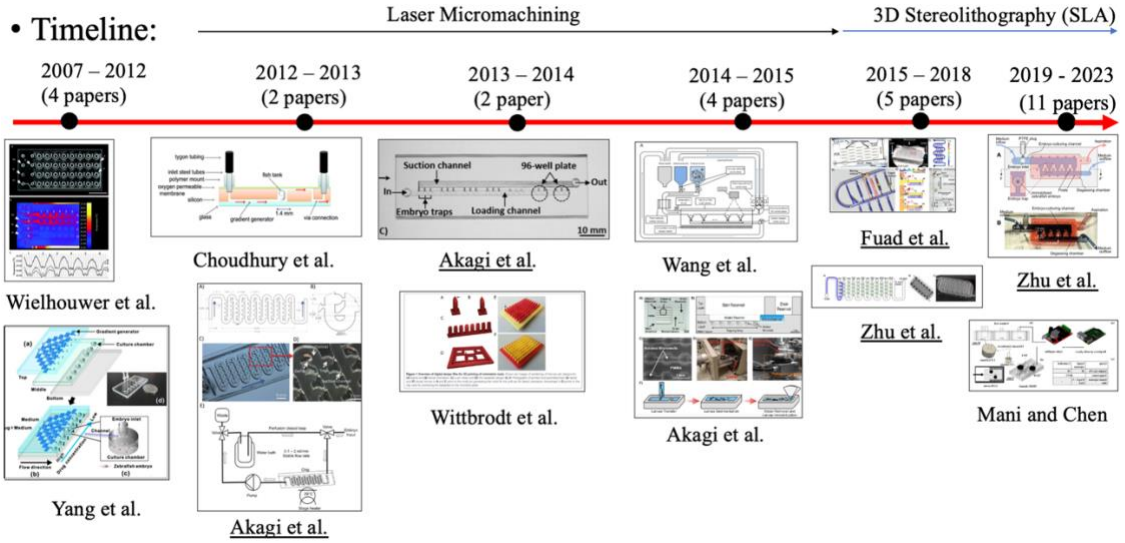

Figure 1.9. The ZOC fabrication methods trend.[28,32–37]

The development of 3D printing, especially the 3D liquid crystal display (LCD) SLA technologies, has significantly reduced the cost in LOC development, making it more accessible to the labs across various fields (Figure 1.10.A).[30] However, one of the concerns for the 3D printing-based LOC fabrication methods is the cytotoxicity and embryonic toxicity of the 3D printing inks. The studies conducted in zebrafish embryos have shown that the 3D printed parts can leach toxic chemicals into the zebrafish culture environments and lead to embryonic abnormalities (Figure 1.10. B). [38,39] Therefore, 3D printing the LOC all at once and used it for cell or small animal studies will not be ideal. To minimize the toxic leaching from the 3D printed parts, using the 3D printer to create a master mold (i.e., replacing the photolithography) and then applying the soft lithography to produce PDMS-glass devices would be ideal for LOC fabrication. (Figure 1.10.C).[39–41]

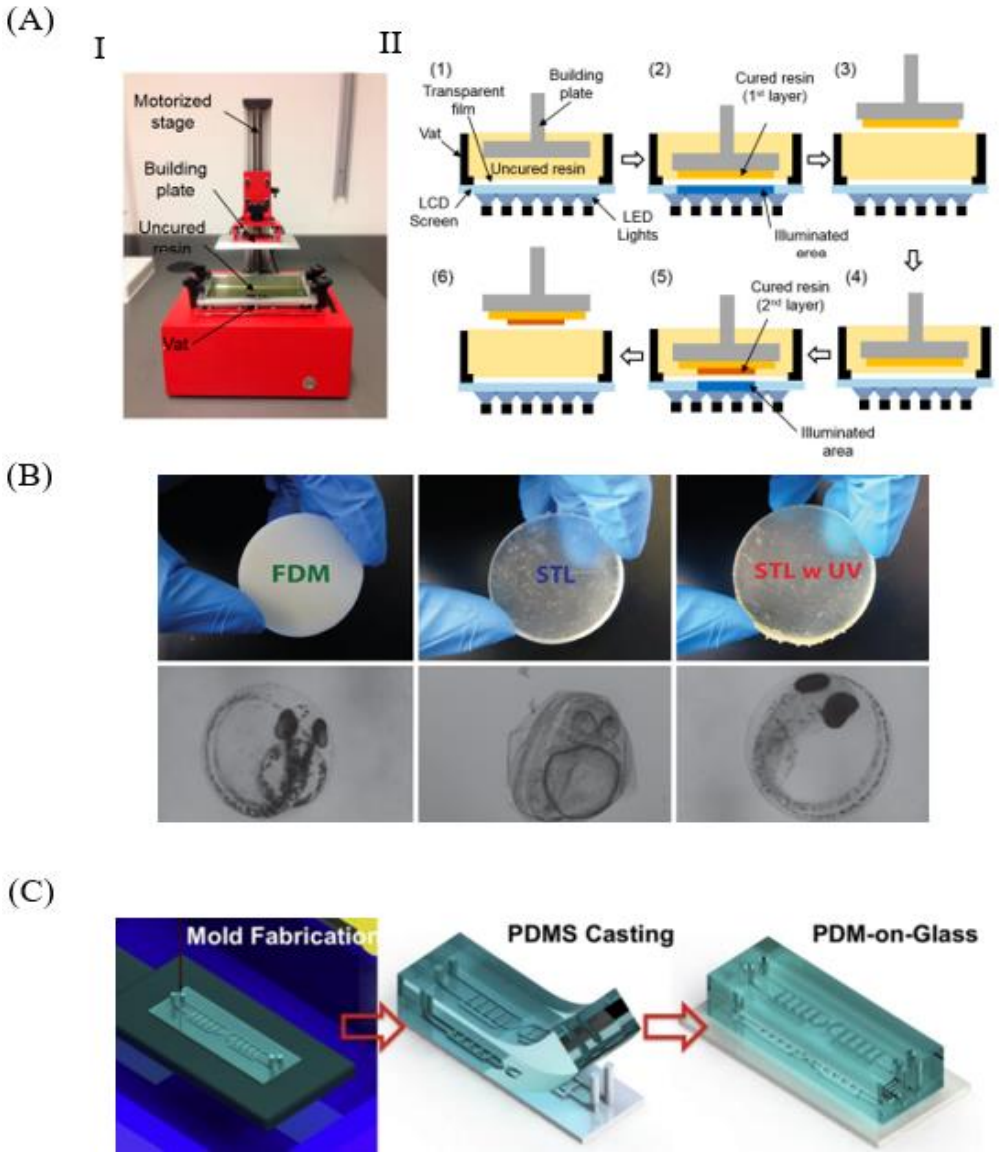

Figure 1.10. 3D SLA technology used in small animal LOC fabrications. A) 3D LCD SLA printer (I) and working principle (II).[30] B) The toxicity of 3D printing inks. Left: zebrafish embryo cultured in acrylonitrile butadiene styrene (ABS) part printed by fused deposition modeling (FDM) 3D printer. Middle: zebrafish embryo cultured photo resin part printed by a commercial SLA 3D printer without UV post-treatment. Right: zebrafish embryo cultured photo resin part printed by a commercial SLA 3D printer with UV post-treatment.[38] C) The recommended 3D printer assisted small animal LOC fabrication method in making PDMS-glass device.[40]

Like the LOCs used in cell and tissue studies, the small animal LOCs achieve high-throughput and high content analysis via steps including sample manipulations (e.g., isolation, sorting, orientation control, etc.), treatments/stimuli, and analysis. In terms of sample manipulations, due to their substantial mass, the momentum required to carry the small animals around in LOC channels is much greater than the required momentum for

cell and tissue manipulations. Therefore, non-contact or extrinsic forces such as electrophoresis force, dielectrophoresis force, and magnetic force which would require huge power consumption are rarely used in small animal manipulations (i.e., energy expansive and potential heat generation). Hydrodynamic force, gravitational force, and droplet are the most used physical mechanisms for high-throughput small animal manipulations (Figure 1.11).[29]

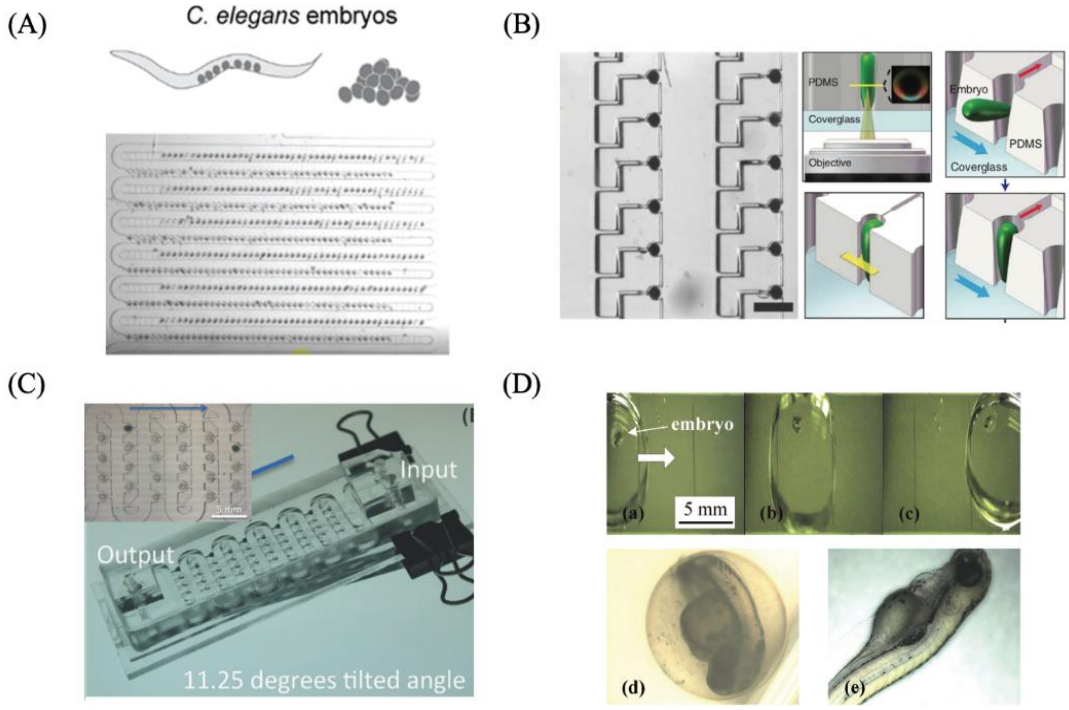

Figure 1.11. The physical mechanisms used to trap and manipulate small animal models. A) Hydrodynamic force is used to trap C. elegans embryos.[42] B) Hydrodynamic force is used to trap and orientated fruit fly embryos.[43] C) Hydrodynamic force and gravitational force are used to trap zebrafish embryos.[32] D) Droplets are used to encapsulate and deliver zebrafish embryos.[44]

Small animal models have intact sensory systems that can respond to various external stimuli such as light, sound, chemicals, and temperature. This makes them valuable tools to study the mechanisms of the sensory systems as well as the behavior and development changes under various stimuli (e.g., sleep, phototaxis, chemotaxis, etc.) Therefore, besides the "omics" analysis (i.e., geonomics, proteomic, metabolomic, etc.), the small animal LOCs have been used extensively for the behavior and development studies (Figure 1.12).[29]

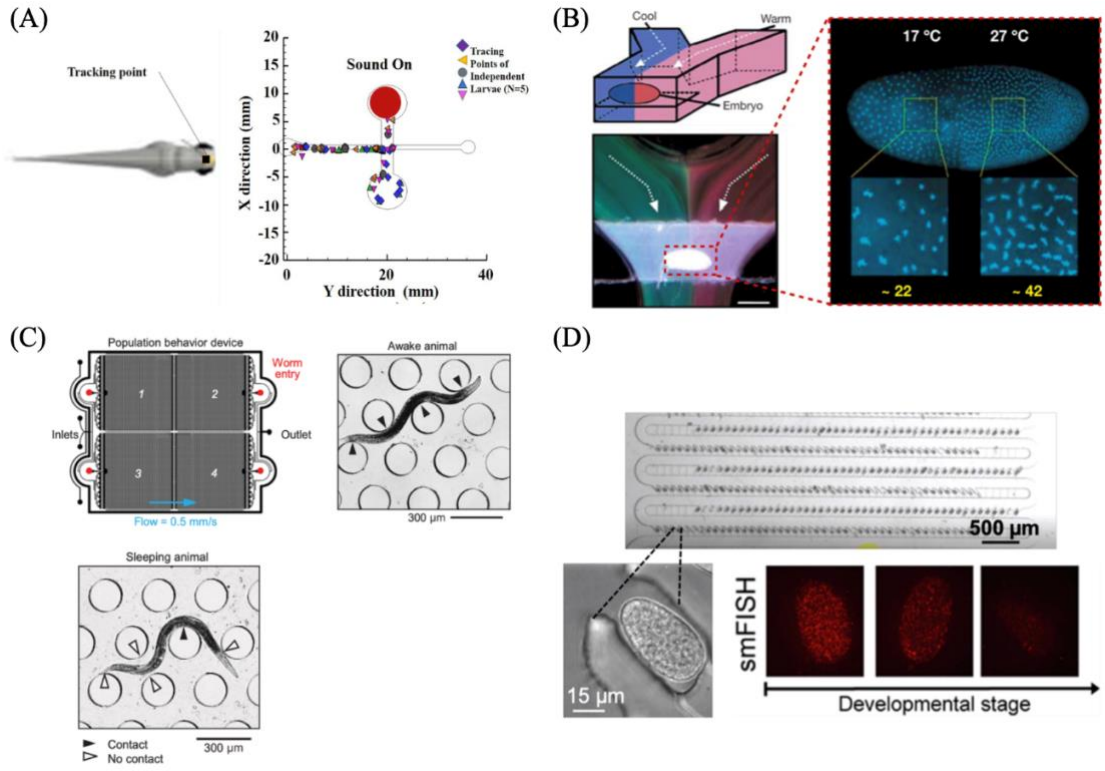

Figure 1.12. The small animal behavior and development analysis using small animal LOCs. A) The ZOC used to trap the zebrafish larvae using acoustic stimulus.[45] B) The fly-on-a-chip used to study the fruit fly embryonic development at different temperatures.[46] C) The C. elegans-on-a-chip used to study the behaviors of C. elegans during sleeping and awaking.[47] D) The C. elegans-on-a-chip used for high-temporal-resolution C. elegans gene expression study.[42]

Unlike the micro- or nano- fluidics that require specialized on-chip and off-chip connectors and flow regulators (e.g., microvalve and actuator) to minimize the flow response lagging, the milli fluidic small animal LOCs usually has a higher precision tolerance in flow control and are largely compatible with readily available, standardized flow control parts and apparatuses.[48] These make these small animal LOCs to be easily coupled with automated liquid handling, imaging, and analyzing systems (Figure 1.13).[29]

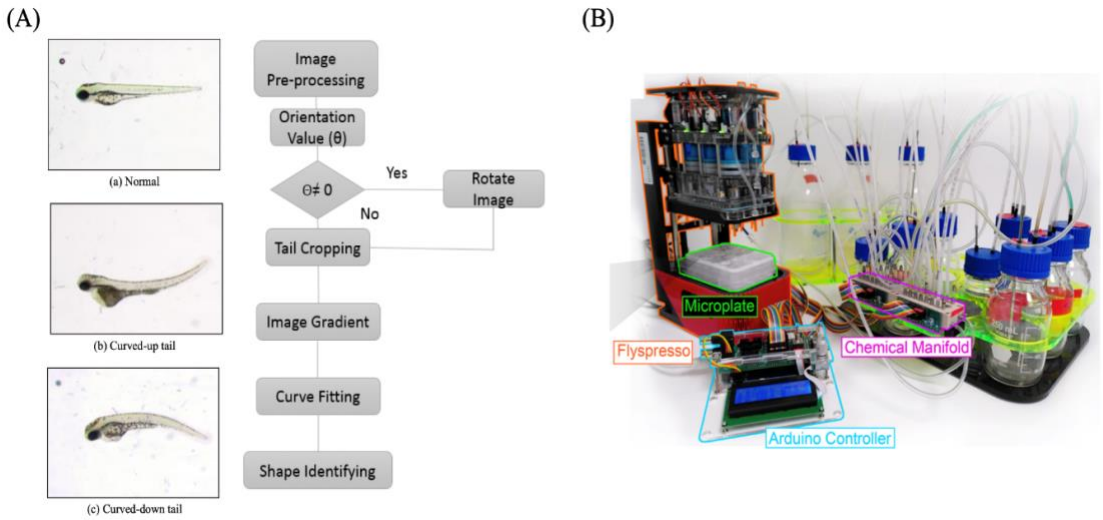

Figure 1.13. Automated imaging and liquid handling systems for small animal studies. A) A computational imaging analysis system for automated zebrafish abnormal tail curvature detection.[49] B) A small, automated liquid handling system for whole mount fruit fly antibody staining.[50]

The application of LOC technologies in small animal studies has skyrocketed in the last two decades. Despite this, the potential of LOCs in small animal studies is still far from being fully explored. New LOC designs and applications are needed to fill the remaining gaps. In addition, the integration of small animal LOCs with other automated systems should be pursued further in order to completely eliminate manual procedures and provide the researchers with a more efficient and streamlined experimental process.

1.2 Outline of the Work

In this dissertation, the LOC technology used in zebrafish studies is the focused research topic and the main content. The overall goal of this dissertation is to develop new ZOCs and establish a zebrafish testing platform to accelerate and improve zebrafish studies. Specifically, Chapter 2 details the development of the ZOCs for automated zebrafish embryo trapping and flow through culture. Chapter 3 presents an application of using the ZOC for whole mount zebrafish antibody staining. In chapter 4, the ZOC device was modified into a concentration gradient generator and was used for the acute fish toxicity test. Chapter 5 concludes all these efforts and provides the future directions.

1.3 References

1. Holland, I. & Davies, J. A. Automation in the Life Science Research Laboratory. *Front Bioeng Biotechnol* **8**, (2020).
2. Hochstetter, A. Lab-on-a-Chip Technologies for the Single Cell Level: Separation, Analysis, and Diagnostics. *Micromachines (Basel)* **11**, 468 (2020).
3. Yousuff, C., Ho, E., Hussain K., I. & Hamid, N. Microfluidic Platform for Cell Isolation and Manipulation Based on Cell Properties. *Micromachines (Basel)* **8**, 15 (2017).
4. Nasiri, R. *et al.* Microfluidic-Based Approaches in Targeted Cell/Particle Separation Based on Physical Properties: Fundamentals and Applications. *Small* **16**, 2000171 (2020).
5. Takagi, J., Yamada, M., Yasuda, M. & Seki, M. Continuous particle separation in a microchannel having asymmetrically arranged multiple branches. *Lab Chip* **5**, 778 (2005).
6. Zhao, W. *et al.* Label-Free and Continuous-Flow Ferrohydrodynamic Separation of HeLa Cells and Blood Cells in Biocompatible Ferrofluids. *Adv Funct Mater* **26**, 3990–3998 (2016).
7. McFaul, S. M., Lin, B. K. & Ma, H. Cell separation based on size and deformability using microfluidic funnel ratchets. *Lab Chip* **12**, 2369 (2012).
8. Kaminski, T. S. & Garstecki, P. Controlled droplet microfluidic systems for multistep chemical and biological assays. *Chem Soc Rev* **46**, 6210–6226 (2017).
9. Zhou, W. *et al.* Microfluidics applications for high-throughput single cell sequencing. *J Nanobiotechnology* **19**, 312 (2021).
10. Lo, S.-J. & Yao, D.-J. Get to Understand More from Single-Cells: Current Studies of Microfluidic-Based Techniques for Single-Cell Analysis. *Int J Mol Sci* **16**, 16763–16777 (2015).
11. Gross, A. *et al.* Technologies for Single-Cell Isolation. *Int J Mol Sci* **16**, 16897–16919 (2015).
12. Cedillo-Alcantar, D. F., Han, Y. D., Choi, J., Garcia-Cordero, J. L. & Revzin, A. Automated Droplet-Based Microfluidic Platform for Multiplexed Analysis of Biochemical Markers in Small Volumes. *Anal Chem* **91**, 5133–5141 (2019).
13. John Meacham & Arpita Bose. MICRO - BIOELECTROCHEMICAL CELL Publication Classification DEVICES AND METHODS OF DETECTING ELECTRON FLOWS . (2020).
14. Ahrberg, C. D., Manz, A. & Chung, B. G. Polymerase chain reaction in microfluidic devices. *Lab Chip* **16**, 3866–3884 (2016).
15. Ma, S.-Y. *et al.* Peanut Detection Using Droplet Microfluidic Polymerase Chain Reaction Device. *J Sens* **2019**, 1–9 (2019).
16. Sundberg, S. O. *et al.* Quasi-digital PCR: Enrichment and quantification of rare DNA variants. *Biomed Microdevices* **16**, 639–644 (2014).
17. Wu, Q. *et al.* Organ-on-a-chip: recent breakthroughs and future prospects. *Biomed Eng Online* **19**, 9 (2020).
18. Leung, C. M. *et al.* A guide to the organ-on-a-chip. *Nature Reviews Methods Primers* **2**, 33 (2022).
19. Huh, D. *et al.* Reconstituting Organ-Level Lung Functions on a Chip. *Science (1979)* **328**, 1662–1668 (2010).
20. Lee, P. J., Hung, P. J. & Lee, L. P. An artificial liver sinusoid with a microfluidic endothelial-like barrier for primary hepatocyte culture. *Biotechnol Bioeng* **97**, 1340–1346

(2007).
21. Marsano, A. *et al.* Beating heart on a chip: a novel microfluidic platform to generate functional 3D cardiac microtissues. *Lab Chip* **16**, 599–610 (2016).
22. Kim, H. J., Huh, D., Hamilton, G. & Ingber, D. E. Human gut-on-a-chip inhabited by microbial flora that experiences intestinal peristalsis-like motions and flow. *Lab Chip* **12**, 2165 (2012).
23. Mastrangeli, M. & van den Eijnden-van Raaij, J. Organs-on-chip: The way forward. *Stem Cell Reports* **16**, 2037–2043 (2021).
24. Musah, S., Dimitrakakis, N., Camacho, D. M., Church, G. M. & Ingber, D. E. Directed differentiation of human induced pluripotent stem cells into mature kidney podocytes and establishment of a Glomerulus Chip. *Nat Protoc* **13**, 1662–1685 (2018).
25. Picollet-D'hahan, N., Zuchowska, A., Lemeunier, I. & Le Gac, S. Multiorgan-on-a-Chip: A Systemic Approach To Model and Decipher Inter-Organ Communication. *Trends Biotechnol* **39**, 788–810 (2021).
26. Hwang, H. & Lu, H. Microfluidic tools for developmental studies of small model organisms -nematodes, fruit flies, and zebrafish. *Biotechnol J* **8**, 192–205 (2013).
27. Wlodkowic, D., Khoshmanesh, K., Akagi, J., Williams, D. E. & Cooper, J. M. Wormometry-on-a-chip: Innovative technologies for in situ analysis of small multicellular organisms. *Cytometry Part A* **79A**, 799–813 (2011).
28. Yang, F., Gao, C., Wang, P., Zhang, G.-J. & Chen, Z. Fish-on-a-chip: microfluidics for zebrafish research. *Lab Chip* **16**, 1106–1125 (2016).
29. Frey, N., Sönmez, U. M., Minden, J. & LeDuc, P. Microfluidics for understanding model organisms. *Nat Commun* **13**, 3195 (2022).
30. Mohamed, M. *et al.* Rapid and Inexpensive Fabrication of Multi-Depth Microfluidic Device using High-Resolution LCD Stereolithographic 3D Printing. *Journal of Manufacturing and Materials Processing* **3**, 26 (2019).
31. Venzac, B. *et al.* PDMS Curing Inhibition on 3D-Printed Molds: Why? Also, How to Avoid It? *Anal Chem* **93**, 7180–7187 (2021).
32. Akagi, J. *et al.* Miniaturized Embryo Array for Automated Trapping, Immobilization and Microperfusion of Zebrafish Embryos. *PLoS One* **7**, e36630 (2012).
33. Fuad, N. M., Kaslin, J. & Wlodkowic, D. Development of chorion-less zebrafish embryos in millifluidic living embryo arrays. *Biomicrofluidics* **11**, 051101 (2017).
34. Wielhouwer, E. M. *et al.* Zebrafish embryo development in a microfluidic flow-through system. *Lab Chip* **11**, 1815 (2011).
35. Wang, W., Liu, X., Gelinas, D., Ciruna, B. & Sun, Y. A Fully Automated Robotic System for Microinjection of Zebrafish Embryos. *PLoS One* **2**, e862 (2007).
36. Zhu, Z. *et al.* A Bubble-Free Microfluidic Device for Easy-to-Operate Immobilization, Culturing and Monitoring of Zebrafish Embryos. *Micromachines (Basel)* **10**, 168 (2019).
37. Panuška, P. *et al.* A millifluidic chip for cultivation of fish embryos and toxicity testing fabricated by 3D printing technology. *RSC Adv* **11**, 20507–20518 (2021).
38. Oskui, S. M. *et al.* Assessing and Reducing the Toxicity of 3D-Printed Parts. *Environ Sci Technol Lett* **3**, 1–6 (2016).
39. Macdonald, N. P. *et al.* Assessment of biocompatibility of 3D printed photopolymers using zebrafish embryo toxicity assays. *Lab Chip* **16**, 291–297 (2016).
40. Fuad, N. M., Kaslin, J. & Wlodkowic, D. Lab-on-a-Chip imaging micro-echocardiography

(iμEC) for rapid assessment of cardiovascular activity in zebrafish larvae. *Sens Actuators B Chem* **256**, 1131–1141 (2018).
41. Zhu, F. *et al.* Three-dimensional printed millifluidic devices for zebrafish embryo tests. *Biomicrofluidics* **9**, 046502 (2015).
42. Charles, S., Aubry, G., Chou, H.-T., Paaby, A. B. & Lu, H. High-Temporal-Resolution smFISH Method for Gene Expression Studies in *Caenorhabditis elegans* Embryos. *Anal Chem* **93**, 1369–1376 (2021).
43. Levario, T. J., Zhan, M., Lim, B., Shvartsman, S. Y. & Lu, H. Microfluidic trap array for massively parallel imaging of Drosophila embryos. *Nat Protoc* **8**, 721–736 (2013).
44. Son, S. U. & Garrell, R. L. Transport of live yeast and zebrafish embryo on a droplet ("digital") microfluidic platform. *Lab Chip* **9**, 2398 (2009).
45. Mani, K. & Chen, C.-Y. A non-invasive acoustic-trapping of zebrafish microfluidics. *Biomicrofluidics* **15**, 014109 (2021).
46. Lucchetta, E. M., Munson, M. S. & Ismagilov, R. F. Characterization of the local temperature in space and time around a developing Drosophila embryo in a microfluidic device. *Lab Chip* **6**, 185 (2006).
47. Lawler, D. E. *et al.* Sleep Analysis in Adult *C. elegans* Reveals State-Dependent Alteration of Neural and Behavioral Responses. *The Journal of Neuroscience* **41**, 1892–1907 (2021).
48. Wang, W. S. & Vanapalli, S. A. Millifluidics as a simple tool to optimize droplet networks: Case study on drop traffic in a bifurcated loop. *Biomicrofluidics* **8**, 064111 (2014).
49. Al-Saaidah, B., Al-Nuaimy, W., Al-Taee, M., Young, I. & Al-Jubouri, Q. Identification of tail curvature malformation in zebrafish embryos. in *2017 8th International Conference on Information Technology (ICIT)* 588–593 (IEEE, 2017). doi:10.1109/ICITECH.2017.8080063.
50. Fuqua, T. *et al.* An open-source semi-automated robotics pipeline for embryo immunohistochemistry. *Sci Rep* **11**, 10314 (2021).

Chapter 2
Development of Milli Fluidic Systems for Zebrafish Embryo Studies

Abstract

Zebrafish (*Danio rerio*) embryo as a small convenient model organism has been widely used in biomedical research. Despite its popularity and the potential for high-throughput analysis, the zebrafish embryo procedures are still largely performed in well plates or petri dishes which involves time-consuming and tedious embryo manual manipulation and liquid transfer. In the last decades, progress has been made to improve the degree of automation and throughput in zebrafish embryo procedures by applying lab-on-a-chip (LOC) technology. The LOC used in zebrafish studies, also known as zebrafish-on-a-chip (ZOC) has shown advantages in allowing high-throughput screening, real-time monitoring, manual step reduction etc. Nevertheless, there is a notable lack of ZOC designs in this field which has become one of the obstacles for ZOC's further application. In this work, two new ZOCs have been developed and validated for automated zebrafish embryo trapping. Moreover, we applied a consumer-grade SLA 3D printer assisted method for ZOC prototyping which is economic and suitable for labs with limited budgets. The proof-of-concept zebrafish embryo culture studies indicate the two ZOCs are feasible for live zebrafish embryo assays and the zebrafish embryonic developments can be manipulated by adjusting the flowthrough conditions. Overall, in comparison to the static petri dish-based method, the ZOCs offer more controllable microenvironments for zebrafish embryo culture as well as a more efficient way for phenotype screening and real-time monitoring. However, the zebrafish embryo culture duration in the ZOC is found limited by the trap geometry and the embryo growth. These findings are valuable for the future optimization of the two ZOCs and will be used to guide the further ZOC applications.

2.1 Introduction

In biomedical research, small animal studies have great advantages over cell lines and tissue studies by allowing researchers to analyze biological processes in the whole organism, a more natural and physiologically relevant environment.[1] Zebrafish (*Danio rerio*) due to its high reproduction rate, small size, body transparency, etc. has become one of the popular small animal models in the biomedical field. However, like most bioassays, the zebrafish related procedures are still largely performed manually in well plates or Petri dishes. Experienced personnel need to go through a series of tedious and time-consuming steps such as embryo transfer, manipulation, imaging, and retrieving which has greatly limited the throughput and reproducibility of these studies. In addition, the static tests performed on well plates or petri dishes can be inadequate for some of the zebrafish studies as the fluidic and chemical microenvironments are not fully controlled. Factors such as liquid evaporation, chemical degradation, oxygen depletion, metabolic inactivation, etc. can lead to results variation, and lower the assay consistency in zebrafish studies.[1,2] Furthermore, high resolution single embryo real-time monitoring is difficult to achieve in the bulk fluidic environment as the movements of zebrafish embryos are not constrained.

Hence, platforms that can provide stable flowthrough environments while holding zebrafish embryos in places throughout the experiment are desired for the zebrafish studies.[3,4]

Unsurprisingly, the implementation of LOC technology for zebrafish studies has received increasing attention in recent years. LOCs are miniaturized chip-based fluidic devices that are usually in micrometer scale (i.e., microfluidic) and have been widely used to perform biological and chemical assays. LOCs offer several advantages over the conventional well plate or Petri dish-based platforms for biological and chemical assay includes: (i) controlled microenvironments;[5] (ii) small sample and reagent requirement;[5] (iii) rapid transfers in high surface-to-volume flowthrough environment;[6] (iv) high-throughput and parallel screening;[7] (v) automated or semi-automated procedures.[8] The LOCs developed for zebrafish studies, also known as ZOCs or milli- fluidic, have channels in millimeter scale. It is a newly emerged LOC class with less than 20 years of history.[9,10] Thanks to the growing demands for the automation in zebrafish research, the ZOC is currently in an accelerated development phase. In recent decades, several ZOCs have been developed for zebrafish studies. For instance, Zhu et al. demonstrated a ZOC for acute zebrafish embryo chemical toxicity test.[11] The group showed that the ZOC enables high-throughput screening and single-embryo-resolution monitoring, which is advantageous for detecting both lethal and sublethal endpoints. Moreover, the chemicals were found to be delivered to the zebrafish embryo more efficiently in the ZOC than in the conventional static well plate.[11] A similar study reported by Akagi et al. showed the shear stress can delay the hatching process of the zebrafish embryo in the ZOC, and therefore needs to be carefully considered when conducting zebrafish studies in ZOC.[4] Another study reported by Fuad et al. have shown the chorion-less zebrafish embryo can also be trapped and cultured in the ZOC device. The vitality of the zebrafish embryo under low shear stress fluidic environment is comparable to the statically cultured zebrafish embryos in the well plate.[4,12] These studies have shown some benefits and potentials of using ZOC for zebrafish studies. Nevertheless, by far only a handful of ZOCs were reported and similar designs were used repeatedly for various zebrafish research purposes.[4,11,12,27] New ZOC designs are urgently needed to further exploit the potential of this novel technology.

In this chapter, two novel ZOCs are developed to automatically trap the dechorionated and unhatched zebrafish embryos for flowthrough culture, respectively. The design and development processes of these two ZOC devices are detailed in the chapter. Moreover, the feasibility of performing live zebrafish embryo assays using these two ZOC is evaluated, and recommendations are given at the end.

2.2 Materials and Methods

2.2.1 Computational Fluid Dynamic Simulation

COMSOL 5.5 (COMSOL 5.5 Inc. Stockholm, Sweden) was used to perform the computational fluid dynamic (CFD) simulation to evaluate the hydrodynamic zebrafish embryo trapping for design I and design II. The “free and porous media flow” was used to simulate the steady state fluidic fields for the initial (i.e., no trap is occupied) and final (i.e.,

all traps are occupied) states of the trapping. The inlet flower rate for design I and design II were set to 10 ml/min and 20 ml/min, respectively. Water was set as the carrying buffer in the simulation. The unhatched zebrafish embryo was modeled as a rigid sphere with 1.4 mm diameter in design I. The dechorionated zebrafish embryo was molded as a cone-shape rigid body with 2 mm overall length and 0.5 mm maximum head diameter. Both dechorionated and unhatched zebrafish embryos were assumed to be located at the bottom of the traps in the simulations.

2.2.2 Design and 3D Printer Assisted Rapid Prototyping

The 2D layout of the milli fluidic device was generated by using AutoCAD (Autodesk Inc. San Rafael, California, USA) and then converted into 3D models in AutoCAD Fusion 360. The negative master model of the milli fluidic device was exported as an STL file and sliced in an Anycubic Photon Workshop slicer (Anycubic Inc. Shenzhen, China) for 3D printing. The master mold was printed by the Anycubic Photon Mono X LCD SLA 3D printer using the Anycubic gray UV resin. Briefly, the layer thickness was set to 50 µm with 16 seconds off time and 2 seconds UV exposure time to avoid the overcuring.[13] After the 3D printing, the master mold was washed in 90% isopropanol for 30 mins and dried in the air. To prevent PDMS (Sylgard 184; DowCorning Corp, Midland, MI, USA) curing inhibition, the 3D printed master model was then UV exposed for 2 hours following a 16-hour heat treatment at 80 ^{0}C.[14] For the PDMS soft lithography, the PDMS elastomer and curing agent were mixed at 10:1 (w/w) ratio and degassed before and after the PDMS casting to remove the air bubbles. The PDMS was then cured for 1 hour at 80 ^{0}C and peeled off from the resin mold. For the tubing and accessory interconnection, 3 mm holes were punched in the PDMS layer with a biopsy punch (Robbins Instruments, Sunnyvale, California, USA). The PDMS layer was bonded with a manually cut microscope glass slide using an air plasma cleaner (Harrick Plasma Inc. New York, USA).

2.2.3 Zebrafish Husbandry and Embryo Dechorionation

Adult wild type zebrafish (EKW line) were raised in the UC Merced fish facility with a 14/10 hour light and dark switching cycle. The zebrafish were fed twice daily with dry feed (300 to 400 pellet size) to ensure healthy development. The zebrafish were randomly paired a night before the mating and spawning. The embryos were collected using a sieve and then rinsed with the E3 buffer to filter out the debris and waste. The collected embryos were cultured in the petri dish filled with E3 buffer at 28.5 ^{0}C and dead embryos were sorted during the development. For embryo dechorionation, the chorions of 24 hpf zebrafish embryos were manually peeled off using micro tweezers (World Precision Instruments, Inc) under a stereomicroscope.

2.2.4 System Setup

A peristaltic pump (Kamoer Fluid Tech Co., Ltd, Shanghai, China) using a 2.3 mm ID and 4.6 mm OD polyurethane tube was used to drive the fluid in the system. The ZOC devices were placed inside a thermal isolated box which is integrated with a Peltier thermal controller to maintain the incubation temperature to be around 28.5 ℃ . To reduce the

oscillation and smoothen the flow, a homemade pulse damper assembled by a 60 ml syringe and a two way-valve (Cole-Parmer Inc.) connected the chip outlet and the peristaltic pump inlet (Figure 2.1). A three way-valve was used to connect the peristaltic pump outlet, a 10 ml loading reservoir, and a waste container to allow both close-loop and open-loop operations (Figure 2.2). Silicone tubes with 2 mm ID and a 3 mm OD were used for the connection. This tubing size allows multiple embryos to be loaded and travel in the system simultaneously. Before operation, the fluidic device was first flushed with 70% (v/v) ethanol to wet the channel wall and prevent bubble formations.

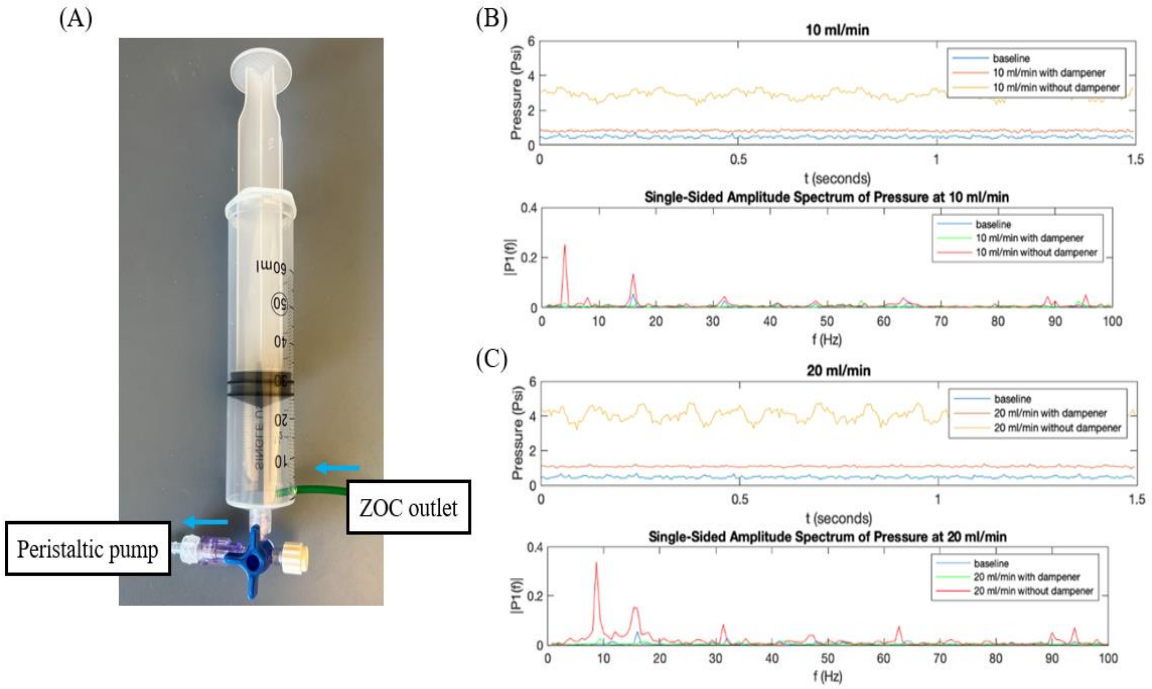

Figure 2.1. Homemade pulse dampener. A) The picture of the homemade pulse dampener using a 60 ml lure lock syringe and a 2-way valve. The air volume inside the syringe is set to be 26 ml. B) Top: The pressure profile measured at the inlet of the peristaltic pump with and without the pulse dampener at 10 ml/min flowrate. Bottom: the pressure profile after fast Fourier transforms. C) Top: The pressure profile measured at the inlet of the peristaltic pump with and without the pulse dampener at 20 ml/min flowrate. Bottom: the pressure profile after fast Fourier transforms.

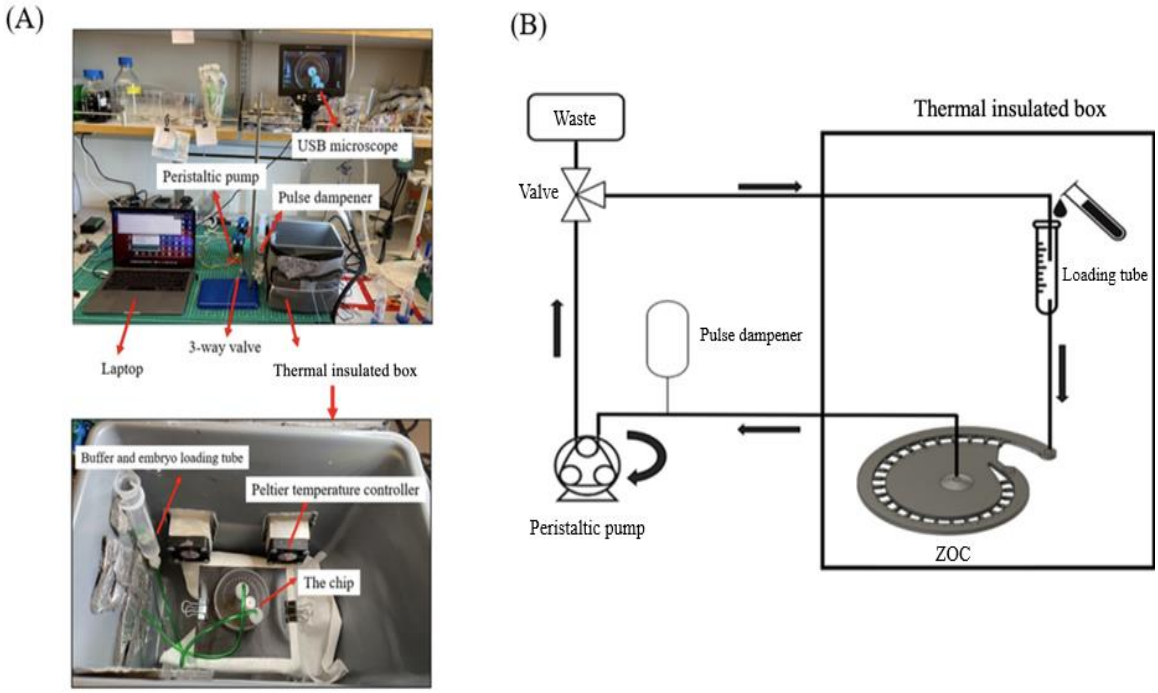

Figure 2.2. The overall system setup. A) Top: The overall setups for the zebrafish embryo trapping and staining system. Bottom: The components inside the thermal insulated box. B) Schematic showing the overall pumping system. The arrows indicate the flow direction during close loop perfusion.

2.3 Device Design and Results

2.3.1 Hydrodynamic Trapping Principle and ZOC Design Considerations

The ZOC-based automatic entrapment of zebrafish embryos is one of the desired features for the ZOC as it can simplify the embryo transfer/placing processes as well as provide consistent microenvironments for embryo development or treatments. The micro-or nano-fluidic devices use mechanisms such as particle sedimentation,[15] hydrodynamic trapping,[16–18] hydrodynamic focusing,[19] electrowetting,[20] droplet encapsulation,[21] etc. to trap or isolate particles. However, for zebrafish embryo, due to its macroscopic volume (millimeter in diameter) and substantial mass (850 to 1050 μg) many of these micro- or nano- particle trapping mechanisms are not practical in milli- fluidic ZOC.[4] In contrast to the micro- or nano- scaled particles, the zebrafish embryos have much higher traveling momentum under perfusion. Furthermore, the gravitational force also contributes to the movements of the zebrafish embryo, in which the sedimentation for the zebrafish embryo is more rapid than micro- or nano- particles.[4] For ZOCs, the hydrodynamic and gravitational forces are the most used trapping mechanisms for automatic zebrafish embryo trapping.[22]

In this study, two ZOC designs aim to study both unhatched (Design I) and dechorionated zebrafish embryos (Design II) are developed. The two ZOC designs utilize hydrodynamic force as the main mechanism for the embryo trapping. To understand the hydrodynamic

zebrafish embryo trapping process as well as to determine the appropriate channel dimensions, electric circuit analogy is used to establish resistive flow models for the ZOCs. Based on the circuit analogy, the volumetric flowrate, pressure difference, and hydraulic resistance along the channel is equivalent to the current, voltage, and resistance in Ohm's law. Hence, the volumetric flowrate, Q is equal to the quotient of pressure difference, ΔP, and hydraulic resistance, R.

$$Q = \frac{\Delta P}{R} \qquad \text{(Eqn. 2.1)}$$

Also, the hydraulic resistance for single phase laminar flow along a section of rectangular channel section is determined by both fluidic properties and the channel geometry and is given by

$$R = \frac{12\,\mu L}{h^3 w}\left[1 - \frac{192}{\pi^5} \times \frac{h}{w} \times tanh\, tanh\left(\frac{\pi w}{2h}\right)\right]^{-1} \qquad \text{(Eqn. 2.2)}$$

Where μ is the dynamic viscosity of the carrying fluid, *L*, *w*, and *h* are the length, width, and height of the rectangular channel section, respectively. A hydrodynamic particle trapping device usually consists of two major channels: (1) an array of trapping channels and (2) a main channel. The steady fluid flow will carry the particles through the main channel and sequentially place single or multiple particles into the traps. The trapping channel's ability to capture the particles from the main channel is based on the relative hydraulic resistances between the trap and the main channel. For instance, particles will be more likely to be drawn into the trap when the hydraulic resistance of the empty trap, R_T, is less than the hydraulic resistance of the main channel, R_M (Figure 2.3.A). When the trap is occupied already, the following particles will bypass the trap as the hydraulic resistance of the occupied trap is now greater than the main channel (Figure 2.3.B). Collectively, the trapping happens when:

$$R_M > R_T \qquad \text{(Eqn. 2.3)}$$

A hydrodynamic trap design usually involves both body and nozzle (Figure 2.2 A). The trap body which usually has a close size to the particle is used to contain the particle whereas, the trap nozzle has a width smaller than the particle diameter is used to retain the particle inside the trap. Notably, the dimensions of the trap nozzle are usually used to adjust the hydraulic resistance of the trap in the fluidic device. The overall hydraulic resistance of the trap can then be calculated by

$$R_T = R_b + R_n \qquad \text{(Eqn. 2.4)}$$

Where, R_b is the hydraulic resistance of the trap body, and R_n is the hydraulic resistance of the trap nozzle.

Separately, the volumetric flowrate relationships between trapping channels and main channel also reflect the particle trapping potential and perhaps a more intuitive way to

understand the hydrodynamic particle trapping process. In the fluidic channel, the primary force that directs the traveling of the particle is the drag force (F_D) which is given by

$$F_D = \frac{1}{2} \times C_D \rho A v^2 \qquad \text{(Eqn. 2.5)}$$

Where, C_D is the drag coefficient, a dimensionless number that describes the resistance of a moving particle to the carrying fluid. ρ is the carrying fluid density. A is the reference area of the object. v is the relative velocity between the object and the carrying fluid. As shown in the equation 2.5, the level of the trapping force is directly related to the velocity of the carrying fluid. When the channel geometry is considered, the particle drawing ability of the trapping channels can also be estimated by the volumetric flowrate relationship between the main channel and trapping channels. For instance, when the volumetric flowrate in the trap channels (Q_T) is higher than the volumetric flowrate in the main channel (Q_M), the particle trapping will be more likely to happen and vice versa (Figure 2.3.A).

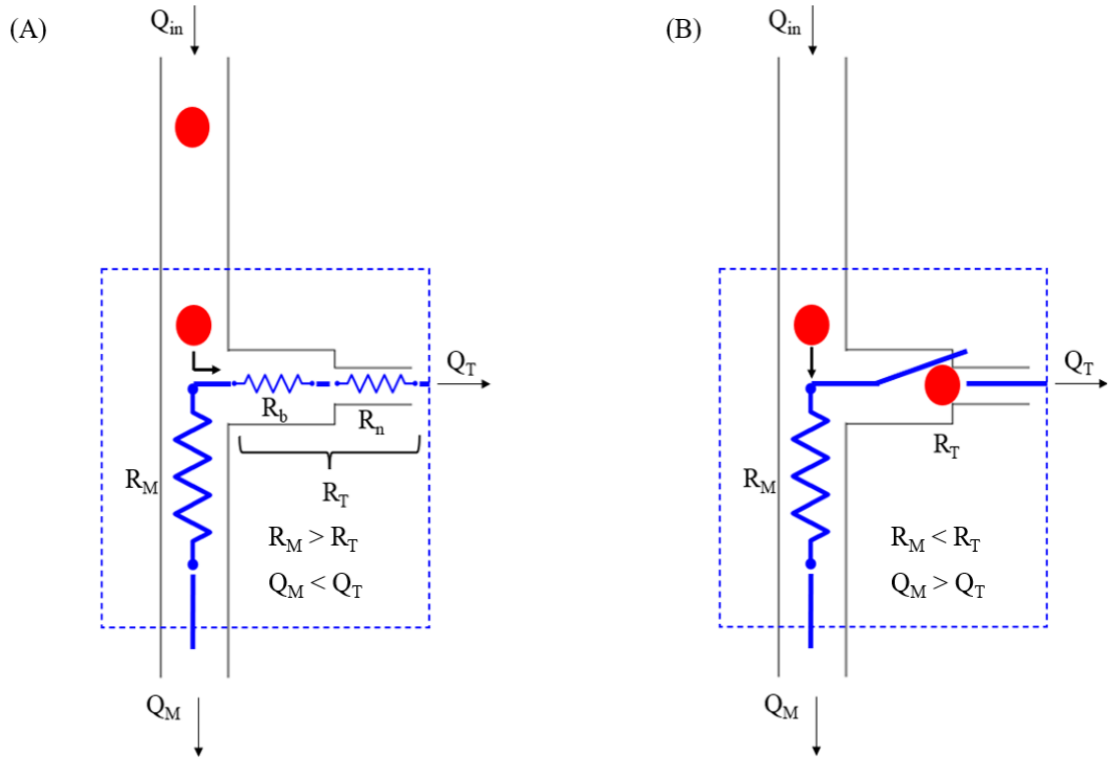

Figure 2.3. Schematic for hydrodynamic particle trapping. A) Particle is drag towards the trapping channel when $Q_M < Q_T$. B) The following particle bypasses the trapping channel when $Q_M > Q_T$.

The two ZOC devices developed in this chapter implements a parallel hydrodynamic trapping configuration in which the traps are parallelly arranged and share the same inlet and outlet with the main channel.[16] Because of the simple channel design, parallel trapping

configuration is suitable for milli fluidic where the design space is precious. The volumetric flowrate as well as the channel hydraulic resistance relationships can be described in a simple model (Figure 2.4).

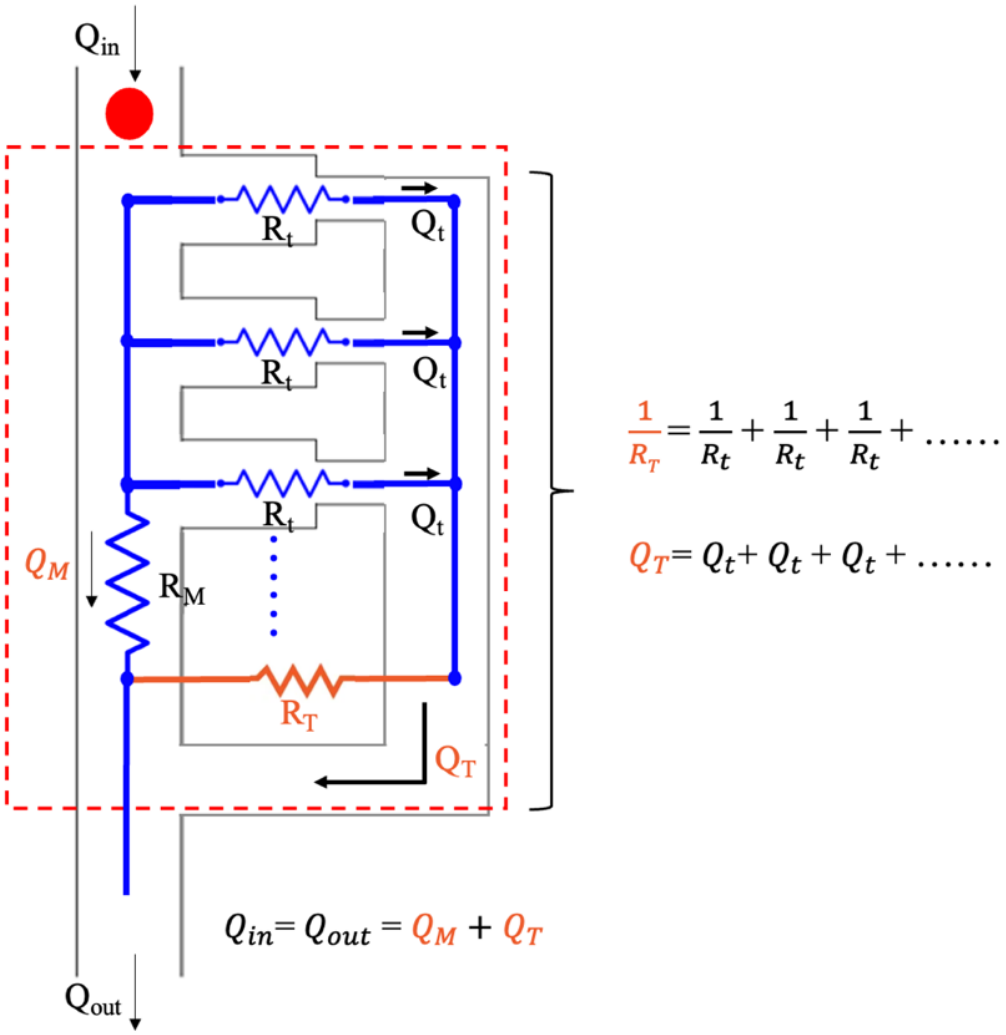

Figure 2.4. The volumetric flowrate and hydraulic resistance relationships in parallel trapping configuration.

Based on the continuity equation, the inlet volumetric flowrate (Q_{in}) is equal to the sum of the volumetric flowrate in the main channel (Q_M) and the overall volumetric flow that go through the trapping channels (Q_T). Similarly, the particle (i.e., zebrafish embryo) is more likely to be trapped happen when the volumetric flowrate that goes through the trapping channels (Q_T) is greater than the volumetric flowrate that goes through the main channel (Q_M). Or in another word, the overall volumetric flowrate that goes through the traps must be greater than 50% of the inlet flowrate to let the trapping happen.

$$Q_T > Q_M = Q_{in} - Q_T$$
$$\Rightarrow \quad Q_T > 0.5 \times Q_{in} \qquad \text{(Eqn. 2.6)}$$

The above equations explain the criteria for hydrodynamic particle trapping under steady state conditions. However, it is important to notice that the particle trapping is a dynamic process in which the hydraulic resistances as well as the volumetric flowrates in the channels are continuously changing as the trapping channels keep being occupied by the particles. Moreover, this dynamic trapping process is complicated and even chaotic for zebrafish embryos as their substantial volume constantly disrupts the fluidic field when traveling in the milli scaled channels. For this, the fluidic field cannot be assumed to be unchanged (i.e., quasi-steady state) throughout the process. Also, the zebrafish embryos are likely to experience more embryo-embryo and embryo-wall interactions in the channel that is not much bigger than their sizes which makes the embryo trapping prediction even harder. Hence, the dynamic trapping process of zebrafish embryo cannot be easily simulated by a single Lagrangian particle tracing model.[23]

To simplify the description of the dynamic trapping and be able to estimate the overall embryo trapping potential of the ZOCs, the initial (i.e., all traps are empty) and final states (i.e., all traps are occupied) of the trapping process are selected and analyzed as they are the only two steady state moments that are certain in this complicated dynamic process. For parallel trapping configuration, it can be easily understood that the overall volumetric flowrate that goes through the traps drops as more traps are occupied during the trapping (i.e., the overall hydraulic resistance of traps increases when more embryos are captured). To maintain a sufficient embryo drawing potential in the ZOCs even at the late stage of the trapping process, the overall volumetric flowrate that goes through the traps (Q_{T_final}) needs to be kept around or greater than 50% of the inlet flowrate (Q_{in}) at the final state.

$$\text{At the final state:} \quad Q_{T\_final} \gtrsim 0.5 \times Q_{in} \qquad \text{(Eqn. 2.7)}$$

The above equation can estimate the overall embryo trapping ability of the ZOC, however, to evaluate the embryo trapping smoothness as well as to predict the usage (i.e., embryo occupation potential) of specific traps, individual trap's embryo drawing ability need to be investigated. Because the movements of the zebrafish embryo are directed by the hydrodynamic drag force (Eqn. 2.5) and the embryos are usually have very closed physical properties (i.e., density, and shape), we define the embryo trapping index (ETP) and use it to evaluate the embryo drawing ability of individual trap.

$$ETP = \frac{V_t}{V_m} \times 100\% \qquad \text{(Eqn. 2.8)}$$

Where, V_t is the average linear velocity towards the trapping channel, and V_m is the average linear velocity at the near main channel section.

For a smoothed trapping, the free embryos need to have the momentum to travel in the ZOC throughout the process without being stopped due to flowrate decreasing in the main channel. Therefore, the inlet flowrate selection as well as the flowrate attenuation rate need to be considered when operating and designing the ZOC with parallel trapping configuration. Moreover, the embryos should not all rush into specific traps during the

trapping which could lead to channel blockage in the ZOC. This means the embryo drawing potential of all empty traps need to be kept at a closed level throughout the trapping process or in another word, no empty traps should have outstanding embryo drawing ability compared to the rest of empty traps. For this, we believe a closed embryo trapping potential for individual empty traps need to be ensured at the initial state as the trapping potential for all the empty traps drop simultaneously during the trapping process in the parallel trapping configuration (i.e., the relationship of embryo trapping potential among all the empty traps mostly preserves towards the end).

All individual the traps at initial state: $ETP \cong$ Constant (Eqn. 2.9)

Collectively, due to the substantial volume and mass, zebrafish embryos experience much larger momentum as well as more complex movements than the micro- and nano- particles during the trapping process. Furthermore, it is not feasible to apply the quasi-steady state assumption to the fluid field when trapping zebrafish embryos, as the macroscopic size of the embryo constantly changes the fluid field. Hence, using the Lagrangian method to predict and estimate the zebrafish embryo trapping ability for ZOC is not cost-efficient. Here, we developed a simple analytic model for embryo trapping potential estimation in the ZOC by targeting the initial, and final states of the zebrafish embryo trapping process. The model as well as other design criteria for the embryo hydrodynamic trapping will guide our ZOC designs discussed in the next section and used for the future ZOC developments.

2.3.2 Design Layouts and Zebrafish Embryo Trapping Analysis

The two ZOCs use a spiral parallel trapping configuration to automatically trap and immobilize the unhatched (Figure 2.5.A) and dechorionated zebrafish embryos (Figure 2.5.B). The spiral ZOC design contains 3 major functional parts: a spiral main channel, an inner suction chamber, and 26 trapping channels that interconnect the main channel and inner chamber. When operating, the inner chamber, which connects to a peristaltic pump, provides a negative pressure to draw the fluids from the main channel via the traps. The trap channels and main channel have different heights for the purposes: 1) to shorten the mass transfer distance in the traps; 2) to prevent bubbles from entering the traps. Also, the main channel for both designs have a width of 3.5 mm which allows multiple embryos to travel simultaneously and let the individual embryo to freely self-rotate. Because the unhatched zebrafish embryo has a larger overall size than the dechorionated zebrafish embryo, the overall channel height as well as the internal volume of the traps for design I is greater than design II. The internal volume for the trap body in design I and design II are about 7.4 μl and 2 μl, respectively which allows only 1 embryo per trap. After trapping, the zebrafish embryo partially blocks the trap nozzle ensuring a flowthrough environment. Here, the trap nozzle length is used to regulate the flow distribution in the trap and main channels. In both ZOCs, the length of trap nozzle decreases from 1 mm for the first trap (i.e., trap closest to inlet) to 0.5 mm for the last trap (i.e., trap at the end of main channel) at a rate of 0.02 mm/trap along the main channel. For zebrafish embryo trapping, this configuration is to ensure a closed hydrodynamic trapping potential at each trap for the purposes of maximizing the usage of the traps and smoothing the trapping process. In addition, this nozzle length changing configuration is also important to minimize the

“procedure lagging” (e.g., mass transfer rate differences) due to the fluid velocity drop in the parallelly arranged traps (i.e., slow down the velocity dropping).

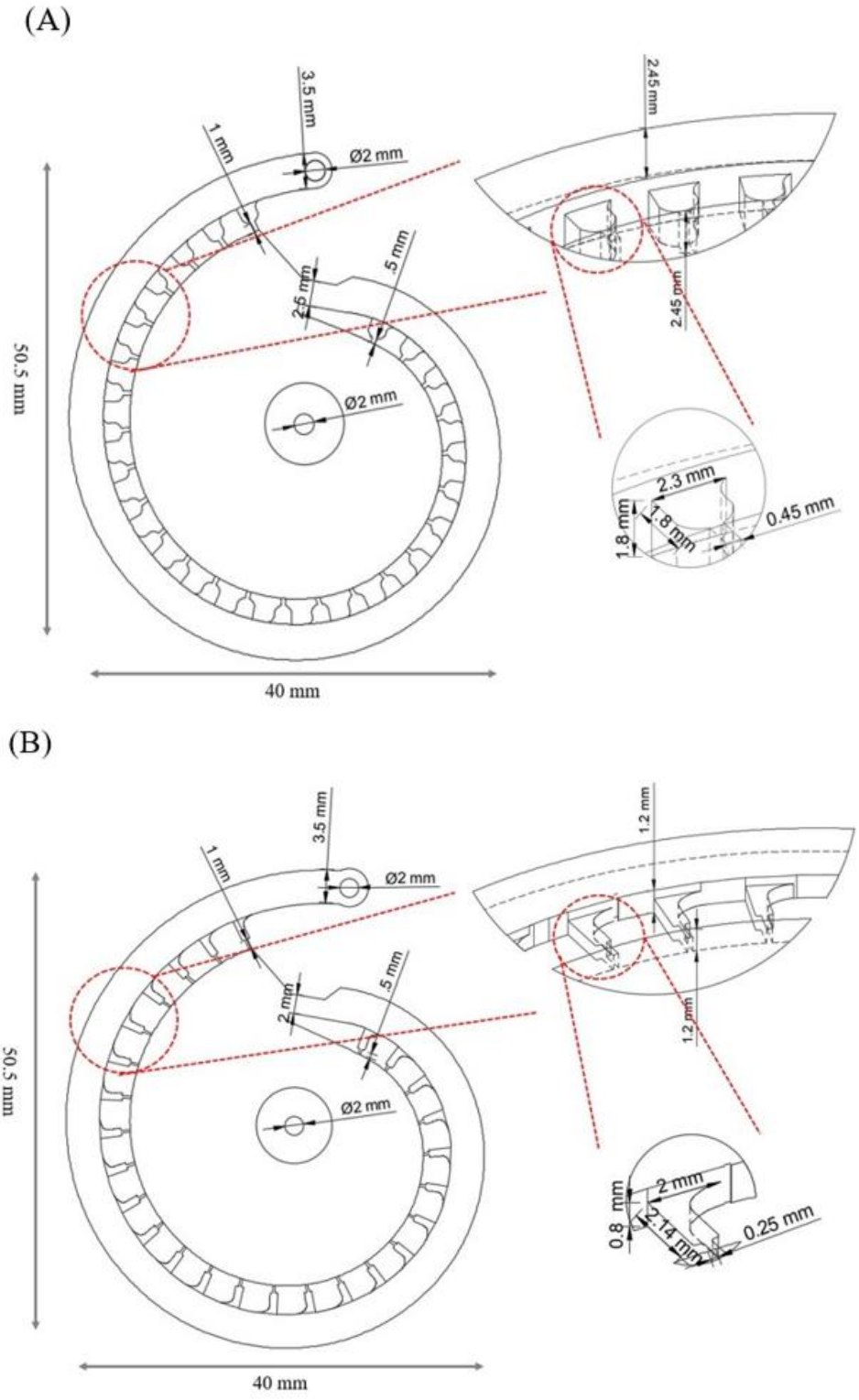

Figure 2.5. The design layouts for the two ZOCs. A) The ZOC design for trapping unhatched zebrafish embryo. B) The ZOC design for trapping dechorionated zebrafish embryos.

Using design II as an example, the zebrafish embryo trapping process can be animated in Figure 2.6.A. For both ZOCs, the traps are arranged parallelly along the spiral main channel and the inner chamber provides a relatively constant downstream pressure (Figure 2.6.B&C). In a simplified circular diagram, the inner chamber can be treated as the ground in the ZOC (Figure 2.6.D). This source-and-sink configuration eases the later fine-tuning as the distribution of hydrodynamic trapping force (i.e., proportional to the pressure drop) is only dependent on the hydraulic resistance of the traps and can be adjusted by modifying the trap nozzle size (i.e., $R_T = R_b + R_n$, Eqn. 2.4).

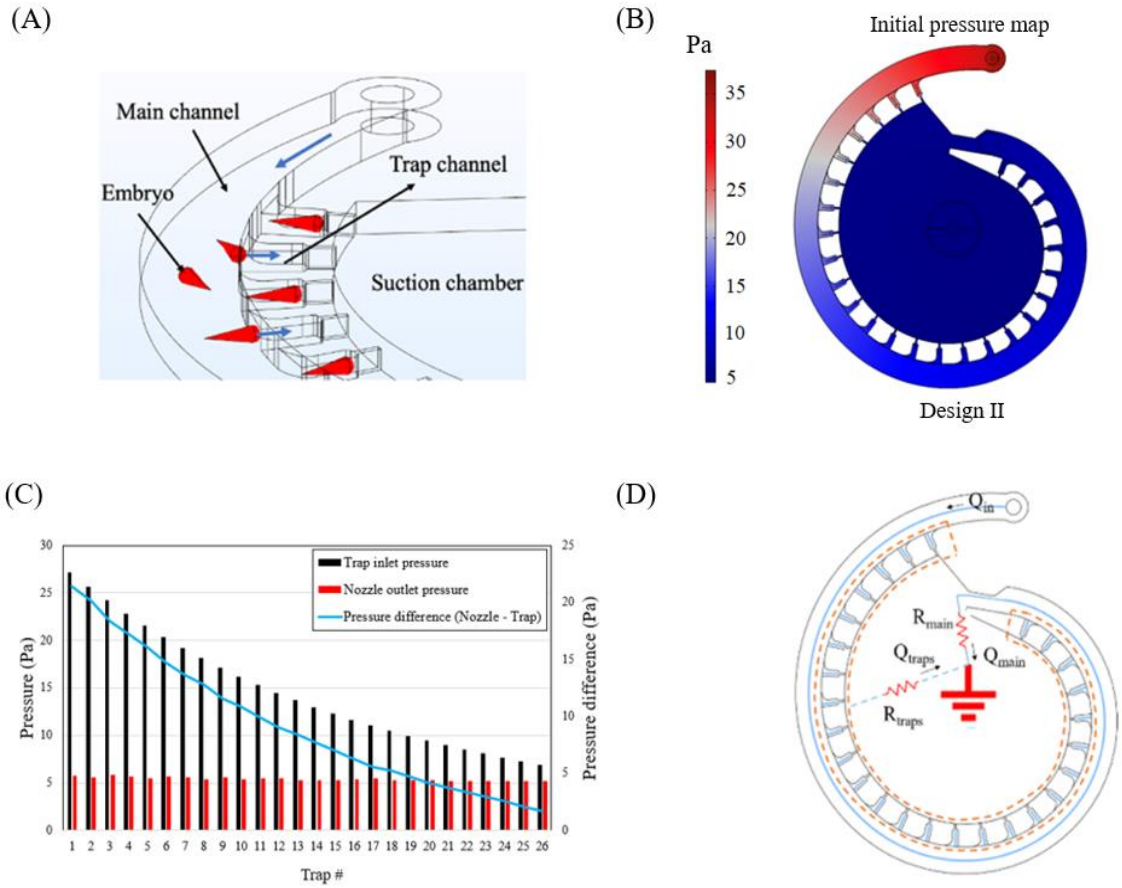

Figure 2.6. The zebrafish embryo trapping principle in the ZOCs. A) Schematic showing the zebrafish embryos are dragged into the traps in design II due to hydrodynamic suction force. B) The pressure maps design II at initial state. C) The pressure and pressure difference distribution near the traps in design II at initial state. D) The simplified circular analogy uses design II as an example showing parallel trapping and source-and-sink configurations in the ZOC.

As discussed in section 2.3.1, the zebrafish embryo trapping in the milli fluidic channel is a complicated dynamic process. Estimating the ZOC's embryo trapping potential by simulating the entire trapping process will be computationally expensive. Therefore, the steady fluidic fields of initial (i.e., all empty traps) and the final (i.e., all occupied traps) states are selected for the CFD simulation to evaluate the overall embryo trapping potential

in the ZOCs (Figure 2.7.A). Based on the CFD simulation, the overall percentage for the flow that go through the traps (i.e., $Q_T/Q_{in} \times 100\%$) drops from 78% and 76% to 53% and 59% during the embryo trapping process in design I and design II, respectively (Figure 2.7.B). This indicates the embryo trapping is getting harder when more traps are being occupied through the process which is consistent with our model in section 2.3.1. Despite this, for both ZOCs the potential for the embryo trapping remains even at the last moment of the trapping process as the flow going through the traps is still higher than the flow going through the main channel (Eqn. 2.6 and Eqn. 2.7).

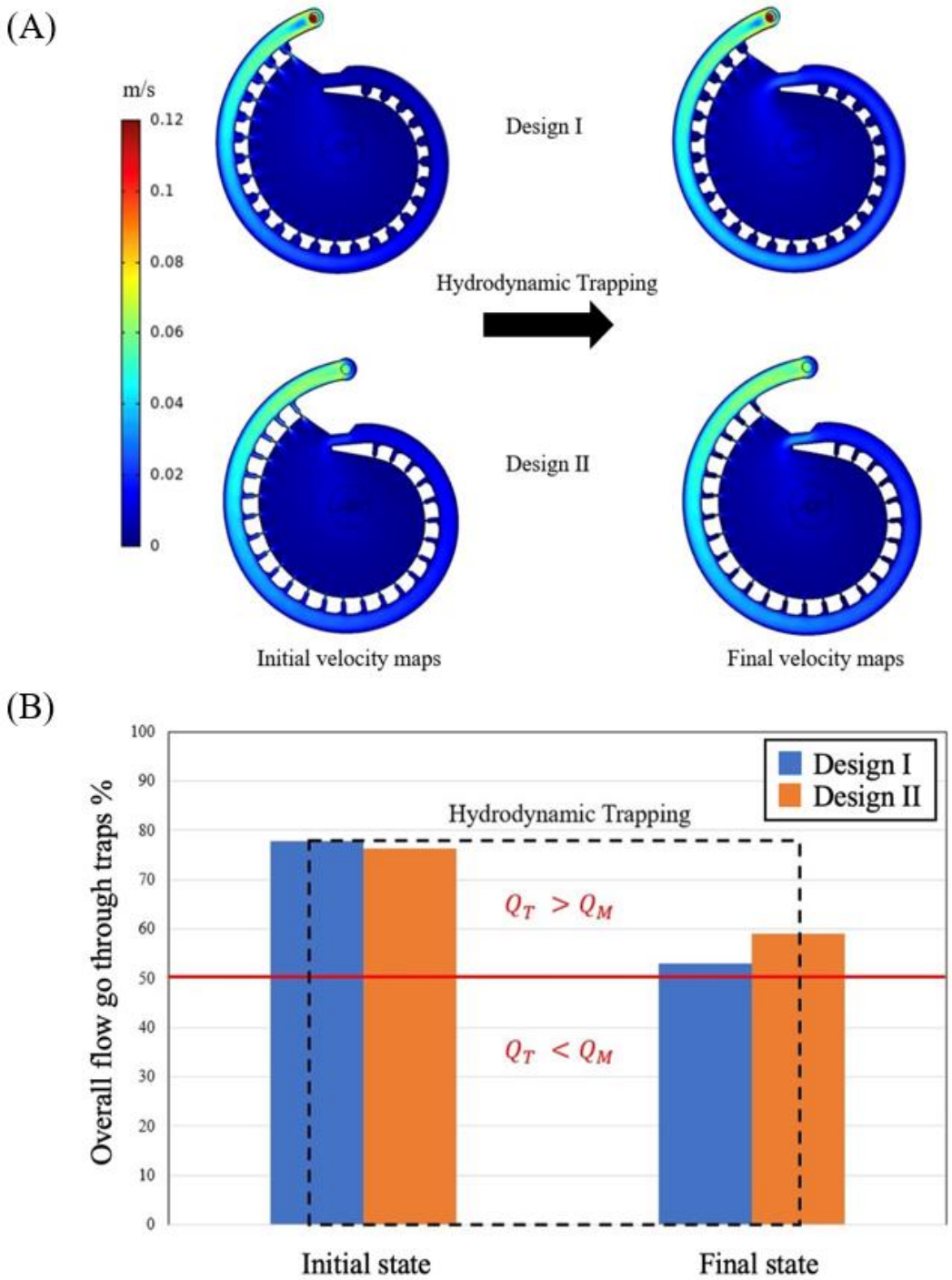

Figure 2.7. Zebrafish embryo trapping evaluation using CFD simulations. A) Top panel: the velocity heatmaps for design I at initial and final trapping states. Bottom panel: the velocity heatmaps for design II at initial and final trapping states. B) The overall trap flow at initial and final trapping states.

The above method estimates the overall zebrafish embryo trapping process in the ZOCs. However, to examine if the zebrafish embryo can be smoothly delivered into the traps as well as to evaluate the potential trap usage rate in the ZOCs, we need to take a close look at the individual trap's embryo drawing ability. The main embryo trapping force in the two ZOCs is the hydrodynamic drag force which is directly proportional to the square of relative velocity between the fluidic flow and moving embryo (Eqn. 2.5). During the embryo trapping in the ZOCs, the zebrafish embryo experiences the hydrodynamic drag forces from the crossflow viz. along the main channel and towards the trap channel. Here, we use the fluidic velocity ratio between the trap channel (V_t) and its near main channel section (V_m) as an index to evaluate the individual trap's embryo drawing ability (i.e., Eqn.2.8: ETP = $V_t \ / \ V_m \times \ 100\%$). For a smoothed embryo trapping process, the zebrafish embryos should not rush into specific traps and the main channel velocity dropping should not be too drastic as these may lower the usage of other traps and lead to main channel blockage. For these purposes, we employed a changing nozzle length design in the two ZOCs (the nozzle length for individual traps decreases from 1 mm to 0.5 mm along the spiral main channel).

To see how the changing nozzle length affects the flow in the main channel and trapping channels, as well as the embryo trapping index (ETP). We then compared two situations in design II in which the changing nozzle length is employed versus not employed (i.e., all nozzles have the same length of 0.5 mm) (Figure 2.8.A). According to the initial state CFD simulations (i.e., all traps are empty), when the changing nozzle length design is not employed in design II, the middle range traps would have outstanding ETP indicating the embryos are more likely to rush into the middle traps during trapping. Moreover, compared to the changing nozzle design, the flow distribution among the parallelly arranged traps is steeper (i.e., drop more quickly), and the flow attenuates more rapidly at the main channel when all the nozzles have the same length (Figure 2.8. B&C&D). These results indicate the changing nozzle design allows the ZOC to have a more evenly distributed embryo trapping ability among individual traps (Eqn. 2.9) and the embryos can maintain a certain level of momentum to loop inside the main channel. In addition to the embryo trapping smoothness improvements, this configuration can also minimize the "procedure lagging" (i.e., delay in mass transfer) in the ZOCs as the trapping channel flowrate distribution is flatten after adjusting the trap nozzle length (Figure 2.8 C).

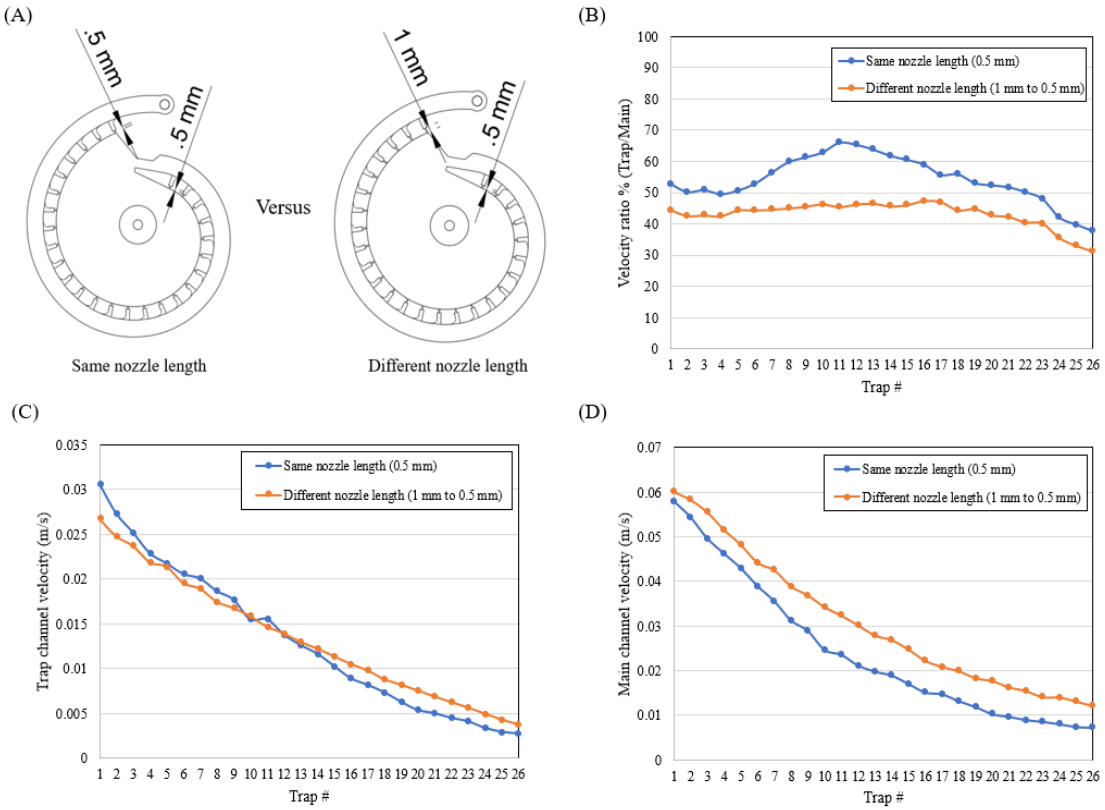

Figure 2.8. The changing trap nozzle length design in ZOC (design II). A) The 2D layouts for the ZOCs with same nozzle length of 0.5 mm (left) and the ZOC with changing nozzle length from 1 mm to 0.5 mm along the main channel (right). B). The ETP for ZOC with (orange) and without (blue) trap nozzle length changes at individual traps. C) The trap channel velocity for ZOC with (orange) and without (blue) trap nozzle length changes at individual traps. D) The main channel velocity for ZOC with (orange) and without (blue) trap nozzle length changes at individual traps. The inlet flowrate is set at 10 ml/min and the CFD simulations are performed at the initial state.

Separately, since the parallel hydrodynamic trapping configuration is used in the ZOC designs, the fluidic velocity levels are expected to change simultaneously in the channels during the embryo trapping. Or in another word, the relationships of the zebrafish ETP among the empty traps will not have too much change during the trapping process. To verify this, we simulated one of the scenarios during the middle of the trapping process in which all the traps are occupied except trap 1,2,13,14,25, and 26. The CFD simulations have shown that the overall ETP drops when more traps are occupied, however, the ETP relationship between the remaining empty traps does not have prominent changes (Figure 2.9). This has proven our assumption mentioned in section 2.3.1 where the embryo trapping potential relationship among all the empty traps would mostly preserves towards the end of the trapping process.

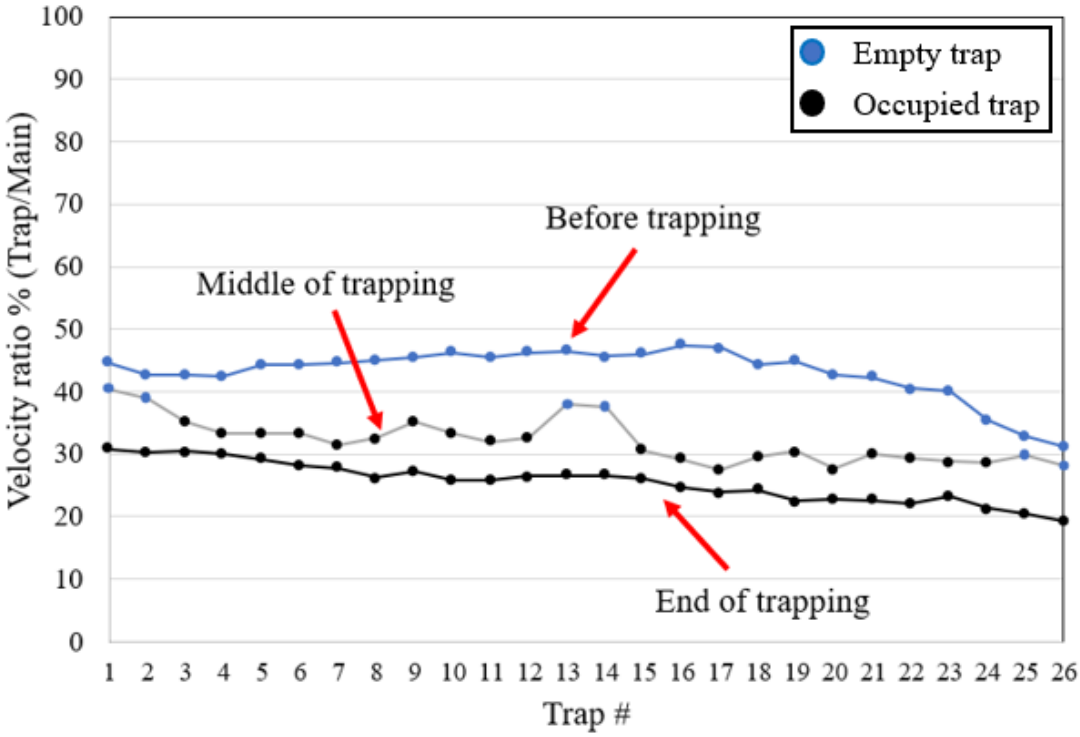

Figure 2.9. The velocity ratio distribution along the traps in design II during embryo trapping process. The blue line indicates the initial state of the trapping. The black line is the final state of the trapping. The gray line is an example during the middle of the trapping process where traps 1,2,13,14,25, and 26 are still empty, and the rest of the traps have been occupied.

We next verify these design considerations by examining the initial steady state velocity maps for the two ZOC designs. The initial state velocity maps indicate that the ETP (i.e., velocity ratios between the trapping channels and local main channel sections) in design I and design II are kept at 46.61± 4.6% and 43.12± 4.07%, respectively (Figure 2.10.A&B). According to the CFD simulation results, we believe the changing nozzle length configuration used in the two ZOC designs allow all the traps to have a closed embryo drawing ability, and therefore can ensure a smoothed trapping process as well as a high trap usage rate.

(A) Design I:

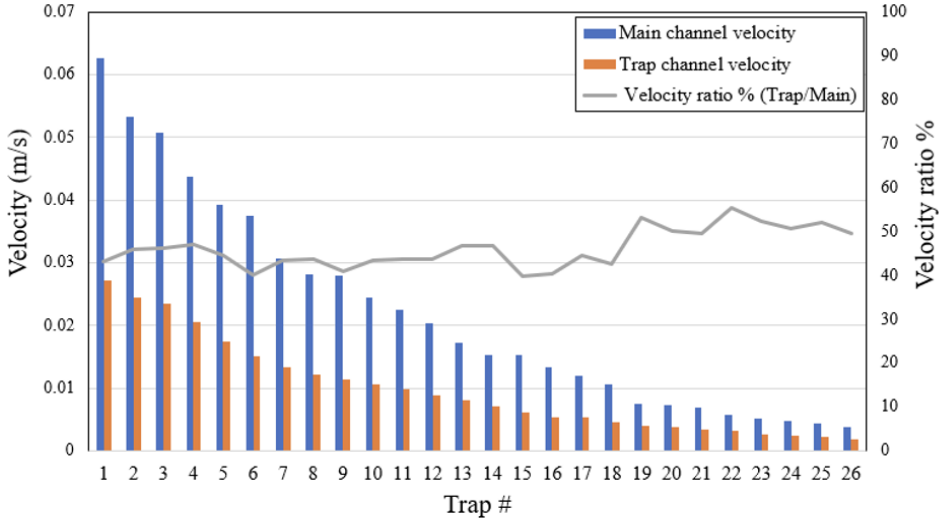

(B) Design II:

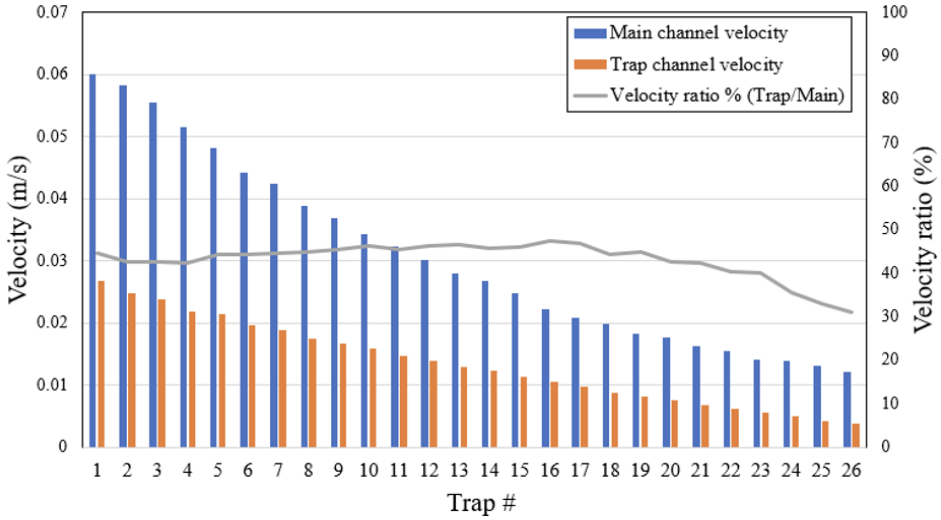

Figure 2.10. The zebrafish embryo trapping smoothness evaluation using CFD simulations. A) The velocity and velocity ratio distribution for the traps in design I. B) The velocity and velocity ratio distribution for traps in design II.

Note the final configurations for the two ZOCs were determined by both CFD simulations and validation experiments. The overall back-and-forth process as well as a series of trial-and-error are not shown here. As our understanding for this trapping configuration gets deeper, the later ZOC design and optimization will be more directional.

2.3.3 Device Fabrication and Inspection

In this work, a consumer-grade LCD SLA 3D printer is used to assist the device prototyping (Figure 2.11.A). Briefly, the negative mold of the ZOC is first printed by the LCD SLA 3D printer (Figure 2.11.B), and then used for PDMS soft lithography to make the PDMS-glass

device (Figure 2.11.C). The complete fabrication process is detailed in section 2.2.2. The reasons for making the PDMS-glass device instead of printing the whole device at once is 1) most commercially available photo resins are toxic to zebrafish embryos,[24] and 2) most photo resins can only reach optical translucent.[25] Compared to the conventional microfluidic fabrication methods, our method eliminates the need for cleanroom fabrication, reduces manual steps, and shortens the fabrication time. Also, the cost for the 3D printer and photo resins are much lower than their industrial or commercial leveled counterparts (e.g., Formlabs). We believe this prototyping method is ideal in making milli fluidic ZOC devices and is suitable for small budget labs.

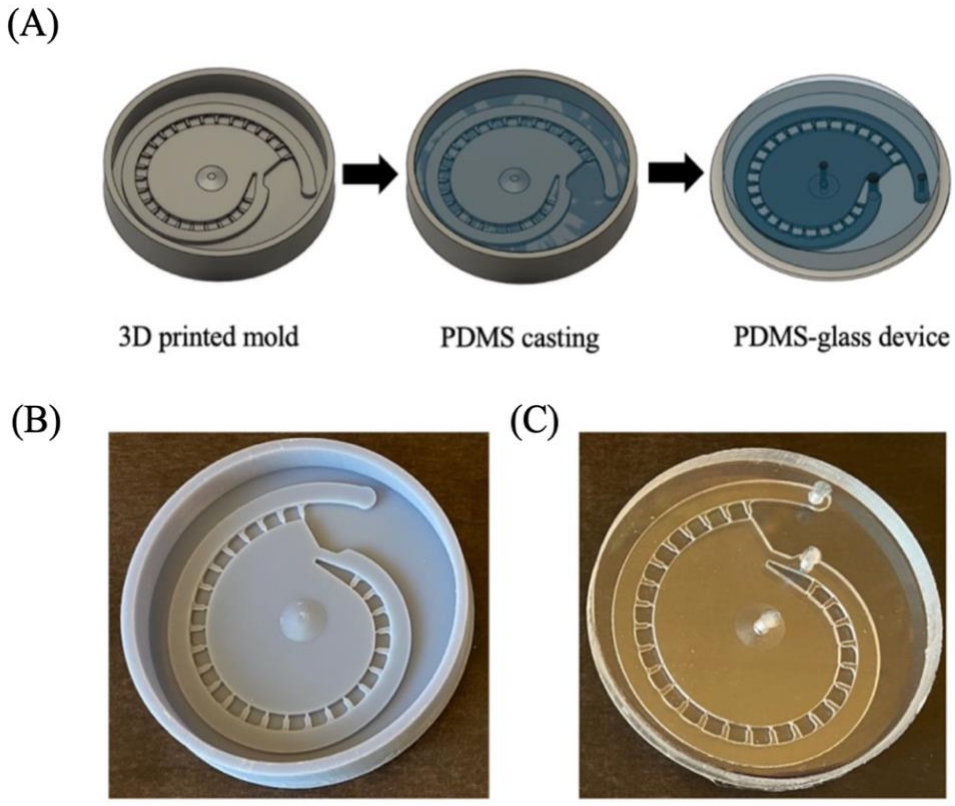

Figure 2.11. The 3D SLA printer assisted ZOC prototyping. A) The ZOC prototyping pipeline. B) Photography showing the 3D SLA printed negative master mold for the ZOC device. C) Photography showing the assembled PDMS-glass device after soft lithography.

The quality and resolution of the device is dependent on the 3D printed negative mold. Therefore, some of the settings in the 3D printer need to be well calibrated to ensure the mold reaches acceptable quality and resolution. The LCD SLA 3D printer used in this work uses a 3840 2400 (4K) LCD screen and an array of UV lamp beads (405 nm) to control the pattern printing at each layer. During the printing, the photo resin is partially cured by the UV light at each layer. The UV exposure time needs to be long enough to ensure the photo resin layers can stick to each other and overcome the gravitational force. However, the UV exposure time also needs to be short enough to avoid overcuring that causes dimension offsets for some small features.[13] Unfortunately, most consumer-grade photo resins are not

provided with very detailed datasheets for dimension specific UV exposure times. Moreover, the same photo resin may have various performances on different brand 3D printers. So, it is important for the users to find out the best UV exposure settings for their prints. In our 3D printer settings, the UV exposure time is set to 2 seconds to minimize the overcuring effect. Also, to minimize the flow disturbance caused by the motions of the build platform, the lifting and retracting speeds of the build platform are set to 0.25 mm/s and 3 mm/s, respectively. Another limitation for this prototyping method is the surface roughness of the 3D printed mold, especially at the edges of the channel. The 3D printer employs an LCD screen with 50 µm by 50 µm pixel size that cannot always fit the edge of design perfectly. Therefore, jagged channel walls are expected to be casted by the LCD SLA 3D printer. To reduce the edge jaggedness of the mold, the anti-aliasing algorithm was applied in the settings (Figure 2.12). To evaluate the fabrication quality, the nozzle width is inspected as it is the smallest feature in the ZOC. The result has indicated that the average nozzle width is about 0.285 ± 0.031 mm (N=5) when the target width is 0.25 mm (Figure 2.12). As expected, the channel wall was also found to be rough, even applied with the highest level of anti-aliasing. The variation of the channel width and the rough channel wall are considered acceptable as only minor hydrodynamic difference is expected to be caused by the small variations and the elastic property of the PDMS would extenuate the mechanical damage on the zebrafish embryo.

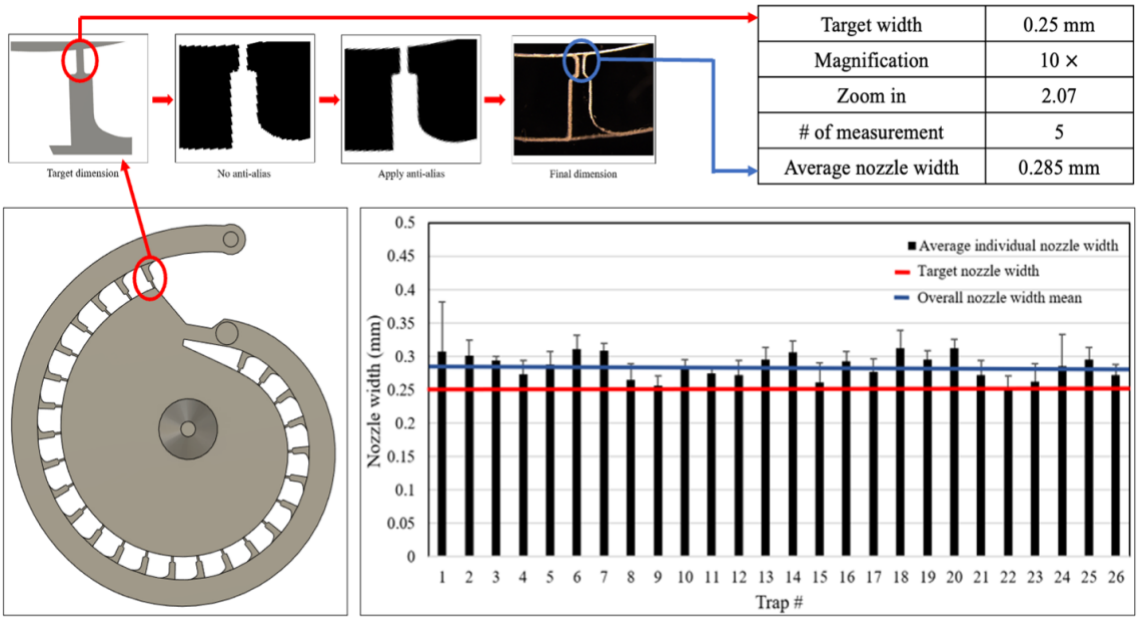

Figure 2.12. Device fabrication inspection. Top left: The anti-aliasing algorithm used to reduce the jaggedness in the channel wall. Top right: The table for the target nozzle width, measured nozzle width, and the settings for the inspection. Bottom left: The CAD drawing of the multi-depth spiral device. Bottom right: The result for the nozzle width inspection (N = 5, error bar ± SD).

2.3.4 Zebrafish Embryo Trapping Validation

The two ZOCs aim to automatically trap and immobilize the zebrafish embryos mainly via hydrodynamic suction force. To validate the trapping process and evaluate the trapping performance of the two ZOC designs, 4 hpf unhatched zebrafish embryo and 24 hpf dechorionated zebrafish embryo were used in the embryo trapping validation tests for the design I and design II, respectively. Because design I has a larger channel dimension than design II, the trapping flowrate used in design I is higher than design II. Here, the embryo trapping flowrate used in design I and design II are set to be 20 ml/min and 10 ml/min, respectively. To maximize the usage of the traps, the gravitational force was also introduced to assist the trapping. At the late stage of the trapping (when most traps were occupied), the device was titled towards the remaining empty traps. Based on the validation test results the average trap occupation rate can reach 86.54 ± 6.57% (N= 6) and 93.03 ± 4.3% (N=16) for design I and design II, respectively. (Figure 2.13. A). Notably, no anesthetic drug such as tricaine was used before or during the zebrafish embryo trapping. This is one of the advantages for ZOC-based zebrafish embryo immobilization as the use of anesthetic drugs may cause bias for the later embryonic development studies. Furthermore, the trap usage distribution showed that the first couple traps were usually skipped by the embryos even with the help of the gravitational force (Figure 2.13. B&C). This is likely due to the high main channel velocity near the inlet which gives the embryo less deviation time to migrate towards the inner wall traps.

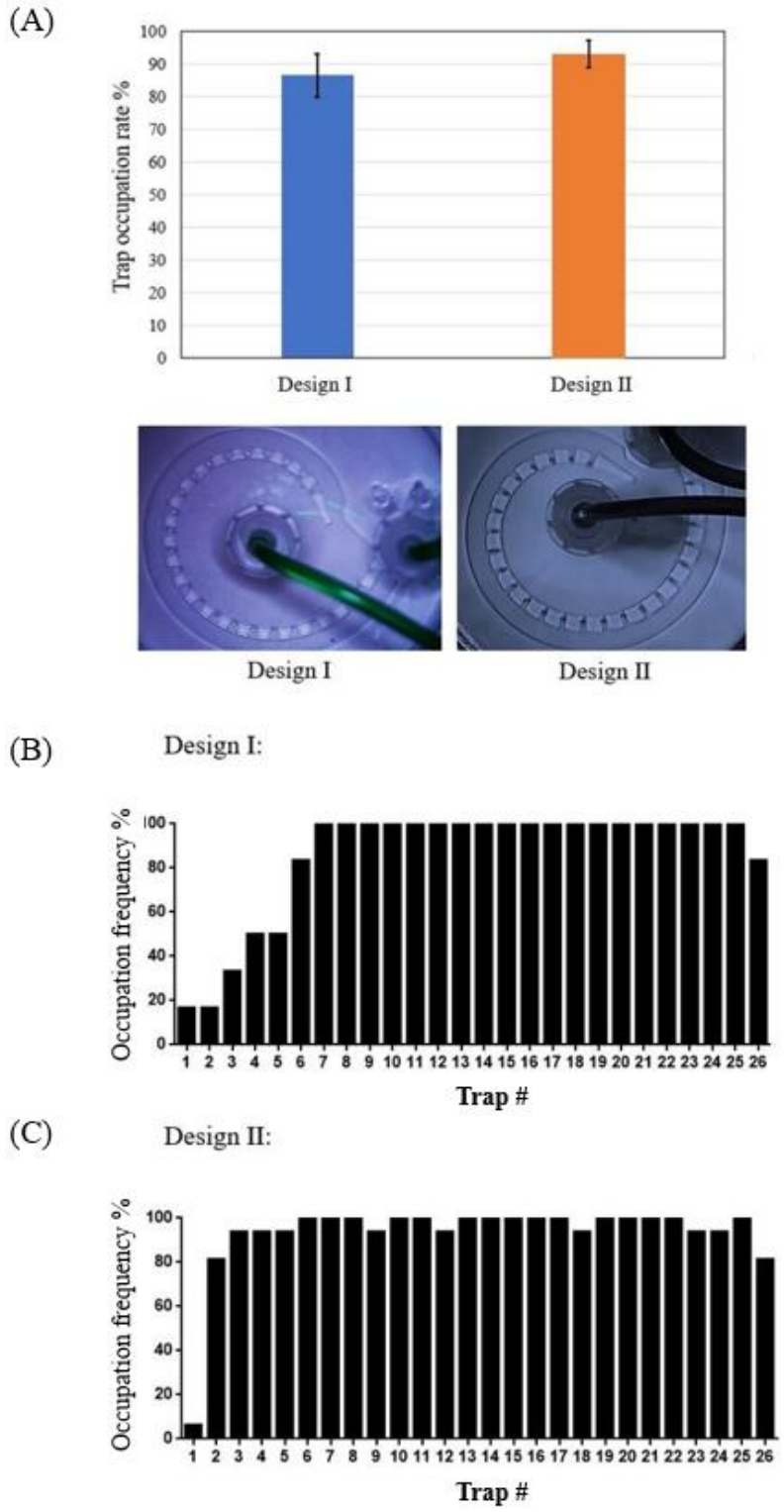

Figure 2.13. Zebrafish embryo trapping validation for the ZOCs. A) Top: the overall trap occupation rate for design I and design II. Bottom: images for the trapping results of design I (N=6, error bar:±SD). and design II (N=16, error bar:±SD). B) The trap usage rate distribution for design I (N =6). C) The trap usage rate distribution for design II (N =16).

In design II, the orientation control of the dechorionated zebrafish embryos was not considered initially. Interestingly, the validation experiments showed that about 92.88 ± 4.44% of trapped embryos in design II had their heads pointing inward after the trapping (Figure 2.14.A). We believe the orientation consistency is contributed by the coupling effects of the body shear stress and the hydrodynamic suction on the dechorionated zebrafish embryo. Briefly, when traveling in the main channel, the head of the cone-shaped zebrafish embryo experiences higher shear stress than its narrowed body. At the same time, the hydrodynamic suction draws the zebrafish embryo towards the inner wall where the traps are located. Because of these, the head of the zebrafish embryo is more likely to rotate towards the inner wall and then be dragged into the trap in the design II (Figure 2.14.B).

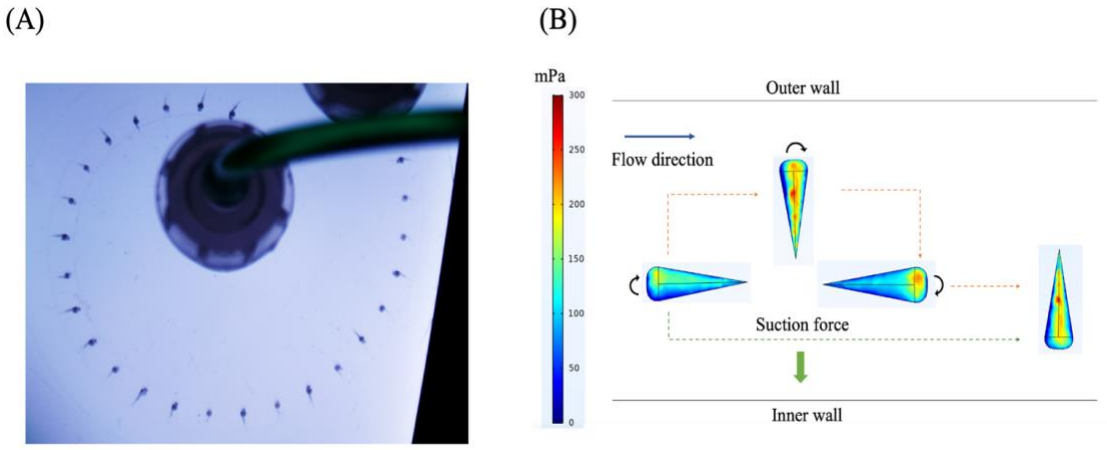

Figure 2.14. Zebrafish embryo body orientations after trapping. A) Image showing most of trapped zebrafish embryos have their heads pointed inward. B) The body shear stress distribution on the 4 potential body orientations of the zebrafish embryo in the main channel (top view). The blue arrow indicates the flow direction. The black arrow indicates the direction of potential embryo body rotation when there is no suction force. The green arrow indicates the direction of hydrodynamic suction force.

To stably transfer the device to various imaging platforms without disturbing the embryos' positions, the buffer is drained out of the two ZOCs after the trapping. Due to the presence of Laplace pressure, the holdup volume of the remaining buffer will form droplets inside the traps (Figure 2.15.A&B). These droplets can wrap around individual zebrafish embryos forming isolated chambers. The encapsulated zebrafish embryos are unlikely to be disturbed by actions such as device unplugging and relocation. Thereafter, the portable device can be transferred to microscope stations for imaging. To our best knowledge, this feature has not been reported by similar ZOCs.[4,11,12,27] The potential usages for this feature in zebrafish studies such as metabolism analysis, hypoxia studies, and toxicity tests may be worth investigating in the future.

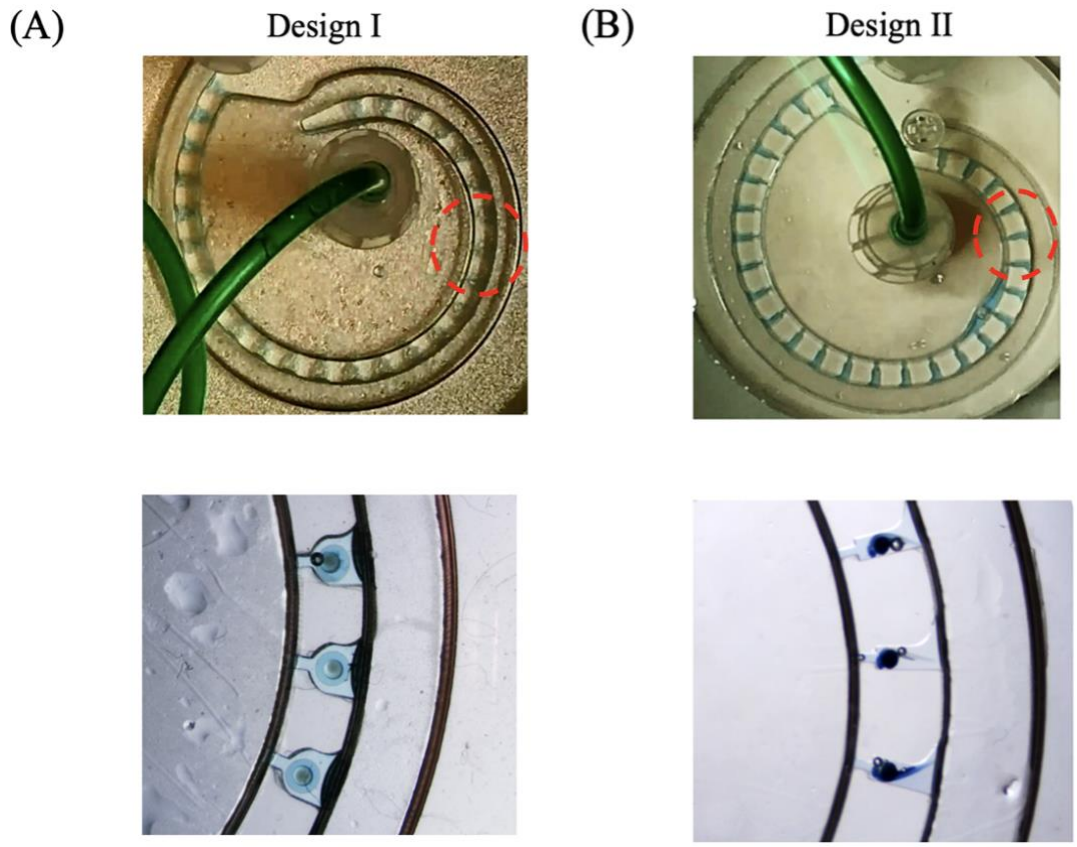

Figure 2.15. The zebrafish embryo droplet encapsulation. A) Top panel: the holdup volume of methylene blue inside the traps in design I. Bottom panel: microscopy images showing the zebrafish embryos are immobilized inside the traps and encapsulated in the droplets due to the presence of the Laplace pressure in design I. B) Top panel: the holdup volume of methylene blue inside the traps in design II. Bottom panel: microscopy images showing the zebrafish embryos immobilized inside the traps and encapsulated in the droplets due to the presence of the Laplace pressure in design II.

2.3.5 ZOC-based Zebrafish Embryo Culture and Imaging

After the trapping, the zebrafish embryos partially block the traps in the ZOC and allow the medium or drug to continuous perfusion through the traps. This allows the establishment of stable microenvironments for the zebrafish embryo which is important for assays such as drug screening and embryonic toxicity studies. The early studies have shown that the ZOC flowthrough systems are feasible for long-term zebrafish embryo culture, yet the perfusion flowrate need to be maintained at certain level to ensure a high embryo survival rate.[3,11] Therefore, for both designs, the zebrafish embryo survival rate during the ZOC-based flowthrough culture was monitored and compared with petri dish static culture. In addition, some studies also suggest that the shear stress exerted by the continuous flow can delay the zebrafish embryo hatching.[4,26] For this, the hatching rates are investigated specifically in design I. Moreover, the zebrafish embryo culture time is primary determined by the geometry and size of the traps as the embryo may escape due to the hatching and

the immobilized embryo will eventually outgrow the size of the trap.[26] Hence, the embryo holding capability for the two ZOC designs are also evaluated during the zebrafish embryos culture experiments. Briefly for experimental setups, the 4 hpf unhatched and 24 hpf dechorionated zebrafish embryos were loaded and immobilized in design I and design II, respectively. After embryo immobilization, the ZOCs were close loop perfused with E3 buffer at 10 ml/min. For the control experiment, a 60 mm Petri dish filled with 20 ml E3 buffer was used for the static zebrafish embryo culture (26 embryos per Petri dish). The temperature for both ZOC-based and static petri dish-based zebrafish embryo culture were kept around 28.5 ℃ and the endpoints were measured every 24 hours.

The zebrafish embryo culture in design I carried on for 120 hours. The results showed that the zebrafish embryo survival rate in design I was comparable to the static petri dish culture (Figure 2.16.A&C). The initial survival rate drops between 4 hpf and 24 hpf were contributed by the unfertilized eggs. Slight decreases in embryo survival rate in the petri dish culture were observed after 24 hpf, while the embryo vitality in design I maintained at a constant level throughout the experiment. Despite no noticeable embryonic development delay was observed in the zebrafish embryos cultured in design I, the hatching was found significantly postponed as less than 10% zebrafish embryos have successfully hatched after 120-hour culture in design I (Figure 2.16. B&D).

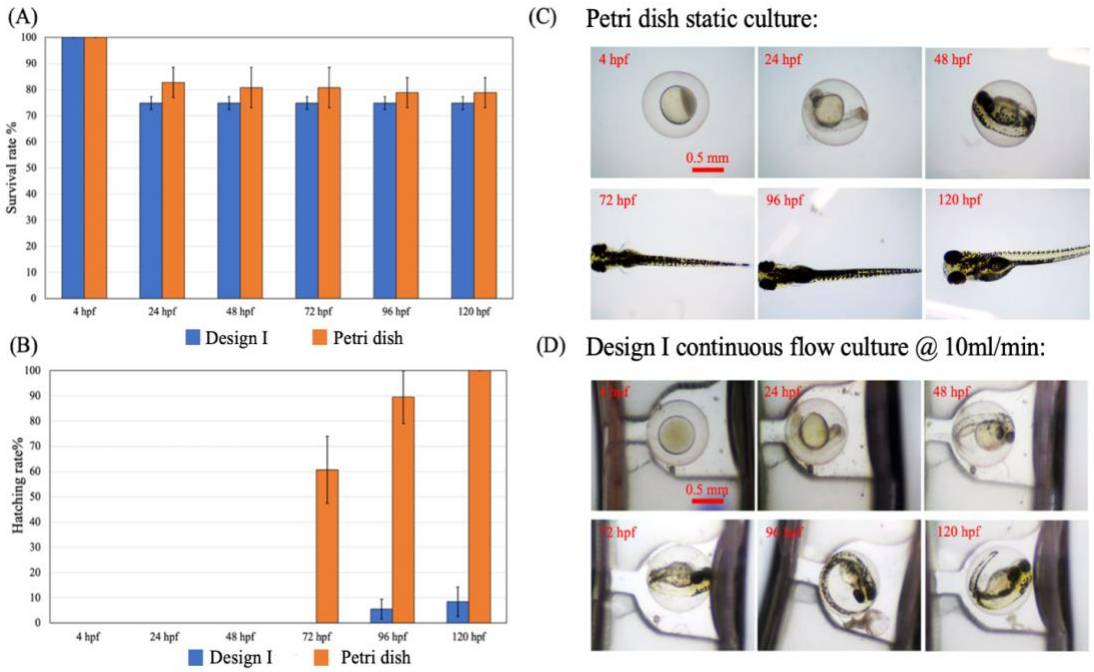

Figure 2.16. The flowthrough zebrafish embryo culture in design I. A) The zebrafish embryos vitality comparison between static petri dish culture and 10 ml/min continuous flow culture in design I (N=2, error bar:±SD). B) The zebrafish embryo hatching delay in design I at perfusion flowrate of 10 ml/min (N=2, error bar:±SD). C) The zebrafish embryonic developments during the 120 hours of culture in the petri dish. D) The zebrafish embryonic developments and hatching delay during the 120 hours of culture in the design I.

Interestingly, the zebrafish embryos immediately begin hatching after disengaging the perfusion at 72 hpf. (Figure 2.17.A). Also, for the hatched zebrafish embryo, the traps can no longer constrain their movements as well as prevent them from escaping during the perfusion (Figure 2.17.B). These findings are consistent with the similar study reported by Akagi et al.[4]

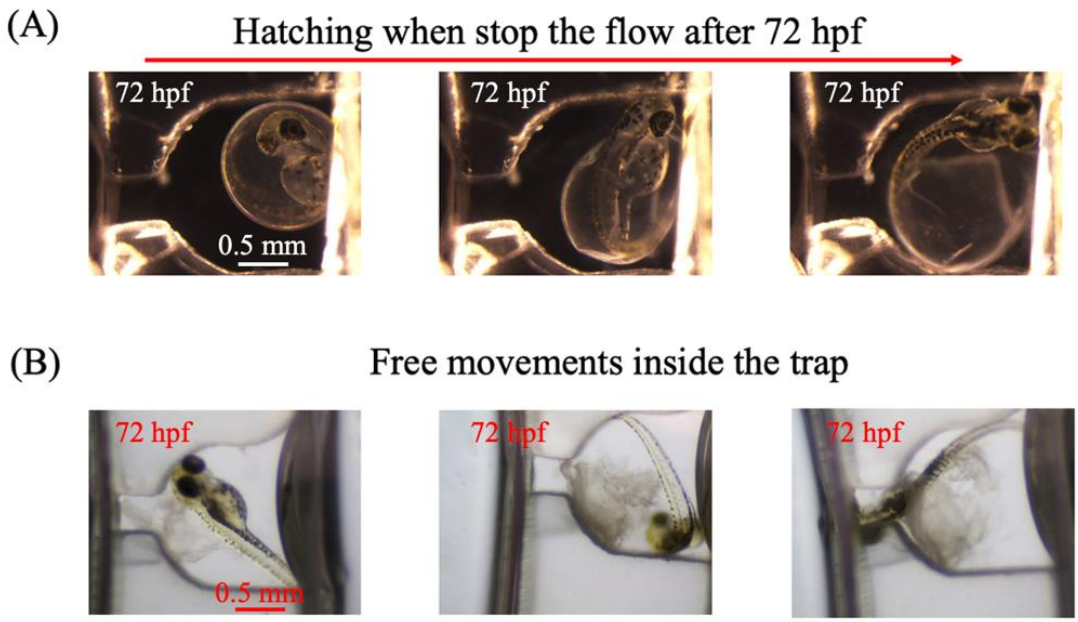

Figure 2.17. The zebrafish embryo hatching in design I after disengaging the flow. A) Microscopy images showing the zebrafish embryo hatching after disengaging the flow. B) Microscopy images showing the trap in design I can no longer restrict the zebrafish embryo body movements after hatching.

Despite the embryo survival rate in design I is comparable to the petri dish static control and no morphology abnormality were found in the embryos cultivated in the flowthrough environment, the shear stress exerted by the fluid flow is believed to be an environmental stress that affects the zebrafish hatching. The similar study reported by Akagi et al showed that the zebrafish embryo hatching rate is shear stress dependent.[4] However, the threshold for the body shear stress that triggers the delay of zebrafish hatching is still unclear.[4] Based on the CFD simulation, the shear stress applied on the zebrafish embryo drops in the parallel arranged traps along the main channel. When perfused at 10 ml/min, a maximum shear stress of 0.0659 Pa is found at the top surface of the embryo located in the first trap (Figure 2.18). This maximum shear stress is close to the 0.0613 Pa reported by Akagi et al. that can cause the hatching delay.[4] Because of the above reasons, we recommend applying lower flowrates during embryo culture and only use the design I for zebrafish embryo studies before 72 hpf in which most embryos are still in chorion.

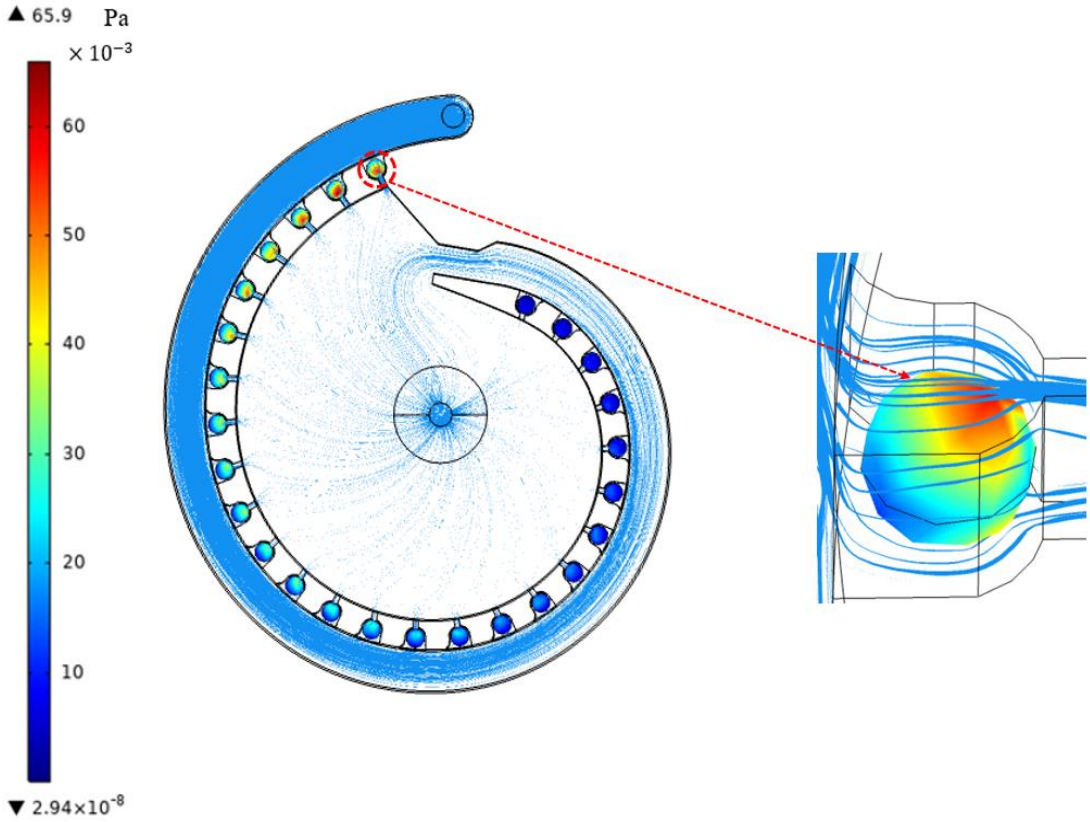

Figure 2.18. The zebrafish embryo body shear stress heatmap in design I at 10 ml/min perfusion flowrate. The zebrafish embryo in trap 1 is selected to show the maximum shear stress level as well as the distribution.

For the zebrafish embryo culture study in design II, the dechorionated 24 hpf zebrafish embryos were used. Like the experiments conducted for design I, the zebrafish embryo survival rate in design II was also found close to the petri dish static embryo culture (Figure 2.19.A). However, with the current trap dimension, the zebrafish embryos were found to already outgrow the trap at around 48 hpf, despite still being immobilized by the hydrodynamic suction force (Figure 2.19.B&C). Furthermore, the size increase of embryo may raise bias for some long-term live zebrafish assays as the trap hydraulic resistance would raise and the fluid field in the design II would vary overtime. Because of these, in the present work, the ZOC-based zebrafish embryo culture in design II only carried on for about 48 hours to minimize the impacts from the size increase of zebrafish embryos.

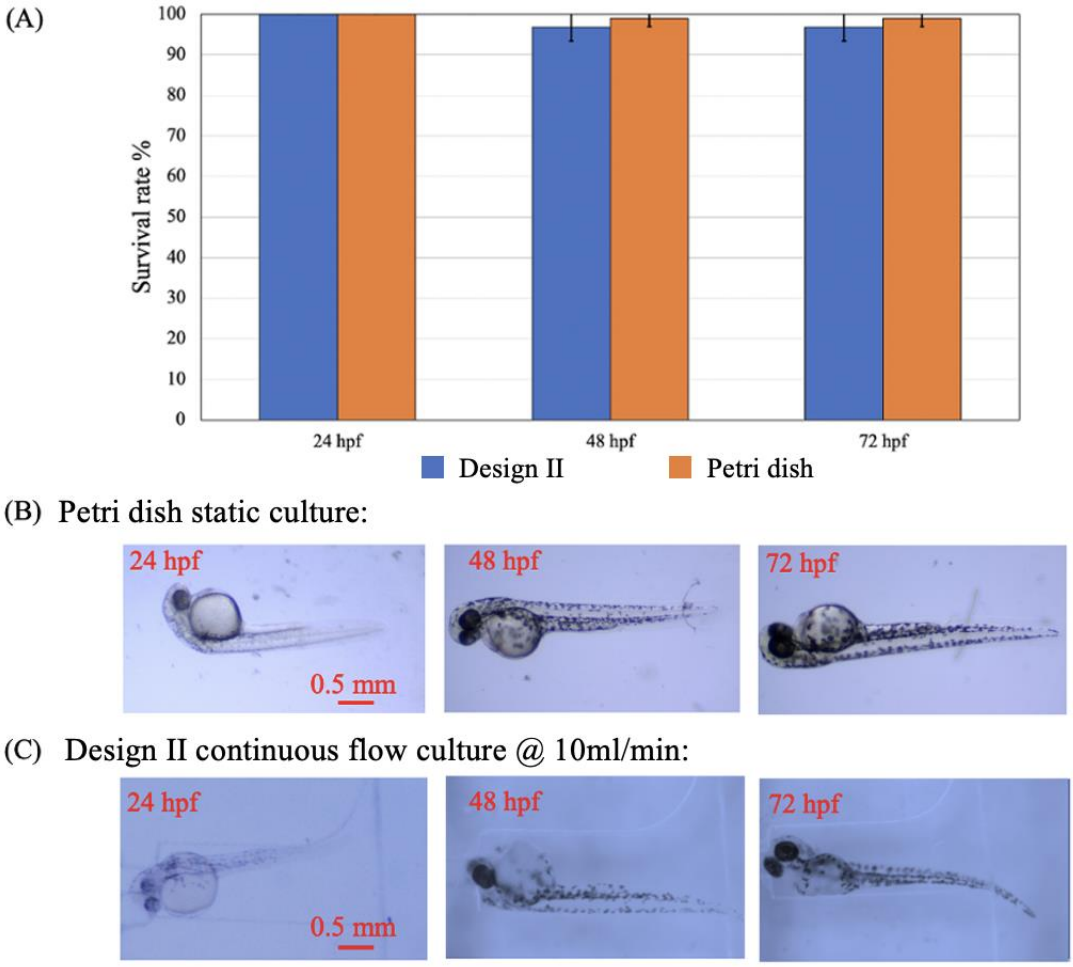

Figure 2.19. The flowthrough zebrafish embryo culture in design II. A) The zebrafish embryos vitality comparison between static petri dish culture and 10 ml/min continuous flow culture in design II (N≥4, error bar:±SD). B) The dechorionated zebrafish embryo development during the 48 hours culture in petri dish. C) The dechorionated zebrafish embryo development during the 48 hours culture in design II.

The continuous flow was also found to stimulate abnormal behaviors in the zebrafish embryos after 48 hpf as some of the zebrafish embryos folded their bodies during the perfusion (Figure 2.20.A). This posture change is likely caused by the crossflow in the trap and main channels as most embryos with folded bodies were observed after 48 hpf where their tails are exposed to the main channel flow. In terms of the shear stress inside the traps, because of a smaller channel dimension, the dechorionated zebrafish embryo in design II experience a higher shear stress than the unhatched embryo in design I when using the same perfusion flowrate (i.e., 10 ml/min). The result of CFD simulation showed that the shear stress hot spot is located only at the upper surface of the zebrafish embryo body. During 10 ml/min close loop perfusion, the zebrafish embryo in the first trap experiences a maximum shear stress of approximately 0.34 Pa which is about 5 times the maximum shear stress applied on the unhatched zebrafish embryo in design I (Figure 2.20.B). A similar study performed by Fuad et al. used a flowrate that can reach a maximum shear

stress of 0.088 Pa.[12] No shear stress induced teratogenic abnormalities or stressed postures were reported by Fuad et al. and the zebrafish embryo can reach all embryonic stages without any significant delays.[12] For this, the zebrafish embryo's body folding may also be contribute by the high perfusion flowrate used in this study (i.e., the maximum shear stress is about 3 times higher than 0.088 Pa). Although no noticeable morphology abnormalities and development postponement were found in the zebrafish embryos cultivated under the high shear stress environment, further investigation is needed to fully understand the embryonic development impacts from the fluidic shear stress. For now, applying low shear stress environments in ZOC-based zebrafish embryo culture will be a safe option to minimize the embryo behavior impacts. All in all, for current trap dimension of design II, we believe design II is only suitable for the acute zebrafish embryo assays (i.e., from 24 hpf to 48 hpf) where the embryo body is still contained in the trap. Also, when selecting the perfusion flowrate for live zebrafish embryo assays, the impacts from the shear stress need to be considered.

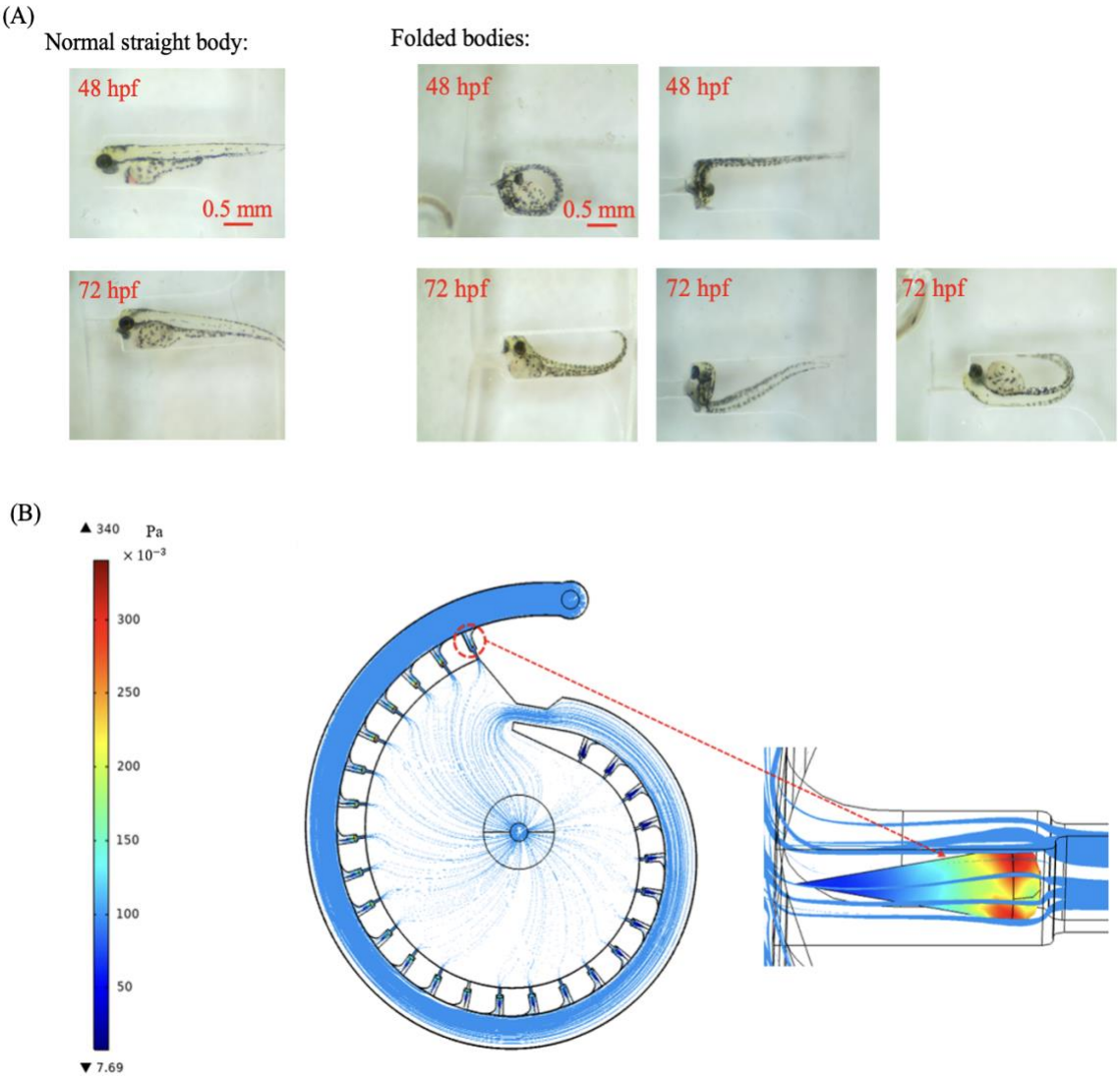

Figure 2.20. The zebrafish embryo abnormal postures under high shear stress flowthrough environment. A) The microscopy images showing some zebrafish embryos folded their bodies in design II during continuous perfusion at 10 ml/min. B) The zebrafish embryo body shear stress heatmap in design II at 10 ml/min perfusion flowrate. The zebrafish embryo in trap 1 is selected to show the maximum shear stress level as well as the shear stress distribution.

In terms of imaging quality, the embryo images taken in the ZOC device have similar clearness and resolution compared to the embryo images taken in the petri dish when using stereomicroscope with a CMOS USB camera under normal light. The CCD camera was also used to take fluorescent images for the 48 hpf transgenic zebrafish embryos *Tg (kdrl:EGFP)* . The vascular endothelial cells in the 48 hpf *Tg (kdrl:EGFP)* zebrafish express green fluorescent protein and can be detected under fluorescent microscopy. In design II, the 48 hpf *Tg (kdrl:EGFP)* zebrafish embryos were encapsulated in E3 buffer after trapping and then moved to the fluorescent microscope for image taking. For comparison, the 0.5% agarose gel was used to immobilize the zebrafish embryos on the plate. The resolution and contrast of the CCD images for the ZOC immobilized embryos is comparable to the images of agarose immobilized embryos as the intersegmental vessels (ISV) in the zebrafish embryo can be clearly visualized in both methods (Figure 2.21).

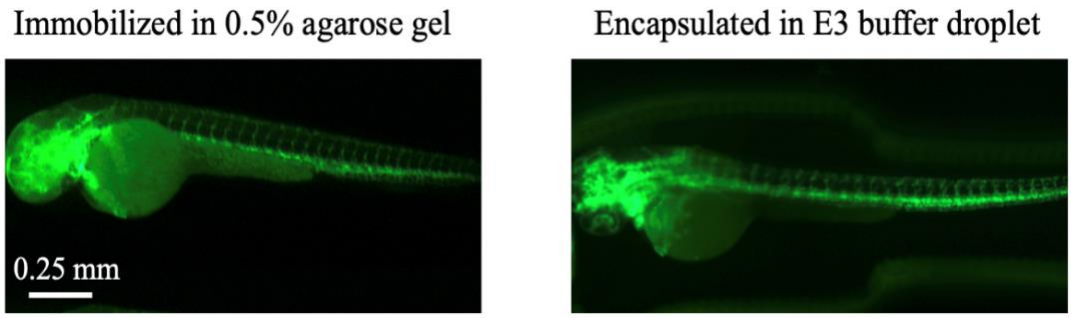

Figure 2.21. The fluorescent images for the 48 hpf *Tg (kdrl:EGFP)* zebrafish embryos. Left: Image taken from the zebrafish embryo immobilized in 0.5% agarose gel. Right: Image taken from the zebrafish embryo encapsulated by E3 buffer droplet in design II. 10× Magnification.

Collectively, both ZOC designs showed feasibility for conducting zebrafish embryo studies and have demonstrated convenience in acquiring phenotype-based data. For live zebrafish embryo studies specifically, the timeframe of performing the tests on the ZOC device depends mainly on the geometry and the dimension of the trap. Also, the embryonic development impact from shear stress needs to be considered when choosing the flowrate for zebrafish embryo culture. For now, it is unclear what is ideal shear stress level for the zebrafish embryo development in the ZOC device. However, based on our results as well as the previous studies, applying a low shear stress in the flowthrough environment is currently the best option for zebrafish embryo culture and other live zebrafish assays.

2.4 Conclusion and Discussion

In this preliminary study, we demonstrated the development process of two ZOC devices for automated zebrafish embryo trapping and flowthrough embryo culture. The ZOCs are rapidly prototyped by a consumer-grade SLA 3D printer assisted method which can meet the resolution requirements in making the milli fluidic ZOCs and is suitable for labs with limited budgets. The ZOC design principles for zebrafish embryo trapping (i.e., hydrodynamic trapping) have been proved to be valid and both ZOCs can achieve over 85% of trap usage rate (i.e., trap occupation rate). For design II, the trapped zebrafish embryos

showed a consistent body orientation pattern which is valuable for high-throughput imaging and phenotype-based screening. Besides, the results of the embryo culture tests indicated that the zebrafish embryos cultivated in ZOCs have a closed vitality to the zebrafish embryos cultivated in the static petri dish. Furthermore, the perfusion flowrate used in the ZOC needs to be carefully selected as the shear stress was found to cause zebrafish embryo hatching delay as well as induce abnormal postures in the chorion-less zebrafish embryos. The specifications of the two ZOCs as well as their recommendations of use are summarized in table 2.1.

Table 2.1 The specifications and recommendations for the two ZOCs.

	Design I	Design II
Total trap number	26	26
Trap usage rate	86.54 ± 6.57%	93.03 ± 4.3%
Orientation control	N.A.	92.88 ± 4.44% head inward
Culture flowrate	<10 ml/min	≤ 2 ml/min
Screening	Parallel comparison	Parallel comparison
Resolution	Single embryo	Single embryo
Zebrafish embryo	Unhatched embryo (0 hpf to 72 hpf)	Dechorionated embryo (24 hpf to 48 hpf)

Despite the two ZOCs being demonstrated to be effective alternatives for the zebrafish embryo culture and phenotype screening, further fine-tuning is needed to maximize the trap usage as well as to extend the experimental duration of the live embryo assays in the two ZOCs. Also, future studies need to be conducted to determine the appropriate fluidic conditions for the live zebrafish embryo studies. All in all, this study offers a robust ZOC configuration for automated zebrafish embryo positioning as well as a simple and effective strategy for ZOC design and validation. This novel ZOC-based zebrafish testing platform has opened new possibilities for zebrafish studies and will be employed in other zebrafish applications in the future.

2.5 References

1. Frey, N., Sönmez, U. M., Minden, J. & LeDuc, P. Microfluidics for understanding model organisms. *Nat Commun* **13**, 3195 (2022).
2. Hwang, H. & Lu, H. Microfluidic tools for developmental studies of small model organisms -nematodes, fruit flies, and zebrafish. *Biotechnol J* **8**, 192–205 (2013).
3. Lammer, E. *et al.* Development of a flow-through system for the fish embryo toxicity test (FET) with the zebrafish (Danio rerio). *Toxicology in Vitro* **23**, 1436–1442 (2009).
4. Akagi, J. *et al.* Miniaturized Embryo Array for Automated Trapping, Immobilization and Microperfusion of Zebrafish Embryos. *PLoS One* **7**, e36630 (2012).
5. Hochstetter, A. Lab-on-a-Chip Technologies for the Single Cell Level: Separation, Analysis, and Diagnostics. *Micromachines (Basel)* **11**, 468 (2020).
6. Cooper, J. M. Challenges in lab-on-a-chip technology. *Frontiers in Lab on a Chip Technologies* **1**, (2022).
7. Levario, T. J., Zhan, M., Lim, B., Shvartsman, S. Y. & Lu, H. Microfluidic trap array for massively parallel imaging of Drosophila embryos. *Nat Protoc* **8**, 721–736 (2013).
8. Streets, A. M. & Huang, Y. Chip in a lab: Microfluidics for next generation life science research. *Biomicrofluidics* **7**, 011302 (2013).
9. Khalili, A. & Rezai, P. Microfluidic devices for embryonic and larval zebrafish studies. *Brief Funct Genomics* **18**, 419–432 (2019).
10. Yang, F., Gao, C., Wang, P., Zhang, G.-J. & Chen, Z. Fish-on-a-chip: microfluidics for zebrafish research. *Lab Chip* **16**, 1106–1125 (2016).
11. Zhu, F. *et al.* Automated Lab-on-a-Chip Technology for Fish Embryo Toxicity Tests Performed under Continuous Microperfusion (μFET). *Environ Sci Technol* **49**, 14570–14578 (2015).
12. Fuad, N. M., Kaslin, J. & Wlodkowic, D. Development of chorion-less zebrafish embryos in millifluidic living embryo arrays. *Biomicrofluidics* **11**, 051101 (2017).
13. Mohamed, M. *et al.* Rapid and Inexpensive Fabrication of Multi-Depth Microfluidic Device using High-Resolution LCD Stereolithographic 3D Printing. *Journal of Manufacturing and Materials Processing* **3**, 26 (2019).
14. Venzac, B. *et al.* PDMS Curing Inhibition on 3D-Printed Molds: Why? Also, How to Avoid It? *Anal Chem* **93**, 7180–7187 (2021).
15. Pretlow, T. G. & Pretlow, T. P. Sedimentation for the separation of cells. *Methods* **2**, 183–191 (1991).
16. Nguyen, M.-A., Srijanto, B., Collier, C. P., Retterer, S. T. & Sarles, S. A. Hydrodynamic trapping for rapid assembly and in situ electrical characterization of droplet interface bilayer arrays. *Lab Chip* **16**, 3576–3588 (2016).
17. Narayanamurthy, V., Nagarajan, S., Firus Khan, A. Y., Samsuri, F. & Sridhar, T. M. Microfluidic hydrodynamic trapping for single cell analysis: mechanisms, methods and applications. *Analytical Methods* **9**, 3751–3772 (2017).
18. Ahmad Khalili, A. *et al.* A Microfluidic Device for Hydrodynamic Trapping and Manipulation Platform of a Single Biological Cell. *Applied Sciences* **6**, 40 (2016).
19. Yuan, X., Glidle, A., Furusho, H. & Yin, H. A 3D hydrodynamic flow-focusing device for cell sorting. *Microfluid Nanofluidics* **25**, 23 (2021).
20. Goellner, B. *et al.* Design Optimization of an Electrowetting Cell Sorter Chip Platform. *Biomedical Engineering / Biomedizinische Technik* **57**, (2012).

21. Zhou, W. *et al.* Microfluidics applications for high-throughput single cell sequencing. *J Nanobiotechnology* **19**, 312 (2021).
22. Yang, F., Gao, C., Wang, P., Zhang, G.-J. & Chen, Z. Fish-on-a-chip: microfluidics for zebrafish research. *Lab Chip* **16**, 1106–1125 (2016).
23. Khoshmanesh, K. *et al.* New rationale for large metazoan embryo manipulations on chip-based devices. *Biomicrofluidics* **6**, 024102 (2012).
24. Macdonald, N. P. *et al.* Assessment of biocompatibility of 3D printed photopolymers using zebrafish embryo toxicity assays. *Lab Chip* **16**, 291–297 (2016).
25. Geisler, E., Lecompère, M. & Soppera, O. 3D printing of optical materials by processes based on photopolymerization: materials, technologies, and recent advances. *Photonics Res* **10**, 1344 (2022).
26. Wielhouwer, E. M. *et al.* Zebrafish embryo development in a microfluidic flow-through system. *Lab Chip* **11**, 1815 (2011).
27. Zhu, Z. *et al.* A Bubble-Free Microfluidic Device for Easy-to-Operate Immobilization, Culturing and Monitoring of Zebrafish Embryos. *Micromachines (Basel)* **10**, 168 (2019).

Chapter 3
Application of using Milli Fluidic System for Whole Mount Zebrafish Antibody Staining

Abstract

Whole mount zebrafish antibody staining (ABS) is a common staining technique for localizing protein information on a zebrafish embryo or larva. However, like most of the bioassays, the whole mount zebrafish ABS is still largely conducted manually through labor intensive and time-consuming steps which affect both reproducibility and throughput of the assay. In this work, we develop a milli fluidic zebrafish-on-a-chip (ZOC) platform that can automatically trap and immobilize the fixed chorion-less zebrafish embryos for the whole mount zebrafish ABS and imaging. With just a single loading step, the zebrafish embryos can be immobilized in the ZOC through a hydrodynamic trapping process. Also, a consistent body orientation (i.e., head point inward) for the trapped zebrafish embryos can be achieved without any additional orientation adjustment device. The proof-of-concept whole mount zebrafish Caspase-3 ABS showed our device can accelerate the overall procedure by reducing at least 50% of washing time in the standard well plate-based manual procedure. Moreover, the result consistency is improved, and manual steps are reduced in our ZOC-based procedure. This work fills the gap in the ZOC application for whole mount zebrafish immunohistochemistry. We hope the device can be accepted by the zebrafish community and be used for other types of whole mount zebrafish ABS procedures or expanded to more complicated *in situ* hybridization (ISH) procedure in the future.

3.1 Introduction

The whole mount zebrafish ABS and ISH using protein and antisense RNA probes are common molecular staining techniques for detecting the protein and gene localization information on zebrafish. The conventional manual procedure for the whole mount zebrafish molecular staining usually takes hours or days to complete and involves a series of tedious and time-consuming steps.[1,2] Moreover, the performance and consistency of the procedure is usually skill dependent. To overcome these limitations, automated liquid handling platforms have been developed to perform the assays. These platforms use robotic arms or hydraulic systems for automated liquid handling and are usually compatible with well plate or tubes. Although they can greatly reduce the labor and improve the consistency of the assays, the platforms are not usually affordable for the labs with limited budgets. In 2021, Fuqua et al. developed an open-source semi-automated platform, *Flyspresso*, for the whole mount fruit fly antibody staining. The *Flyspresso* utilizes a programmed gas-powered hydraulic system for liquid handling which is portable and is compatible with

various staining procedures.[3] The open-source platform provides an economic way for developing customized automated platforms for whole organism assays. However, it is not a "sample-in and answer-out" platform as the specimens still need to be retrieved and manually mounted for imaging. Moreover, the shaking or repeat pipetting-based mass transfer enhancements in tube and well plate limits the room for process optimization and time reduction.[3] To address these limitations, one way is to integrate the automated platform with lab-on-a-chip (LOC) fluidic device.

In the last decades, numerous LOC platforms have been developed and employed to perform ABS and ISH. Most of them are used for the biomarker detection at cell and tissue levels.[4–10] These devices have demonstrated that both sensitivity and specificity of the assay can be improved in the controlled microenvironments and the procedure can be sped up by enhancing the convective mass transfer.[4,8–10] Despite these, the LOC platforms for the whole organism ABS or ISH were rarely reported. In 2012, Akagi et al. developed a milli fluidic device that can automatically trap, immobilize, and provide micro perfusion in zebrafish embryo culture. Integrating with a USB microscope, the system can be used for long term real-time *in situ* monitoring during fish embryo toxicity tests (FET).[11] Notably, the whole mount zebrafish Trypan blue staining was performed using the milli fluidic device and staining process was found accelerated by micro perfusing at high flowrate.[11] Although Trypan blue is not a macromolecular probe, the proof-of-concept study provide evidences that the mass transfer can be enhanced with high perfusion flowrate even for the whole mount zebrafish.

From engineering and economic perspectives, integrating the fluidic device, especially micro- or nano- fluidic, with the automated platforms is indeed debatable. The main controversy lies in the complexity of the use, as well as the high cost associated with the device fabrication and development. Nevertheless, these concerns may not apply to milli fluidic devices. Compared with the conventional microfluidic device, the milli fluidic device used for some whole organism studies usually has more resolution tolerance.[12,13] Also, because the subject (i.e., whole organism) is at macroscopic level, applications such as trapping,[11] sorting,[14] drug dosage generation,[15,16] etc. can be realized by applying relatively simple channel geometry and the results are unlikely to be susceptible to defects.[17] Furthermore, with the assistance of micro-milling machines[11] or 3D printers,[12,18,19] new milli fluidic devices can be rapidly made and tested. Also, manufacturing processes such as injection molding and hot embossing can be easily adapted for mass production of milli fluidic devices at relatively low cost. Collectively, in contrast to the micro- or nano- fluidic device, the milli fluidic device has more potential to be incorporated with the automated liquid handling platforms and more likely to achieve the automation procedure level of "sample-in and answer-out".

In this study, the milli fluidic ZOC device used for zebrafish embryo trapping and the whole mount zebrafish embryo ABS is modified from the ZOC design II (i.e., ZOC for trapping dechorionated zebrafish embryo) reported in chapter 2. The feasibility of using the ZOC for the whole mount zebrafish embryo ABS is examined and the performance is compared with the well plate-based procedure.

3.2 Materials and Methods

3.2.1 Computational Mass Transfer and Fluid Dynamic Simulations

COMSOL 5.5 (COMSOL 5.5 Inc. Stockholm, Sweden) was used for the fluid dynamic and mass transfer simulations to evaluate the flowthrough conditions and mass transfer processes in ZOC. Specifically, the "free and porous media flow" was used to simulate the steady state fluidic fields. The steady state fluidic field for the final state of trapping is then coupled with "the transport of diluted species in porous media" to simulate the buffer replacement during the flushing process in a time-dependent study. The inlet flowrate was set to be 10 ml/min for both trapping and flushing simulations. Water was used as the carrying fluid in the simulations and the diffusion coefficient for the IgG antibody was defined as 1×10^{-7} cm^2/s.[10] To determine the maximum shear stress applied on the zebrafish embryos during the perfusion, the inlet flowrate was set to 20 ml/min as it is the maximum flowrate for the current system. The dechorionated zebrafish was molded as a cone-shape rigid body with 2 mm overall body length and 0.5 mm maximum head diameter. The Reynolds number (Re) is calculated as

$$Re = \frac{\rho u L}{\mu} \qquad \text{(Eqn. 3.1)}$$

Where, ρ is the density of the fluid, u is the local flow velocity, L is the characteristic length of the channel, and μ is the dynamic viscosity of the fluid.

The highest Re number is found to be 306 when applying the highest perfusion speed (20 ml/min) in the ZOC (Figure 3.1). This indicates the flow characteristic of ZOC is within the laminar regime ($Re < 2100$).

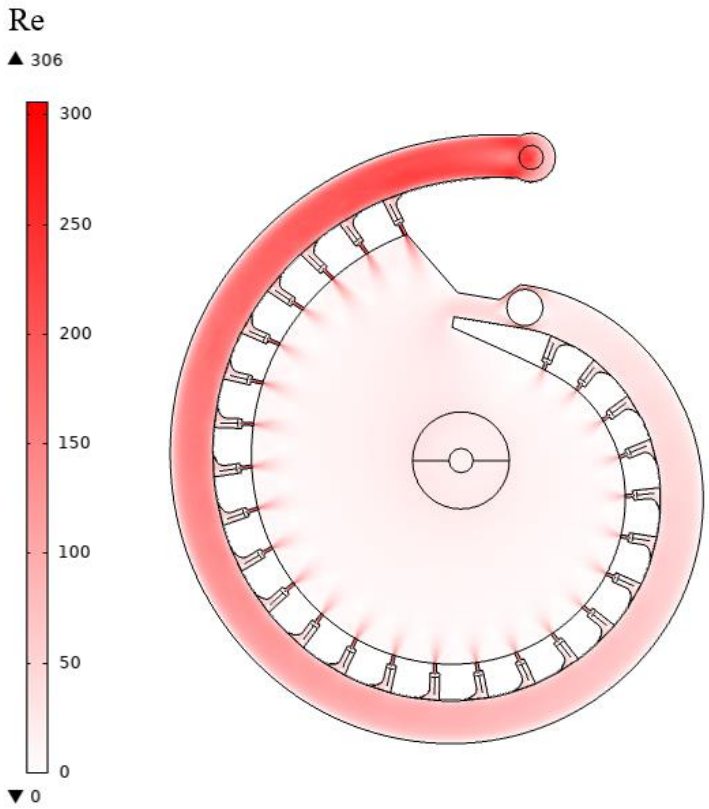

Figure 3.1. The Re number heatmap for the ZOC when perfusing at 20 ml/min with the flow restrictor add-on.

3.2.2 Zebrafish Embryo UV Treatment and Fixation

Before the UV treatment and fixation, 24 hpf embryos were manually dechorionated and then transferred into a petri dish (~ 100 embryos per dish) filled with 15 ml E3 buffer. To activate the Caspase-3 cleavage, the embryos were then exposed under the UV lights (~ 0.44 W/cm^2) in the biosafety cabinet (NuAire Inc. Plymouth, USA) for 2 hours following 8 hours recovery in an incubator at 28.5 °C. The treated embryos were fixed in 4% formaldehydes/PBST for overnight at 4 ^{o}C and then stored in 100% methanol at – 20 ^{o}C for later staining (Figure 3.2).

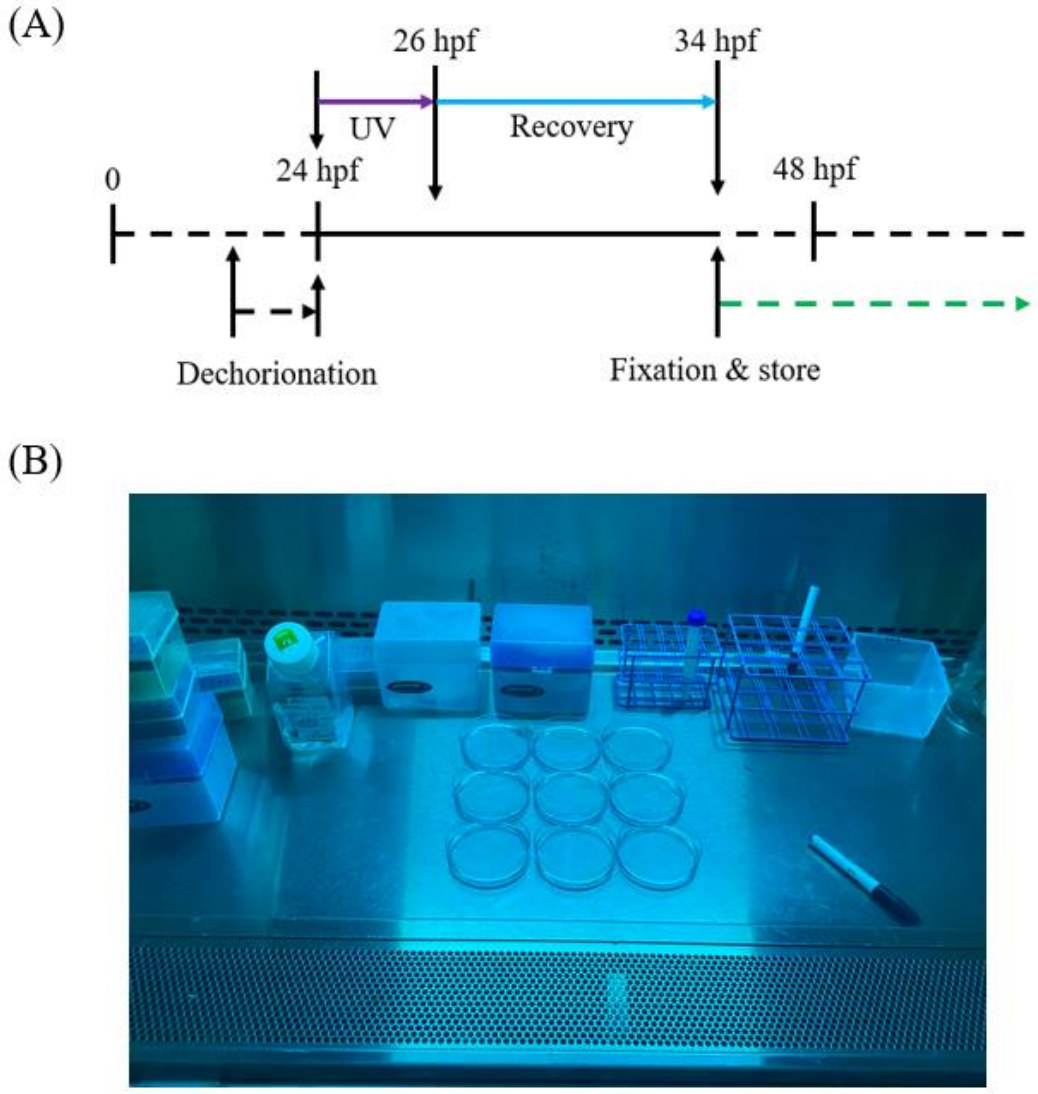

Figure 3.2. Zebrafish Embryo Caspase-3 cleavage activation and sample preparation. A) The schedule for the zebrafish embryo Caspase-3 cleavage activation treatments and sample preparation. B) The image showing the dechorionated zebrafish embryos were under UV treatment.

3.2.3 Whole Mount Zebrafish Caspase-3 Antibody Staining

The procedures for the well plate-based and ZOC device-based whole mount zebrafish Caspase-3 ABS are listed in Table 3.1. The sample preprocessing for both plate-based and device-based procedures are performed in the 24-well plate. A belly-dancer (IBI Scientific Inc., Iowa, USA) was used to provide medium level shaking for the plate-based and off-chip steps. For the plate-based whole mount zebrafish Caspase-3 ABS, 10 to 15 embryos were loaded per well in a 24-well plate. For the device-based whole mount zebrafish Caspase-3 ABS, the number of embryos tested on the device was dependent on the trapping

result. The flowrate and time for each staining step in ZOC was kept constant at 10 ml/min and 2 hours, respectively. The dilution ratios for the primary antibody and secondary antibody were kept at 1:1000 (Cell signaling technology #9661, -Caspase-3, Rabbit) and 1:200 (Invitrogen #31686, -Rabbit Rhodamine, 0.5 mg/ml in stock), respectively.

3.2.4 Imaging and Signal Quantification

The fluorescence images were acquired under the confocal microscope (Leica Biosystem Inc.) with 100 × magnification, 15% laser power, and 800 volts digital gain. The laser beam scanned the zebrafish embryo along the Z direction every 5 μm to get the sliced images. The sliced images were then stacked to form a Z projected image using the maximum intensity. ImageJ was used to analyze the signal levels on the Z-projected images by applying masks with threshold level of 100 on the 8-bit gray scale images.

3.3 Results

3.3.1 Fixed Zebrafish Embryo Trapping and ZOC Flow Settings

The ZOC device used in this chapter is the same as the ZOC design II in chapter 2 (Figure 2.4.B). In short, the ZOC device contains 3 major functional parts: a spiral main channel, an inner suction chamber, and 26 trapping channels that interconnect the main channel and inner reservoir. Hydrodynamic suction was used as the main trapping and immobilization force in this design. When operating, the inner chamber, which connects the peristaltic pump at the outlet, provides a negative pressure to draw the fluids from the main channel via the traps. The pumping system is also the same as in chapter 2. As detailed in section 2.2.4, depending on the procedure, the close and open loop perfusion modes can be switched via a 3-way valve. In addition, the ZOC was fabricated by the consumer-grade 3D printer assisted rapid prototyping method which is more economic than the previously reported methods (section 2.2.2).[19,20] The embryo trapping validation experiment showed that ZOC can reach an overall trap occupation rate of 93.6 $\pm$ 4.0% (N = 24) when trapping dechorionated fixed zebrafish embryos. The trap occupation frequency distribution in the ZOC was similar to design II in which trap 1 is usually skipped during the embryo trapping (Figure 3.3.A). Moreover, similar body orientation pattern was also observed in the trapped embryos as 93.7$\pm$ 4.3% have their heads point inward after trapping (Figure 3.3.B). It is important to be noted that PBST, rather than water, was utilized as the carrying buffer in the fixed embryo trapping, as the embryo become hydrophobic after fixation.

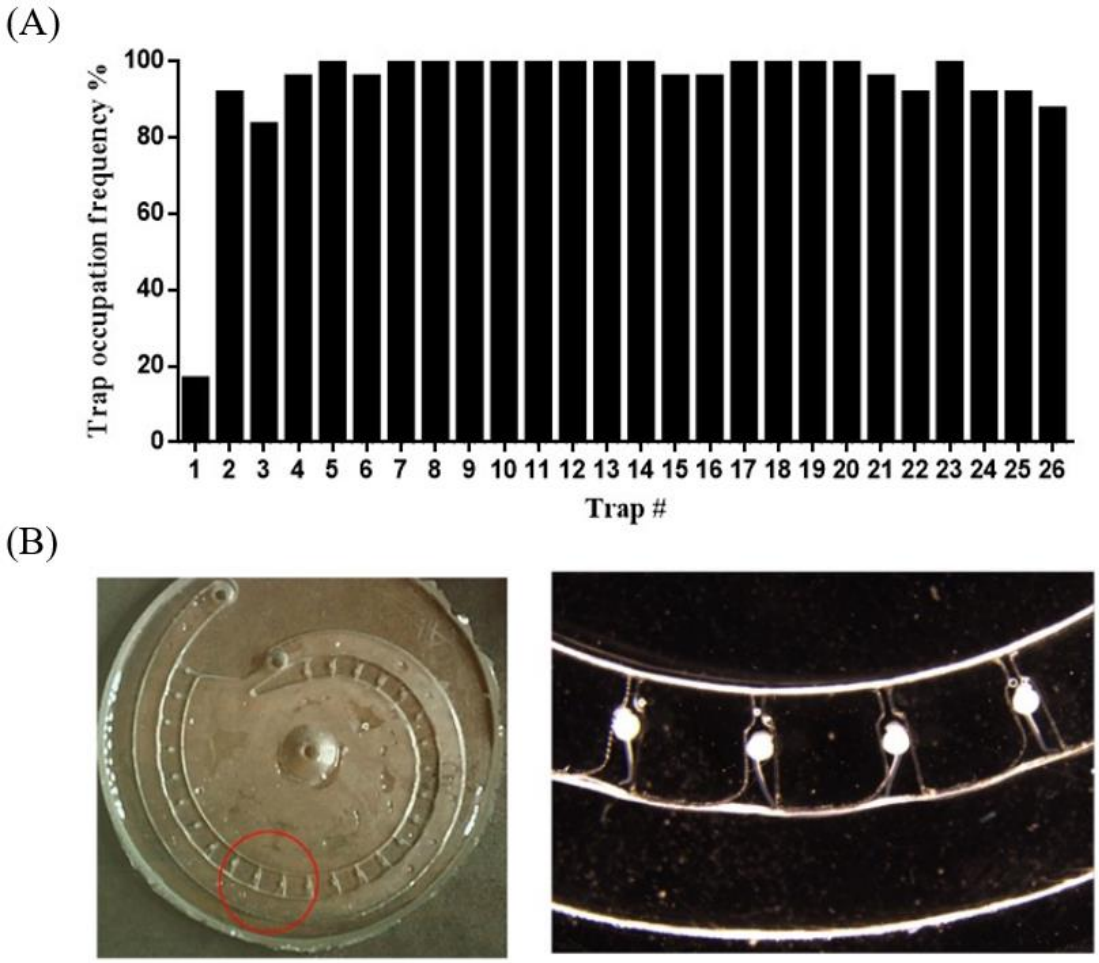

Figure 3.3. Fixed chorion less zebrafish embryos trapping validation. A) The trap occupation rate for each individual trap in the ZOC (N= 24). B) Microscopy images showing the zebrafish embryos are immobilized inside the traps and encapsulated by the PBST droplets due to the presence of the Laplace pressure.

The ZOC employed here utilizes a simple spiral parallel trapping configuration. However, the limitation for this configuration is also obvious as the flowrate in the individual traps drops along the spiral main channel.[21] This is not ideal for the ZOC-based ABS because the convective mass transfer rate is now different at each trap and the last trap always takes the longest time to complete the mass transfer. To minimize this procedure lagging, a M3 screw is used as a flow restrictor (FR) to partially block the narrowed main channel section during the ZOC-based ABS. Based on the CFD simulation, the add-on of the FR can boost the flowrate in the traps as well as close the flowrate differences among the traps (Figure 3.4).

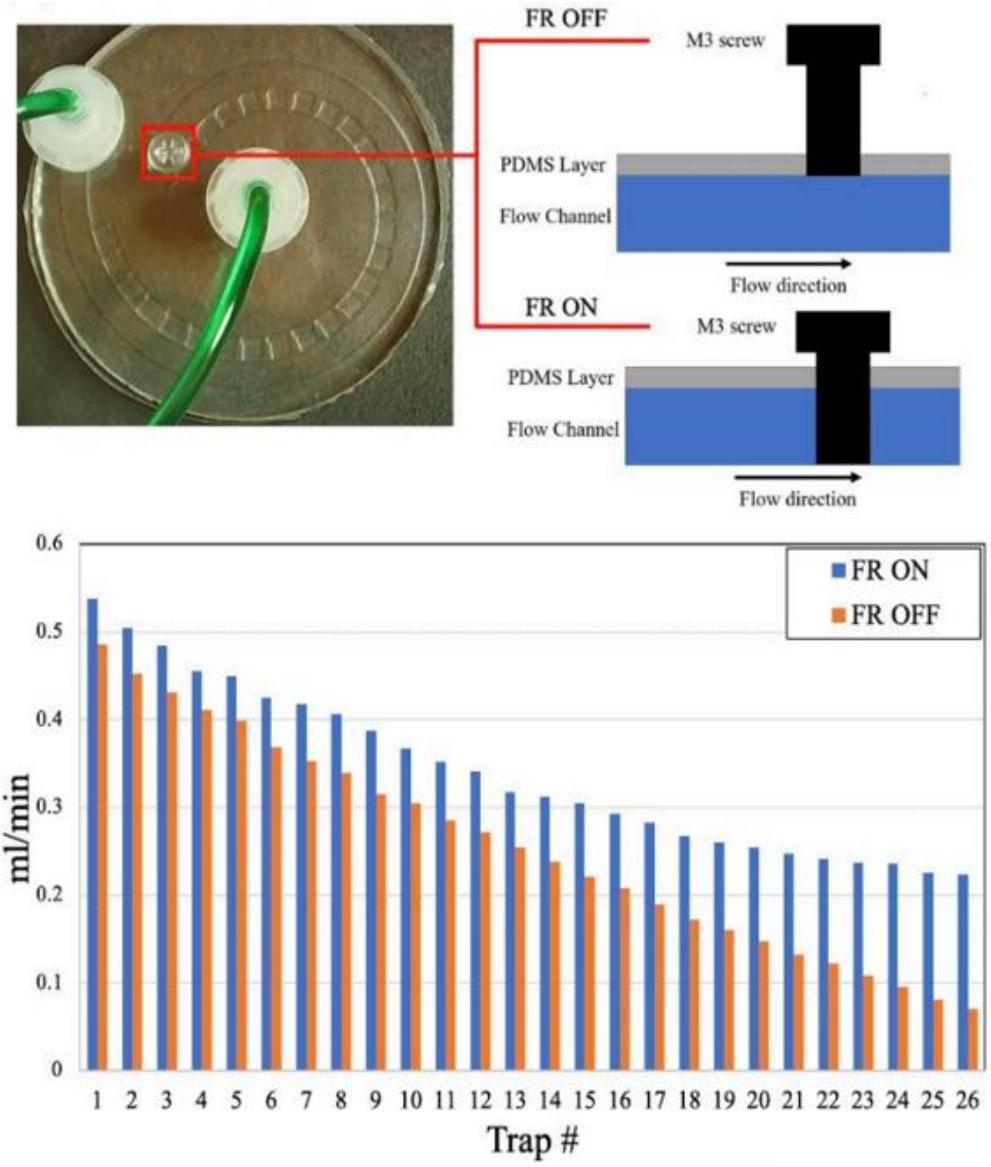

Figure 3.4. CFD simulation for different flow settings. Top: The flow restrictor (FR) ON and OFF modes for the ZOC. Bottom: The flower rates at each individual trap at FR ON (blue) and FR OFF (orange) modes.

The validation experiments using the methylene blue/PBST also confirmed that the FR ON mode enhances the perfusion in the traps (Figures 3.5. A&B) as it took less time for the dye to fill the traps. Here, the flowrate for both the CFD simulations and validation experiments was set to 10 ml/min.

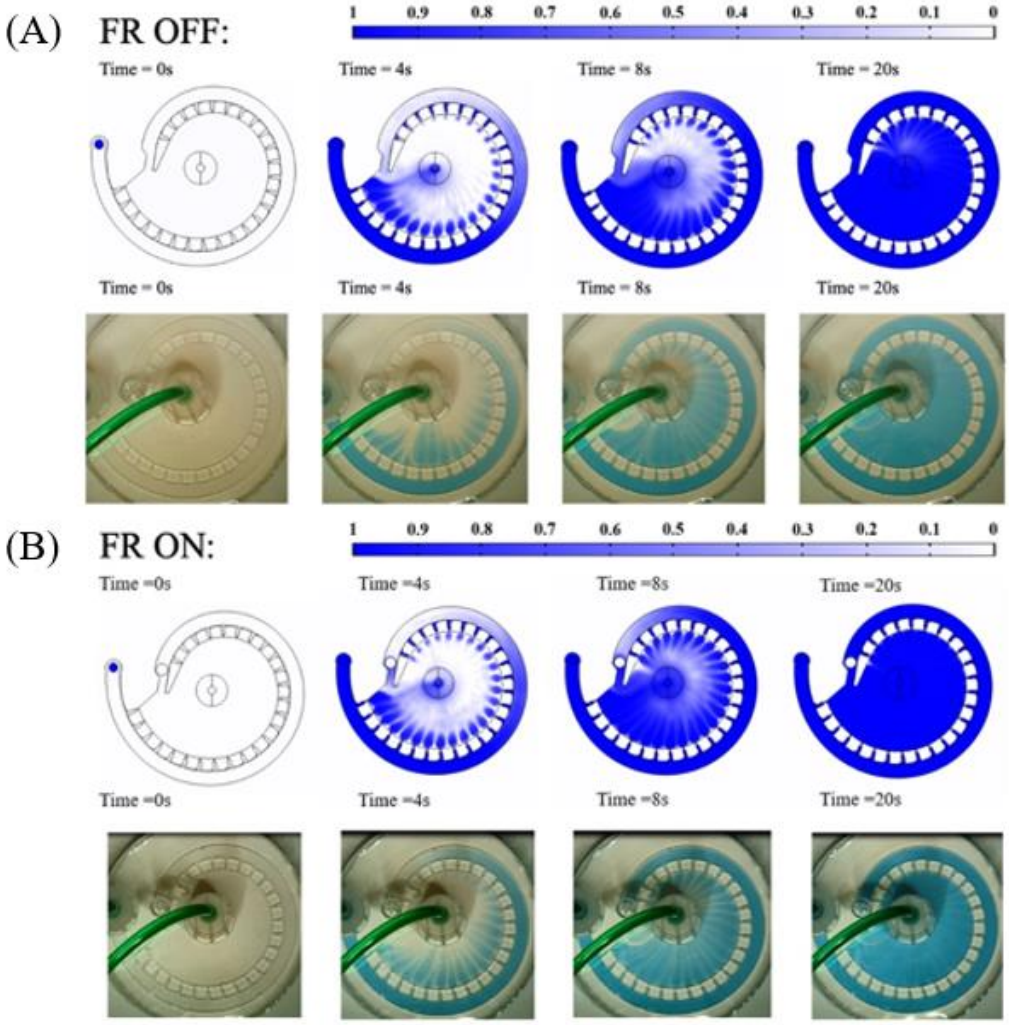

Figure 3.5. Validation experiments for different flow settings. A) The perfusion simulation (top) and validation (bottom) for FR OFF mode at 10 ml/min inlet flowrate. B) The perfusion simulation (top) and validation (bottom) for the FR ON mode at 10 ml/min inlet flowrate.

During the buffer switching, the old buffer will first be flushing out in the system. To ensure the overall system is replaced by the new buffer and all the holdup volume inside traps is cleaned up, the system is then flushed with the new buffer in the open loop before switching to the close loop circulation. In the simulation, the staining buffer (i.e., the PBDT with antibody) was set to be replaced by the PBDT washing buffer at 10 ml/min. The simulation showed that it takes about 7 seconds (i.e., 4 seconds for the new buffer to reach the last trap and 3 seconds for the buffer replacement) to flush out the staining buffer in the last

trap (Figure 3.6). However, the ZOC channels are not completely cleaned as the old buffer remains accumulated at the center chamber. Also, 7 seconds is not enough for the new buffer to fill the entire system (i.e., the device plus tubing) at 10 ml/min as the minimum system volume is about 6 ml. To completely flush out of the old buffer from the system, the flushing process need to carry on for at least another 23 seconds to an overall 30 second flushing time. Both simulation and validation experiments using methylene blue/PBST have shown that the system can be completely replaced by the new buffer after flushing for 30 seconds at 10 ml/min. Note, during the buffer switching, the FR is turned OFF (i.e., M3 is lifted) to prevent the potential bubble blocking.

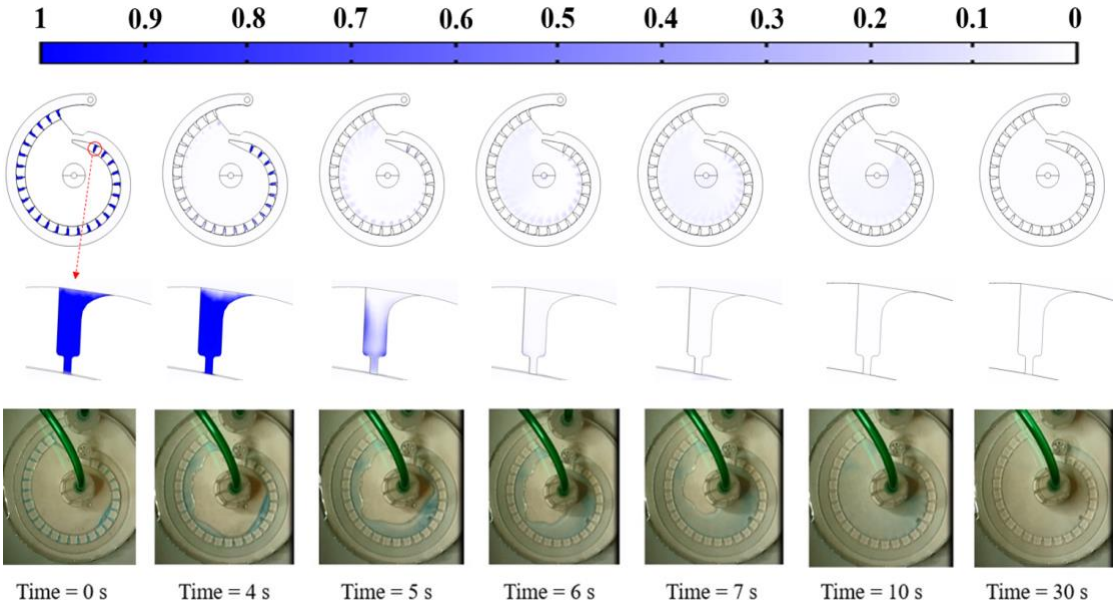

Figure 3.6. The buffer flushing simulation and validation for the ZOC. Top panel: the overall mass transfer simulation for the flushing process. Middle panel: mass transfer simulation for the last trap (i.e., 26th trap) during open loop flushing. Bottom panel: the flushing validation experiment using methylene blue/PBST. The flushing flowrate for both simulation and experiment are 10 ml/min.

One of the concerns for the ZOC-based ABS is the shear stress during the perfusion may cause damage to the fixed embryo. The CFD simulation showed that when the perfusion flow is at 20 ml/min and the FR is turned ON, the maximum shear stress applied on the embryo is about 0.672 Pa and the shear stress hot spot is located at the upper surface of the embryo body (Figure 3.7). Despite the shear stress level being about double the shear stress level used in the live embryo experiments (Figure 2.20.B), we believe it is unlikely to damage the fixed zebrafish embryos as tissue becomes more rigid and less fragile after formaldehyde fixation. Indeed, most observed embryo damages were during the off-chip pipetting and embryo transferring.

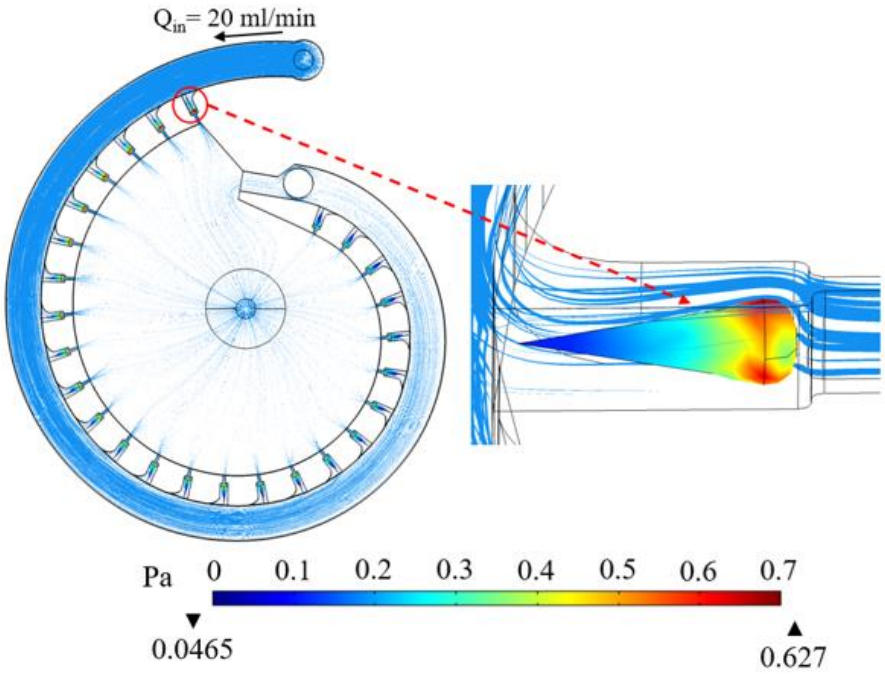

Figure 3.7. The body shear stress heatmap for fixed zebrafish embryo in the ZOC at 20 ml/min with FR ON. The embryo in the first trap is selected to show the maximum shear stress level as well as the shear stress distribution.

3.3.2 Multi Depth Channel for Bubble Prevention

The air bubble introduction is the major cause of biases for the ZOC-based zebrafish assays. Bubbles can obstruct the trap during the perfusion, interfere with the embryo imaging, and induce backflow, all of which can adversely affect the accuracy and reliability of the assay results. As most PDMS-glass ZOC devices are integrated with open pumping systems, the air may enter the device through both inlet and the gas permeable PDMS layer leading to the formation of liquid-gas flow in the channels. Likewise, in our current system setup, the flow is driven by a peristaltic pump. To reduce the pulsing caused by the peristaltic pump, the buffer loading tube must open to the air. Therefore, air can potentially be introduced into the ZOC channel during the operation. By far, the only attempt to prevent the air bubbles in the ZOC device is made by Zhu et al. The group reported a bubble free ZOC device by bonding a PDMS vacuum layer on top of the PDMS embryo culture channel layer.[18] In their study, the negative pressure in the vacuum chamber can effectively remove the bubbles from the embryo culture channel.[18] However, the multilayer PDMS device will complicate the fabrication steps and the additional PDMS layer may affect the signal detection during the imaging. Moreover, the application of external negative pressure may affect the zebrafish embryo culture environment such as oxygen level. Here, we demonstrated a simple channel geometry-based bubble prevention method for the single layer ZOC.

In our current system setting, buffer switching, and high flowrate perfusion are the two situations where most bubble introduction events occur. Nevertheless, the types of bubbles

that are introduced in these two situations are different, as are the underlying bubble formation mechanisms. During the buffer switching step, the channel was first emptied and the new buffer together with air was then perfused into the channel. The bubbles introduced during the buffer switching step are usually large or medium sized bubbles (Figure 3.8.A). These bubbles which usually have larger size than the trap is unlikely to enter the trap during the perfusion. However, the presence of large bubbles may cause pressure fluctuations, induce backflow, and as a result disturb the trapped embryos.[25] Our ZOC offers a spacious main channel for the large bubbles which can minimize the pressure fluctuations caused by their movements and thus unlikely to disturb the trapped embryo. Also, because of their large radius, the large air bubbles experience less capillary retaining force in the main channel and therefore can be easily flushed out of the ZOC. Note the narrow section at the end of the main channel may prevent the large bubbles from being removed. Increasing the flushing flowrate or slightly tilted ZOC device can help to remove the large bubbles stuck at the end of the main channel.

When operating at the highest perfusion flowrate (i.e., 20 ml/min), micro bubbles were found in the channels (Figure 3.8.B). This is because air was introduced with the buffer at high pumping speed creating dispersed bubble flow (i.e., very low gas velocity but high liquid velocity) in the ZOC.[22] Besides, the use of detergents such as Triton X-100 and Tween 20 also aggravates the formation of the micro bubbles. In our ZOC, because the main channel height is greater than the trapping channels, micro bubbles travel near the top surface of the main channel and are unlikely to enter the traps.

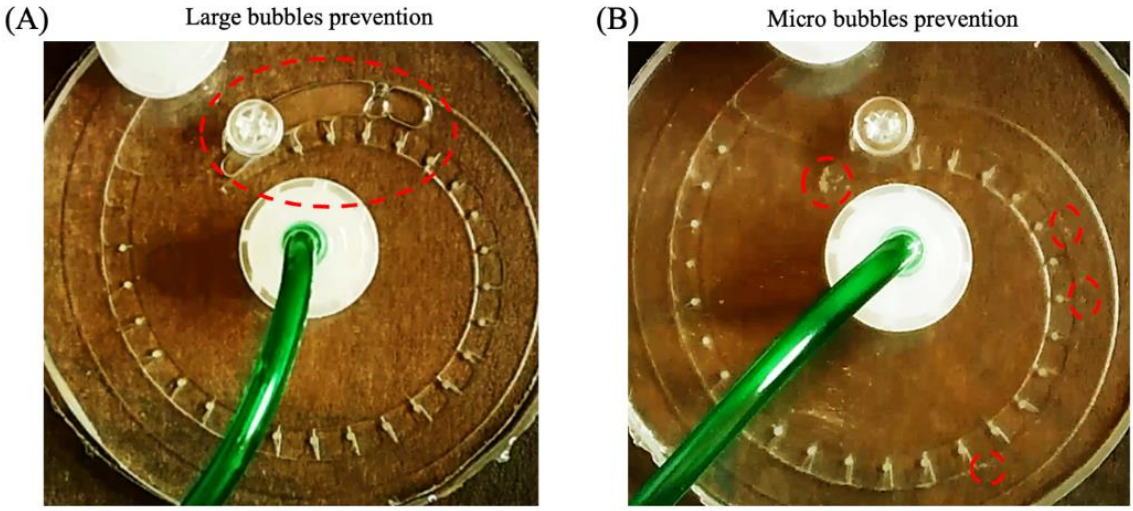

Figure 3.8. The bubble formations and prevention in the ZOC multi-depth channels. A) The large bubble formed during buffer switching can be easily flushed out by increasing the flowrate or slightly tilting the device. B) The micro bubbles formed at high perfusion flowrates are traveling near the top surface of the main channel and not entering the traps due to the channel height difference.

All in all, the multi-depth channel design in the ZOC can prevent both large and micro bubbles from entering the traps, yet further optimizations are needed to completely prevent

bubbles from entering the traps.

3.3.3 ZOC-based Whole Mount Zebrafish Caspase-3 Antibody Staining

The whole mount zebrafish Caspase-3 ABS is a well-established assay to detect the level of cell apoptosis in the zebrafish.[1] To induce the Caspase-3 cleavage, we applied UV light, a common environmental stress triggering apoptosis pathway, on the zebrafish embryo.[23] To investigate if the whole mount zebrafish ABS can be improved in the flowthrough environment, we next perform the whole mount zebrafish Caspase-3 ABS using the ZOC and compared the results with conventional plate-based manual procedure. The procedures for the well plate-based and ZOC-based whole mount zebrafish Caspase-3 ABS are shown in Table 3.1.

Table 3.1. Whole mount zebrafish Caspase-3 ABS procedures.

Steps		Time			
		Plate-based	ZOC-based		
Pre-processing	75% Methonal/ 25% PBST	5 mins	5 mins	OFFChip	RT
	50% Methonal/ 50% PBST	5 mins	5 mins		
	25% Methonal/ 75% PBST	5 mins	5 mins		
	100% PBST	10 mins × 2	10 mins × 2		
	Acetone permeabilization	7 mins	7 mins		-20℃
	Total pre-processing	42 mins	42 mins		
Staining & Washing	100% PBST	10 mins × 3	30 mins + trapping	ONChip	RT
	100% PBDT blocking	60 mins	60 mins		
	Primary anrtibody	120 mins	120 mins		
	100% PBDT washing	40 mins × 3	60 mins @ 20 ml/min		
	Secondary antibody	120 mins	120 mins		
	100% PBDT washing	40 mins × 3	60 mins @ 20 ml/min		
	Total staining and washing	570 mins	450 mins		
Total time		612 mins	492 mins		

The general whole mount zebrafish ABS procedure involves both staining and washing steps.[1] To ensure the antibody can sufficiently bind to the antigen, the staining time is usually kept at an extended level (e.g., overnight). Despite no systematic study has been conducted to investigate how the fluidic flow can affect the antibody-antigen interaction in the whole mount zebrafish, the studies performed in tubes or well plates suggested that the macromolecular (i.e., antibody and RNA probes) staining usually take longer in older embryos as the tissue became denser.[1,2] The intact tissue of the zebrafish embryo certainly affects the antibody penetration. Therefore, optimizing the whole organism staining procedure by reducing the staining time may result in loss of sensitivity. The washing step,

on the other hand, is for the removal of the nonspecific binding after the staining step and is crucial for the specificity of the procedure. Targeting the washing steps will be a safer option for the optimization of the whole organism staining as the true signal is ensured with sufficient staining time. Also, the manual buffer refreshing steps can be avoided in ZOC washing as the wash buffer is circulated in a close loop. For these, the washing steps were targeted in the whole mount zebrafish Caspase-3 ABS procedure for optimization. Briefly, in the ZOC, two flowrates viz., 10 ml/min and 20 ml/min were used to perform 30 mins, 60 mins, 90 mins, and 120 mins washings after each staining step (Figure 3.9.A, top panel). To ensure the consistency and sufficient Casapse-3 binding, the flowrate and time for the two staining steps were kept constant at 10 ml/min and 120 mins, respectively. For comparison, the same washing times were tested in the plate-based procedure using a 24-well plate. After the procedure, the Caspase-3 signals were measured from the zebrafish embryos encapsulated by the PDST droplets in the ZOC (i.e., the holdup volume of PDST wash buffer due to the Laplace pressure) and 0.5% agarose in well plate.

Based on the experiment results, the washing process was found to be accelerated by using the ZOC as significant intensity differences were found at 30 mins, 60 mins, and 90 mins between the well plate-based and ZOC-based washings (Figure 3.9.A, bottom panel). Also, the samples were found already sufficiently washed at 60 mins when the washing flowrate is 20 ml/min in the ZOC. In addition, a significant intensity difference was found between the two tested washing flowrates at 60 mins which implied a higher washing flowrate in ZOC can speed up the washing process. The two tested washing flowrates in ZOC showed insufficient washing at 30 mins as the intensities for both flowrates were significantly higher than the control (i.e., 2-hour washing in well plate), and no significant intensity difference can be distinct between them.

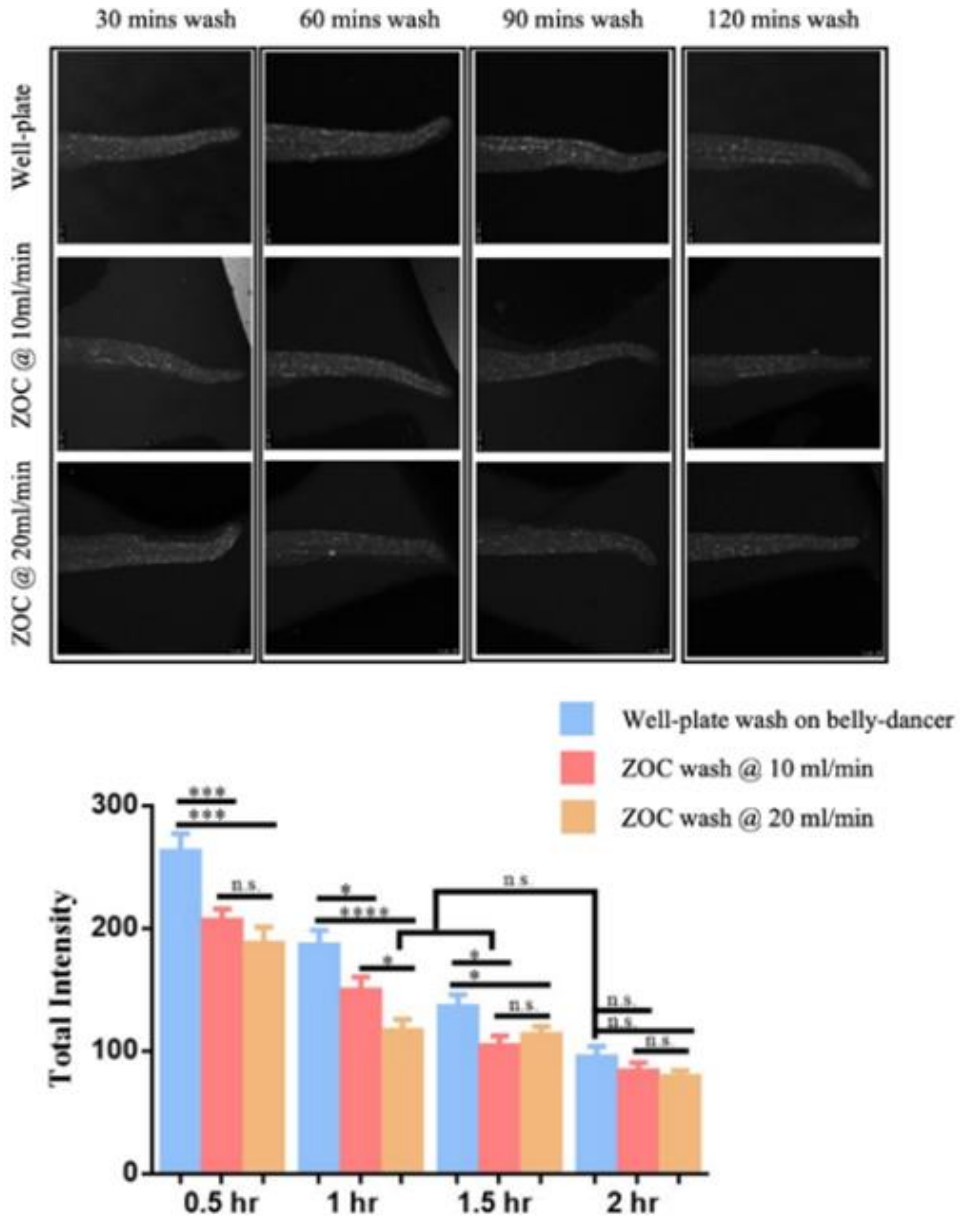

Figure 3.9. ZOC-based versus. Well plate-based whole mount zebrafish Caspase-3 ABS. Top: gray scale images of the tail and trunk for 34 hpf UV treated zebrafish embryo after Caspase-3 ABS. (Vertical axis: well plate-based ABS and ZOC-based ABS at different washing flowrates; Horizontal axis: different PBDT washing times). Bottom: The quantified signal levels for well plate-based ABS (measured in 0.5% agarose) and ZOC-based ABS (measured in PBDT droplets) at different PBDT washing times and flowrates. (N≥3, n≥10, error bar: +SEM.)

Regarding the image taking environments, the intensity measured from PBDT droplets inside the ZOC has a slightly decreased signal when compared to the intensity measured in the 0.5% agarose gel. This is likely due to the power attenuation when the fluorescent laser travel through the thick PDMS layer (i.e., 6.2 mm) above the embryos. Despite this,

the Caspase-3 signal measured from the PDST droplet in ZOC and from 0.5% agarose in well plate showed no significant difference in intensity levels (Figure 3.10.A). We next normalized the intensity of all the experimental results measured by respective means and the consistency of the ZOC-based procedure is found higher than that of the manual well plate-based procedure (Figure 3.10.B). Also, the consistency of the assay is improved when applying higher washing flowrate in ZOC.

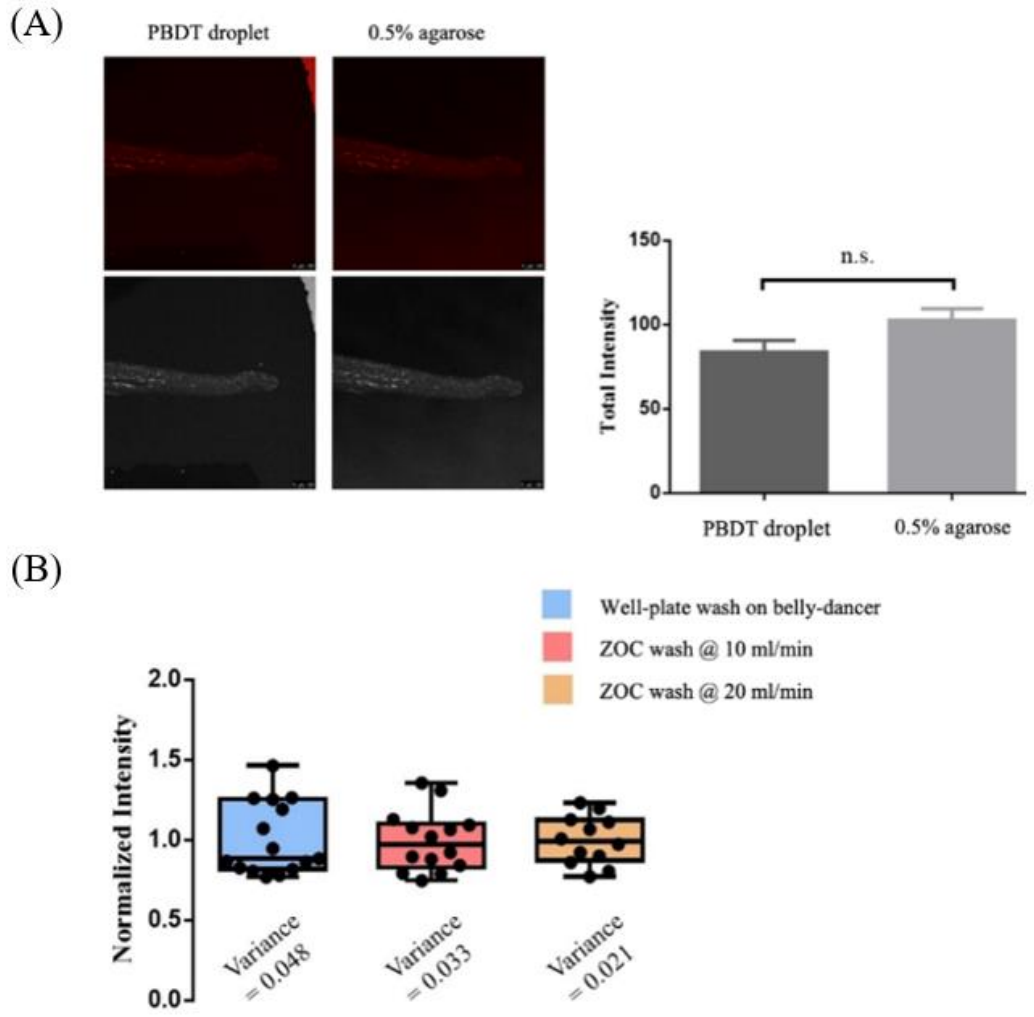

Figure 3.10. The image quality and result consistency comparison between ZOC-based and Well plate-based methods. A) The signal levels for the same set of embryos measured from PBDT droplet in ZOC and in 0.5% agarose in well plate, error bar: +SEM. B) The experiment variances for ZOC-based and well plate-based whole mount zebrafish Caspase-3 ABS (N ≥12).

All in all, the ZOC-based whole mount zebrafish ABS outperforms the conventional plate-based manual approach by reducing both manual steps and time while increasing the consistency of the results (Figure 3.11). This highlights the benefits of miniaturization and mechanization of zebrafish assays.

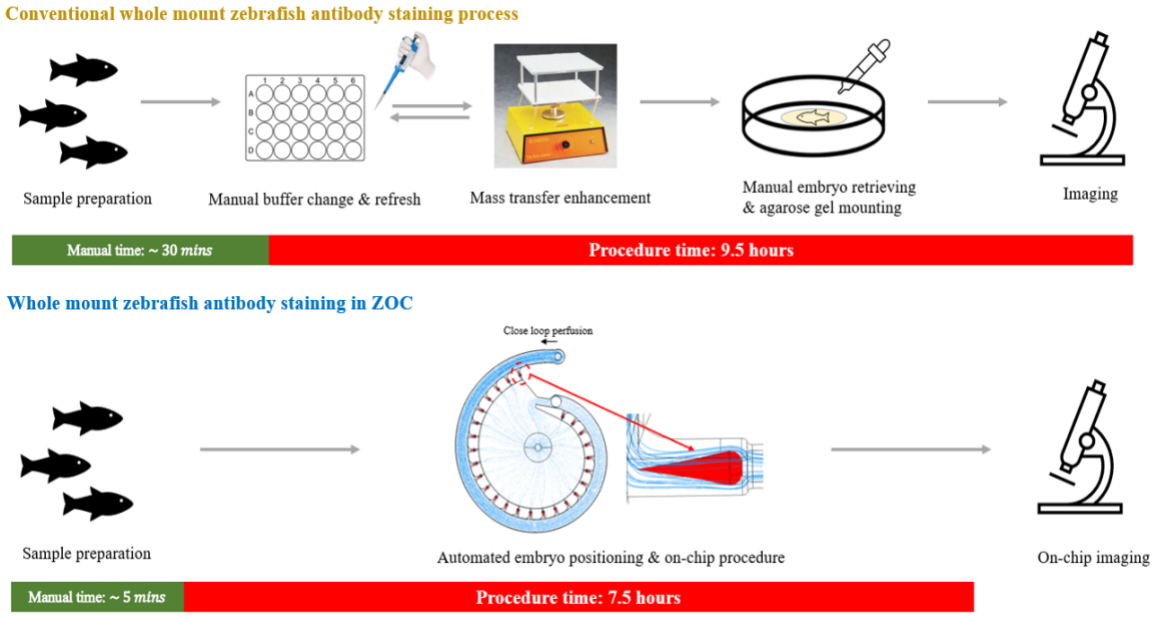

Figure 3.11. The manual steps and procedure time comparison between the conventional well plate-based method (Top) and ZOC-based method (Bottom).

3.4 Conclusion and Discussion

ZOC may have experienced significant growth lately, but it is still in the early development phase.[11,16,20] The needs for optimizing and automating the time consuming and labor-intensive procedures such as whole mount zebrafish ABS and ISH is still largely unfulfilled. To fill the gap, we developed a multi-depth spiral ZOC that can trap, immobilize, and perform the whole mount Caspase-3 ABS on the chorion-less zebrafish embryo.

The ZOC used in the study applies the classic hydrodynamic trapping mechanism to trap chorion-less zebrafish embryos in the close loop perfusion system. The developed ZOC showed a trap usage rate that is comparable to the previously reported zebrafish embryo trapping platforms,[11,19] but with a more convenient loading procedure as multiple embryos are allowed to enter the ZOC at the same time. Also, the body orientation preference (i.e., head point inward) found when trapping the cone-shaped fixed zebrafish embryo will be useful in the applications that require parallel phenotype comparison. This phenomenon may also provide some insights for the trapping and sorting of non-spherical particles in other fluidic devices. In addition, the trapped embryos were found to be encapsulated in the droplets after draining out the buffer. The encapsulation of embryos in droplets makes the ZOC portable and allows the ZOC to access various imaging platforms after trapping. This feature, which has not been reported by similar ZOCs, may have potential to be used for applications such as drug screening, metabolite analysis, hypoxia study etc.

In this study, for the first time, the complete procedure of the whole mount zebrafish ABS was performed and optimized on a ZOC system. We proved that the overall procedure for the whole mount zebrafish Caspase-3 ABS procedure can be accelerated by employing a

higher perfusion flowrate. We believe this finding also applies to other whole mount ABS procedures. Also, we hope our ZOC can be accepted by the zebrafish community and encourage various staining procedures to be tested on it.

The current ZOC design and system setting still have limitations that need to be optimized in the future. First, the close loop system used in ZOC-based procedure requires more reagent volume (i.e., ~2 times for washing and ~6 times for staining) compared to the well plate-based procedure due to off-chip volumes contributed by the tubing and pump. The large reagents consumption could be reduced by shortening or reducing the size of the tubing. Also, the effect of large reagent consumption may be minimized by conducting large scale tests (i.e., connect multiple ZOCs in series) or by reusing the reagents.[3] Second, although the multi-depth ZOC can prevent large- or micro- sized bubbles from entering the traps, the medium sized bubbles may still occasionally enter the traps during the perfusion. This is the major cause of bias in the study as the trapped bubbles will not only affect the flow conditions in the traps but also block the embryo during the imaging. Therefore, a special bubble trapping or breaking device[24] could be added at the ZOC inlet to trap the medium size bubbles or break the medium size bubble into micro bubbles. Finally, the current procedure still requires the operator to manually load the embryos and switch the buffers during each step. The manual buffer switching process can be eliminated by integrating the ZOC with automated imaging and liquid handling platforms[3] in the future to reach the degree of "sample-in and answer-out".

3.5 References

1. Sorrells, S., Toruno, C., Stewart, R. A. & Jette, C. Analysis of Apoptosis in Zebrafish Embryos by Whole-mount Immunofluorescence to Detect Activated Caspase 3. *Journal of Visualized Experiments* (2013) doi:10.3791/51060.
2. Thisse, B. & Thisse, C. In Situ Hybridization on Whole-Mount Zebrafish Embryos and Young Larvae. in 53–67 (2014). doi:10.1007/978-1-4939-1459-3_5.
3. Fuqua, T. *et al.* An open-source semi-automated robotics pipeline for embryo immunohistochemistry. *Sci Rep* **11**, 10314 (2021).
4. Vanderhoeven, J., Pappaert, K., Dutta, B., Van Hummelen, P. & Desmet, G. DNA Microarray Enhancement Using a Continuously and Discontinuously Rotating Microchamber. *Anal Chem* **77**, 4474–4480 (2005).
5. Nguyen, H. T. *et al.* Microfluidics-assisted fluorescence in situ hybridization for advantageous human epidermal growth factor receptor 2 assessment in breast cancer. *Laboratory Investigation* **97**, 93–103 (2017).
6. Maïno, N. *et al.* A microfluidic platform towards automated multiplexed in situ sequencing. *Sci Rep* **9**, 3542 (2019).
7. Huber, D., Voith von Voithenberg, L. & Kaigala, G. V. Fluorescence in situ hybridization (FISH): History, limitations and what to expect from micro-scale FISH? *Micro and Nano Engineering* **1**, 15–24 (2018).
8. Ciftlik, A. T., Lehr, H.-A. & Gijs, M. A. M. Microfluidic processor allows rapid HER2 immunohistochemistry of breast carcinomas and significantly reduces ambiguous (2+) read-outs. *Proceedings of the National Academy of Sciences* **110**, 5363–5368 (2013).
9. Brajkovic, S. *et al.* Microfluidics-based immunofluorescence for fast staining of ALK in lung adenocarcinoma. *Diagn Pathol* **13**, 79 (2018).
10. Kao, K.-J. *et al.* A fluorescence in situ hybridization (FISH) microfluidic platform for detection of HER2 amplification in cancer cells. *Biosens Bioelectron* **69**, 272–279 (2015).
11. Akagi, J. *et al.* Miniaturized Embryo Array for Automated Trapping, Immobilization and Microperfusion of Zebrafish Embryos. *PLoS One* **7**, e36630 (2012).
12. Fuad, N. M., Kaslin, J. & Wlodkowic, D. Lab-on-a-Chip imaging micro-echocardiography (iμEC) for rapid assessment of cardiovascular activity in zebrafish larvae. *Sens Actuators B Chem* **256**, 1131–1141 (2018).
13. Zhu, F. *et al.* Three-dimensional printed millifluidic devices for zebrafish embryo tests. *Biomicrofluidics* **9**, 046502 (2015).
14. Panuška, P. *et al.* A millifluidic chip for cultivation of fish embryos and toxicity testing fabricated by 3D printing technology. *RSC Adv* **11**, 20507–20518 (2021).
15. Yang, F. *et al.* An integrated microfluidic array system for evaluating toxicity and teratogenicity of drugs on embryonic zebrafish developmental dynamics. *Biomicrofluidics* **5**, 024115 (2011).
16. Li, Y. *et al.* Zebrafish on a Chip: A Novel Platform for Real-Time Monitoring of Drug-Induced Developmental Toxicity. *PLoS One* **9**, e94792 (2014).
17. Frey, N., Sönmez, U. M., Minden, J. & LeDuc, P. Microfluidics for understanding model organisms. *Nat Commun* **13**, 3195 (2022).
18. Zhu, Z. *et al.* A Bubble-Free Microfluidic Device for Easy-to-Operate Immobilization, Culturing and Monitoring of Zebrafish Embryos. *Micromachines (Basel)* **10**, 168 (2019).
19. Fuad, N. M., Kaslin, J. & Wlodkowic, D. Development of chorion-less zebrafish embryos

in millifluidic living embryo arrays. *Biomicrofluidics* **11**, 051101 (2017).
20. Yang, F., Gao, C., Wang, P., Zhang, G.-J. & Chen, Z. Fish-on-a-chip: microfluidics for zebrafish research. *Lab Chip* **16**, 1106–1125 (2016).
21. Nguyen, M.-A., Srijanto, B., Collier, C. P., Retterer, S. T. & Sarles, S. A. Hydrodynamic trapping for rapid assembly and in situ electrical characterization of droplet interface bilayer arrays. *Lab Chip* **16**, 3576–3588 (2016).
22. Gaseated Fluids (Gas-Liquid Mixtures). in *Underbalanced Drilling: Limits and Extremes* 109–195 (Elsevier, 2012). doi:10.1016/B978-1-933762-05-0.50010-3.
23. Zeng, Z., Richardson, J., Verduzco, D., Mitchell, D. L. & Patton, E. E. Zebrafish Have a Competent p53-Dependent Nucleotide Excision Repair Pathway to Resolve Ultraviolet B–Induced DNA Damage in the Skin. *Zebrafish* **6**, 405–415 (2009).
24. Fu, T., Ma, Y., Funfschilling, D. & Li, H. Z. Dynamics of bubble breakup in a microfluidic T-junction divergence. *Chem Eng Sci* **66**, 4184–4195 (2011).
25. Stucki, J. D. & Guenat, O. T. A microfluidic bubble trap and oscillator. *Lab Chip* **15**, 4393–4397 (2015).

Chapter 4
Application of using Concentration Gradient Generator for High Resolution Zebrafish Embryo Dose-Response Screening

Abstract

Acute zebrafish fish embryo toxicity (FET) test is a simple and robust assay in assessing the acute toxicity of chemicals and has been implemented in the zebrafish-on-a-chip (ZOC) platforms for high-throughput endpoints screening. By far, most ZOCs can only achieve a sole function in performing the acute FET tests: either concentration gradient generation or automated zebrafish embryo entrapment. A multifunctional device that can include both functions in conducting FET tests is highly desired. In this work, we presented an innovative multifunctional concentration gradient generator (CGG) that can accomplish both zebrafish embryo positioning and concentration gradient generation at the same time. The feasibility of this new CGG design has been examined in the acute FET test for caffeine overdose effect study. The CGG-based acute FET test has proved effective in detecting the sublethal endpoints and conducting dose-response analysis. This work provides an alternative tool for the acute FET test. We hope the new CGG device can be accepted by the research community to explore its potential by testing more chemicals.

4.1 Introduction

Zebrafish (*Danio rerio*) embryo is commonly used in chemical toxicity tests to identify the harmful effects of the chemical at different concentration levels. The toxicity tests performed in the zebrafish embryo are usually more physiological relevant than the cell based in vitro studies as the complexity of a living organism is considered. Most significantly, due to their small size, transparent body, and rapid growth features, zebrafish embryos are well-suited for high-throughput phenotype-based *in situ* screening. Furthermore, the tests performed on zebrafish embryos can have less ethical problems as the use of live adult fish are avoided.[21] The Organization for Economic Co-operation and Development (OECD) has developed the guidelines for the acute fish embryo toxicity (FET) test (TG 236, 2013) using zebrafish embryo, which serve as one of the golden standards for assessing acute chemical toxicity.[1]

The increasing use of zebrafish embryos in the acute chemical toxicity tests also facilitates the development of ZOC for the FET test. The ZOC, as discussed in the previous chapters, allows precise microenvironment control, real-time embryo monitoring, high-throughput parallel comparison, and automated embryo positioning. However, there is still a notable lack of ZOC designs for the FET tests. By far, none of the reported ZOC platforms can achieve both automatic concentration gradient generation and zebrafish embryo immobilization at the same time.[2–4] Also, most of the ZOC platforms are developed to conduct toxicity tests on the zebrafish embryos that are still protected in chorion.[5] The zebrafish chorion, an acellular envelope which serves as a molecular barrier to protect the embryos from stress and toxicities in the surrounding environment. However, during the FET test, the chorion can slow down or stop the chemical penetration leading to various

chemical exposure levels for embryos, and thus leading to heterogeneous phenotype detection.[5] For these, the zebrafish embryo dechorionation technique is used to improve the accuracy and sensitivity of FET tests.[1] In 2017, Fuad et al. reported a milli fluidic device for automatic immobilizing of dechorionated zebrafish embryos and can be used for FET test.[5] This proof-of-concept study consistent with our preliminary study in chapter 2, demonstrated the dechorionated zebrafish embryos can develop normally in ZOC and sub-lethal endpoints of zebrafish embryo such as tail curvature, pericardial edema, yolk sac abnormality, etc. can be easily detected on the milli fluidic device. One of the limitations for the milli fluidic device reported by Fuad et al. is the entrapped zebrafish embryos cannot be exposed under different chemical concentrations which turn off the capability for parallel dose-response comparison. In 2012, Choudhury et al. reported a microfluidic perfusion platform with chemical gradient generation feature for zebrafish embryo toxicity test. The microfluidic platform uses a Christmas tree-like multi-channel to continuously generate various chemical dosages downstream in the fish tanks.[6] The major drawback for this platform is the embryos need to be loaded individually to the fish tanks (i.e., multi-depth traps) which can be labor intensive for large scale tests.[6] Moreover, the fish tanks cannot fully restricts the embryo movements, especially after hatching which limits the data acquisition rate and high-resolution monitoring. Currently, none of the reported ZOC platforms can achieve both automated embryos immobilization and dosage generation at the same time. Therefore, the development of ZOC platforms to achieve both functions is desired for the acute FET tests.

In this work, we develop a multifunctional concentration gradient generator (CGG) that can automatically immobilize the dechorionated zebrafish embryos and generate chemical gradients for acute FET tests. We demonstrate the innovative CGG platform has advantages in identifying the concentration-dependent sublethal endpoints and conducting high-resolution dose-response analysis which can be served an alternative tool for the acute FET tests.

4.2 Materials and Methods

4.2.1 Computational Mass Transfer and Fluid Dynamic Simulations

The CFD and mass transfer simulation were performed by COMSOL 5.5 (COMSOL 5.5 Inc. Stockholm, Sweden) to evaluate the hydrodynamic zebrafish embryo trapping and the concentration gradient generation in CGG. The “free and porous media flow” was used to simulate the steady state fluidic fields for the initial (i.e., no trap is occupied) and final (i.e., all traps are occupied) states of the trapping process. The trapping inlet flower rate was to 10 ml/min. Water was set as the carrying buffer in the simulation. The dechorionated zebrafish embryo was molded as a cone-shape rigid body with 2 mm overall length and 0.5 mm maximum head diameter. Also, the zebrafish embryos were placed at the bottom of the traps in the simulation. For the concentration gradient generation simulations, “the transport of diluted species in porous media flow” physics was used and was coupled with the steady state fluidic field when all the embryos were on board (i.e., all traps are occupied). The diffusion coefficient (D) of the caffeine/trypan blue mixture in water is

defined as 2.21×10^{-6} cm^2/s.[7] The inner wall inlet of the CGG was set to perfuse with 2 mg/mL caffeine and the outer wall inlet was set to perfuse with E3 buffer (i.e.,0 mg/mL caffeine). The mass transfer *Péclet* number ($Pé$) is calculated as:

$$Pé = \frac{Lu}{D} \qquad \text{(Eqn. 4.1)}$$

Where, L is characteristic length, u is the local relative velocity between the two miscible streams, and D is the diffusion coefficient.

4.2.2 Overall System Setup

The overall system was upgraded from the system used in Chapter 3. As shown in Figure 4.1, a syringe pump compatible with two 60 ml syringes was added for concentration generation purposes. A two-way valve (i.e., valve 1) was added to block the loading tube during dosage generation. Also, a three-way valve was placed at the outlet of the CGG to switch between the close loop embryo trapping/perfusion and dosage generation modes. The main concern during the concentration gradient generation was the embryo dislocation due to the backflow. Therefore, the pumps need to be turned off before valve switching and the valve switching order should follow their denoted numbers (e.g., switch valve 1 first then valve 2).

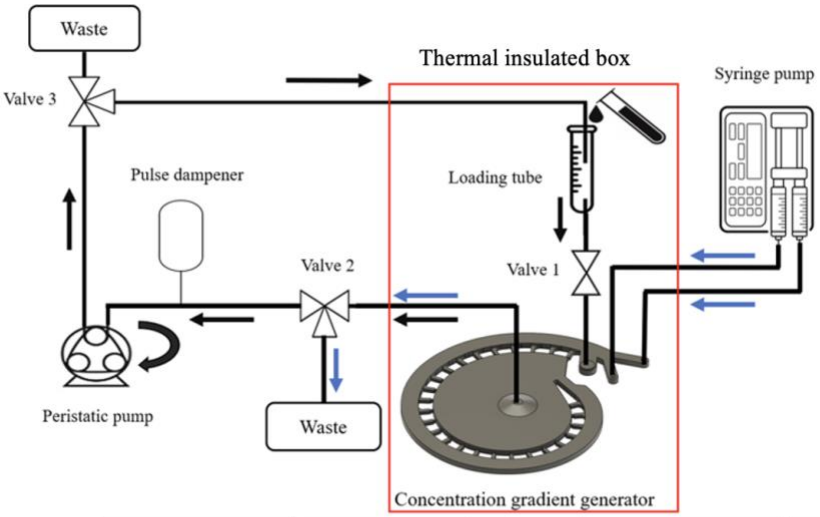

	Peristatic pump	Syringe pump	Valve 1	Valve 2	Valve 3
Close loop Trapping/Perfusion	ON	OFF	ON	To pulse dampener	To loading tube
Gradient generation	OFF	ON	OFF	To waste	Bypass
Flushing	OFF	OFF	ON	To waste	Bypass
Draining	ON	OFF	ON	To pulse dampener	To waste

Figure 4.1. Schematic showing the overall system setup. Black arrow indicates the flow direction when using the peristaltic pump. Blue arrow indicates the flow direction when using syringe pump during concentration gradient generation. The bottom table shows the operation modes and corresponding apparatus states.

4.2.3 Acute Zebrafish Embryo Caffeine Toxicity Tests

The adult wild type zebrafish (EKW line) which were raised in UC Merced fish facility were randomly paired a night before the mating and spawning. The eggs were collected using a sieve and then rinsed with the E3 buffer to filter out the debris and waste. The collected eggs were cultured in a petri dish filled with E3 buffer at 28.5℃. The unfertilized eggs and dead embryos were sorted before/after the incubation. The chorions of 24 hpf zebrafish embryos were manually peeled off using micro tweezers (World Precision Instruments, Inc) under a stereomicroscope about 2 hours before the tests. The dechorionated zebrafish embryos then were treated with different caffeine concentrations in 24 well plate (10 embryos per well) and different concentration gradients in CGG (26 embryos per CGG) for 2 hours. The caffeine was replaced by the E3 buffer after the 2-hour treatment in both well plate and CGG. Next, the zebrafish embryo was recovered in the well plate and CGG for 24 hours. The flowrate in CGG during the 24 hours of recovery process was set to be 2 ml/min. The temperature is maintained at 28.5℃ throughout the test. Images and endpoints were taken and recorded after 2-hour treatment and 24-hour recovery, respectively (Figure 4.2). Finally, the dose-response analysis is performed in Prism (GraphPad Software)

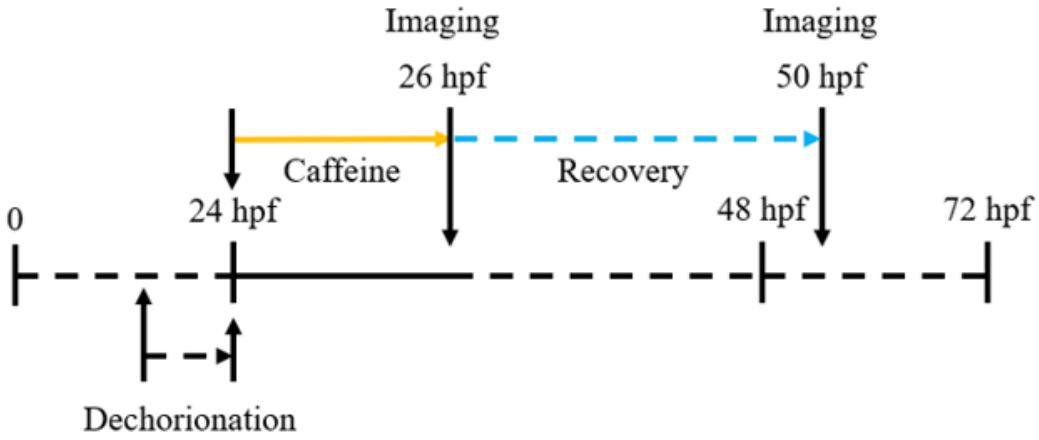

Figure 4.2. The schedule for the zebrafish embryo acute caffeine overdose study.

4.2.4 Imaging and Intensity Measurements

The zebrafish embryos images were taken using a stereomicroscope with a digital camera (AmScope Inc., USA). An LED plate (AmScope Inc. USA) was used as the light source for the imaging. A MATLAB script is developed to quickly estimate the caffeine concentration levels at individual traps via trypan blue gradient images (Figure 4.3.A). Specifically, an intensity profile along the traps is generated by inputting the steady state concentration gradient images and the coordinates of the traps to the MATLAB script. On the intensity profile, the trypan blue intensities inside the traps are displayed as upper peaks while the gaps between traps are flat signals. The peak signals on the intensity profiles then convert to the caffeine concentrations using the concentration versus intensity standard curve for trypan/caffeine buffer (Figure 4.3.B). Note the light intensity at each trap was measured in 8 bits and the intensity of trypan is calculated as 255 – light intensity.

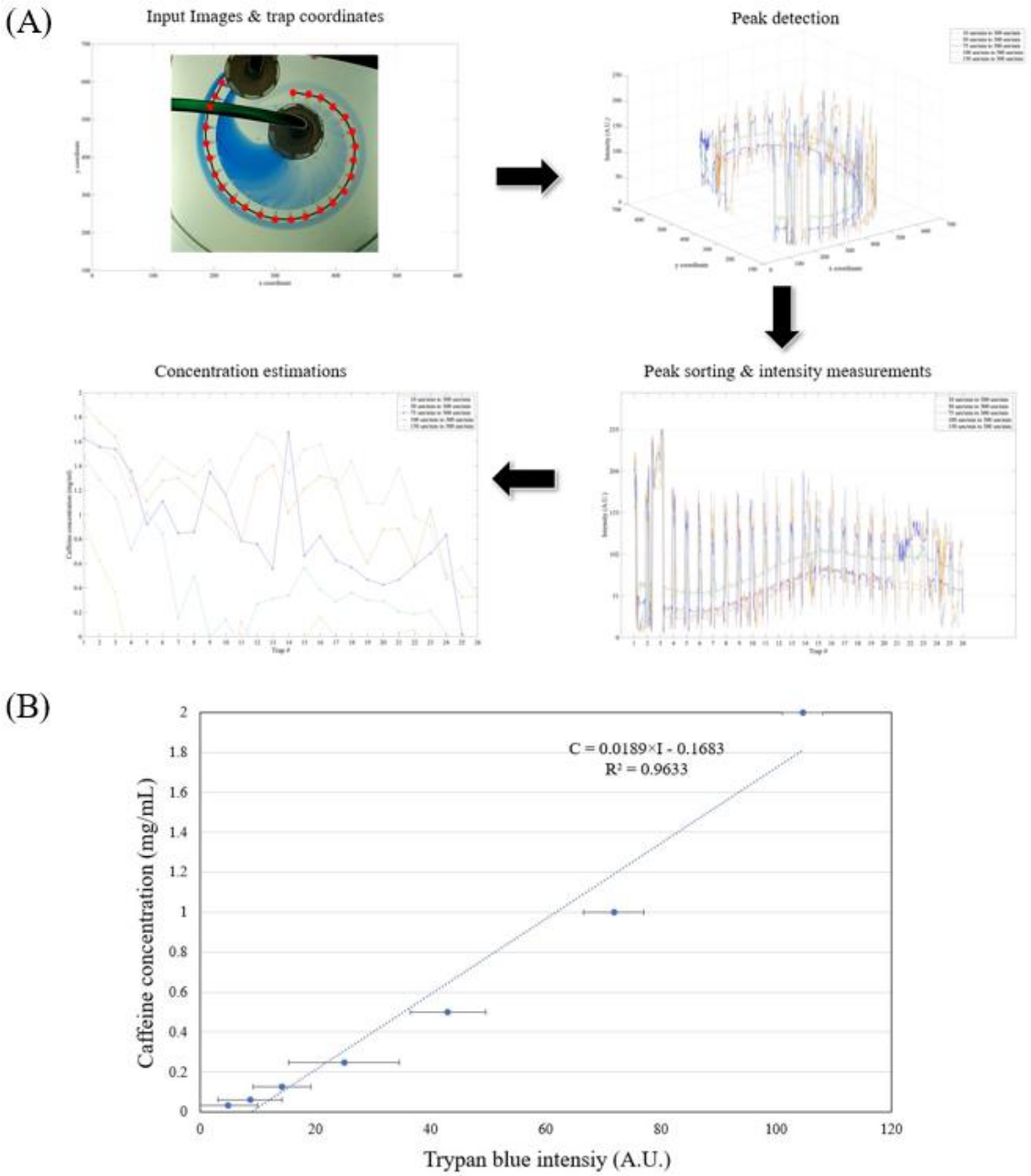

Figure 4.3. Caffeine concentration level measurements using MATLAB script. A) The overall caffeine concentration measurement process in the MATLAB script. B) The caffeine concentration versus trypan blue intensity curve.

4.3 Device Design and Results

4.3.1 Concentration Gradient Generator Design Layout

The CGG used in this Chapter is modified from the ZOC design II developed in chapter 2. To further improve the trap usage and integrate with the new concentration gradient

generation feature, the inlet for the zebrafish embryo /buffer loading is moved to the trap side of the main channel (i.e., inner wall). The height of the main channel and inner chamber is increased to 1.4 mm and the height of the traps is decreased to 0.7 mm for the purpose of preventing bubbles, especially the medium sized bubble, from entering the traps. Also, the nozzle length for the traps has now decreased from 0.8 mm to 0.45 mm at a rate of 0.014 mm/trap along the spiral main channel to compensate for the loss of hydrodynamic suction force due to the height adjustments (Figure 4.4. A). For the dynamic chemical concentration gradient generation, a Y branch is added at the main channel. After the zebrafish embryos are immobilized inside the traps, two miscible buffers with different chemical concentrations are perfused through the two inlets (i.e., inner wall inlet and outer wall inlet) at the Y branch. The two miscible streamlines then mix along the main channel to create various concentration levels inside the traps (Figure 4.4. B). At steady state, the concentration levels are stable inside the traps creating steady microenvironments for the acute FET.

(A)

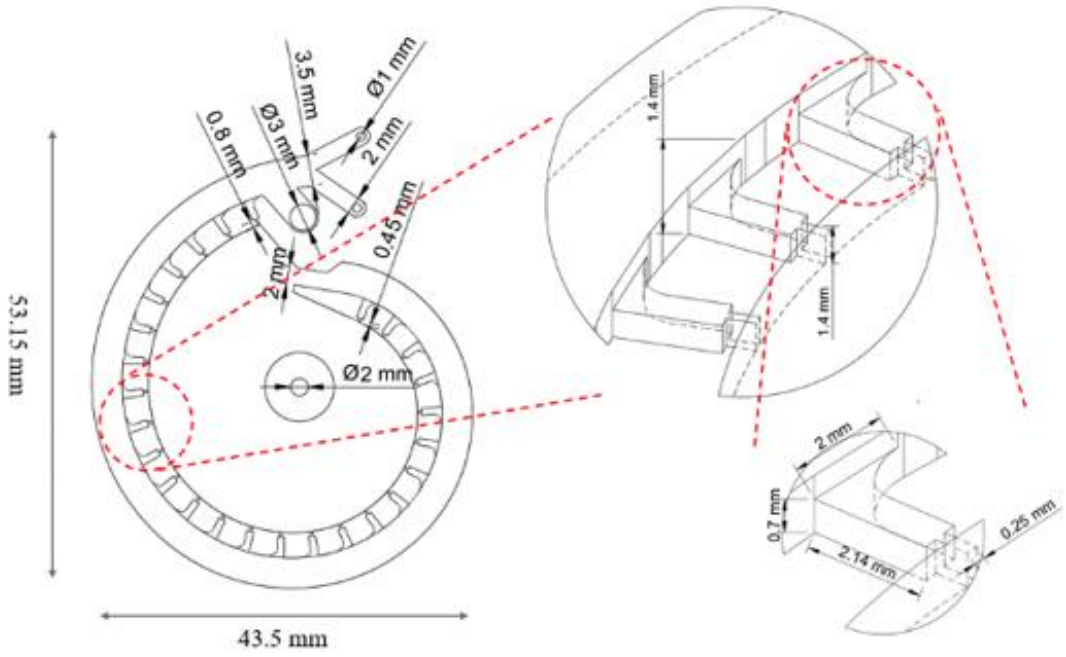

(B)

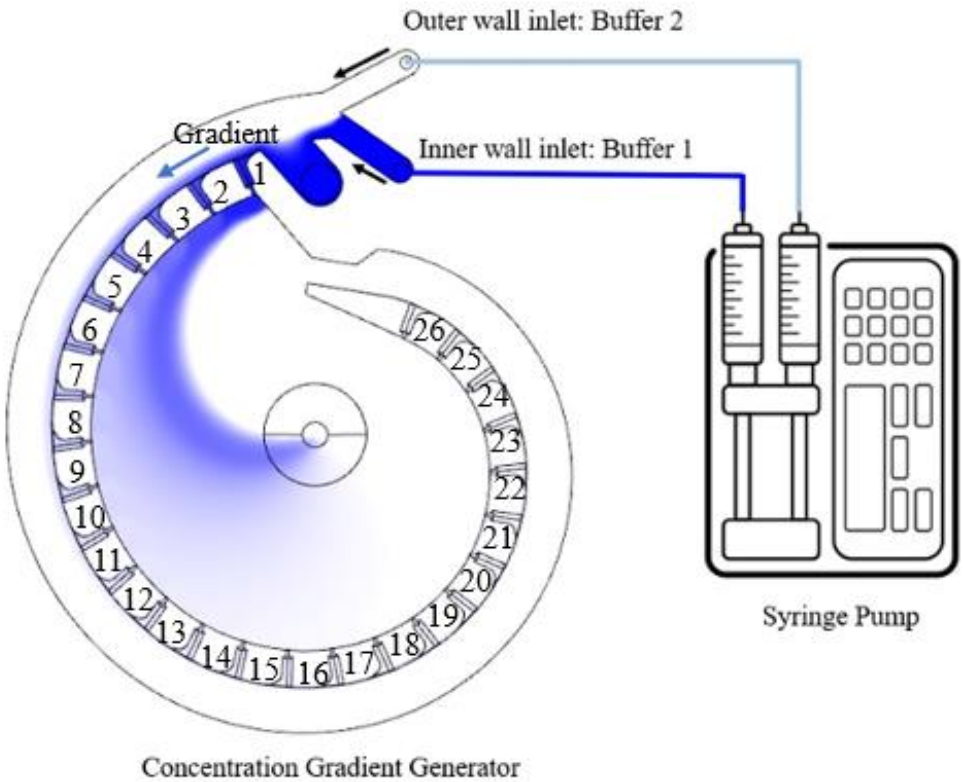

Figure 4.4. The CGG for acute FET tests. A) The CGG design layout. B) schematic for the dynamic concentration gradient generation. The trap orders are labelled by the numbers.

4.3.2 Zebrafish Embryo Trapping Estimation and Validation

Same as the process demonstrated in section 2.3.2, the zebrafish embryo trapping potential in the CGG was analyzed by using the CFD simulations. Briefly, the initial (i.e., all traps are empty) and final (i.e., all traps are occupied) states of the hydrodynamic trapping process were selected for the analysis. As explained in section 2.3.1, the overall flowrate that travels through the traps is the indicator for the overall hydrodynamic trapping potential of the CGG. The CFD simulations showed that flowrate that go through the traps drops from 87.5% of inlet flowrate to 53.7% of the inlet flowrate after the hydrodynamic trapping which indicating that the CGG can preserve sufficient embryo trapping ability even at the last moment of the trapping process (Figure 4.5. A). The velocity distribution of the CGG at the initial state is also analyzed to estimate the trapping smoothness as well as the trap usage rate. The velocity distribution map showed that the velocity ratios between the trapping channels and near main channel sections (i.e., the embryo drawing ability index, ETP) are maintained at a relatively constant level (Figure 4.5.B). This indicates a smoothed process for embryo trapping as no traps with outstanding embryo drawing ability.

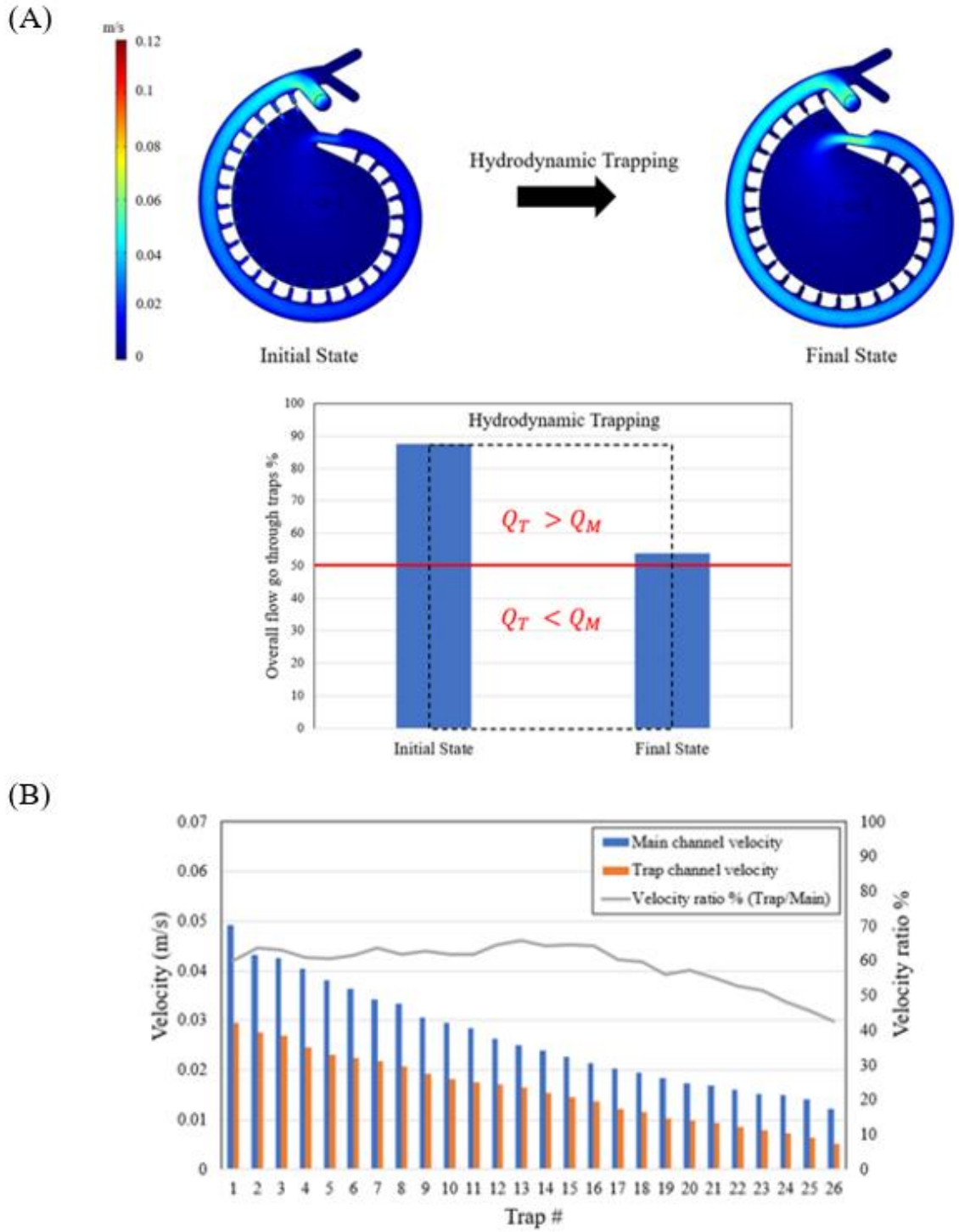

Figure 4.5. Zebrafish embryo trapping estimation in the ZOC. A) Top panel: the velocity heatmaps for initial and final states of trapping. Bottom panel: the overall trap flowrates at initial and final states of trapping. B) The velocity and velocity ratio distribution for each individual trap.

Like the embryo trapping validation performed in section 2.3.2 and section 3.3.1, the dechorionated 24 hpf wild type zebrafish embryos were used for the closed loop hydrodynamic trapping. The flowrate was set to be 10 ml/min and the E3 buffer was used as the carrying buffer. Also, no anesthetic drug such as tricaine was used to treat the zebrafish embryos prior to the trapping. The results showed that the trap occupation rate for the CGG can reach 98.4$\pm$ 2.2% (N= 24) which is higher than the 93.03$\pm$ 4.35% (N= 16) for the design II reported in chapter 2 (Figure 4.6.A). Consistent with what was found in chapter 2, most of the captured zebrafish embryos had their head point inward inside the traps, given an overall head inward rate of 88.08$\pm$4.73% (N= 24) in the CGG which is slightly lower than the 92.88 ± 4.44% (N= 24) measured in design II (Figure 4.6.A). Additionally, after the modifications from design II (i.e., embryo loading inlet location and channel dimensions), the occupation rate of the first trap in the CGG has significantly increased from 6.25% to 79.2% (Figure 4.6.B &C).

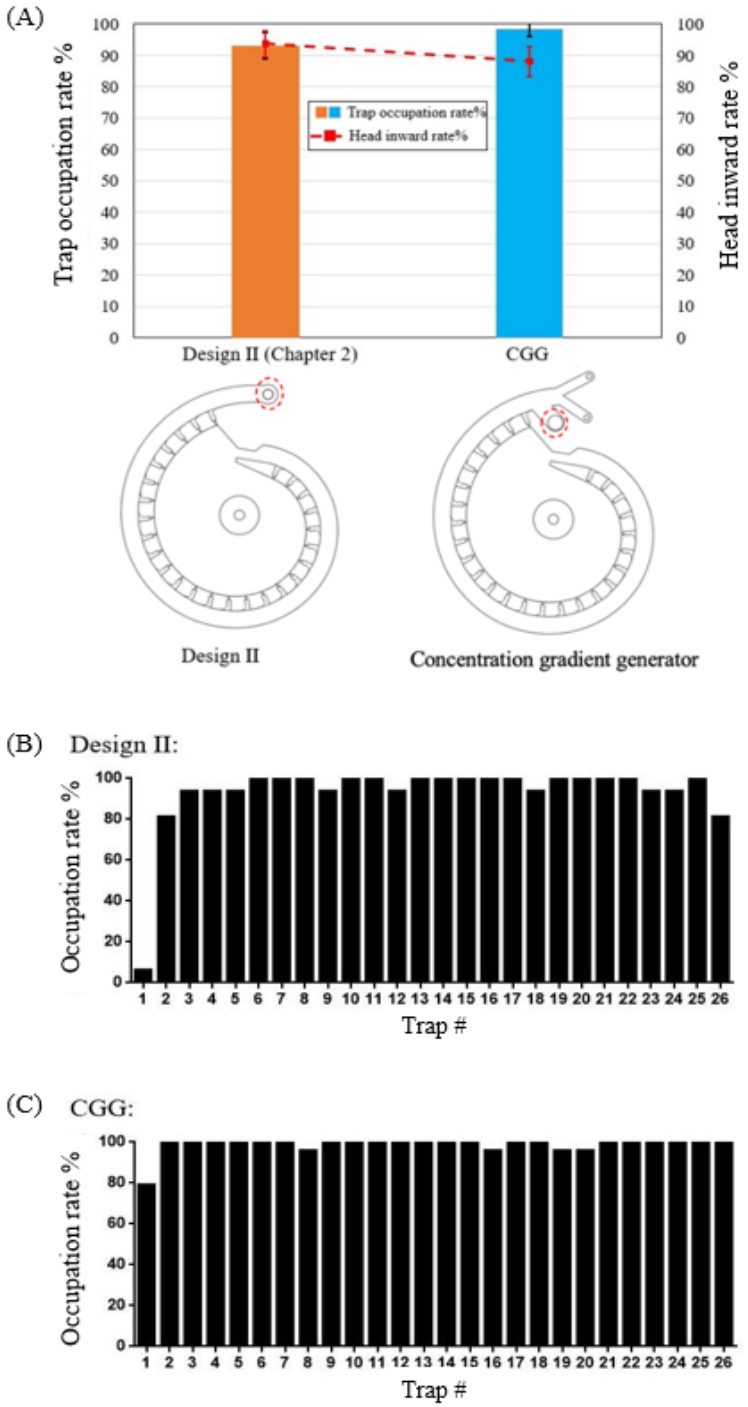

Figure 4.6. The zebrafish embryo trapping performance comparison between design II and CGG. A) Top panel: the overall trap occupation rate bar graph for design II (N= 16, error bar:±SD) and CGG (N= 24, error bar:±SD) and head inward rate line plot (red dash line) for design II (N= 16, error bar:±SD) and CGG (N= 24, error bar:±SD). Bottom panel: the configuration difference between design II and CGG. Red circle indicates the embryo loading inlets. B) The trap occupation frequency distribution in design II (N= 16). C) the trap occupation frequency distribution in CGG (N= 24).

4.3.3 Dynamic Concentration Gradient Generation

The CGG uses a Y-junction to mix the two introduced buffers along the spiral channel and create various concentration levels in the traps. Before using CGG for live zebrafish embryo testing, a quick validation experiment using whole mount zebrafish trypan blue staining was performed to verify the CGG's viability for concentration gradient generation. In this preliminary test, the inner wall and outer wall inlets were perfused with 0.04% Trypan blue/E3 buffer at 25 $\mu l/min$ and E3 buffer at 125 $\mu l/min$, respectively (Figure 4.7.A). After the 20-min staining, the parallelly placed fixed zebrafish embryos developed a decreasing trypan blue intensity along the spiral main channel (Figure 4.7.B). This indicates the CGG can treat the embryos with varies chemical concentrations inside the traps, and the 26 concentration levels are decreasing along the spiral main channel. Furthermore, the gradient can be varied by adjusting the flowrates at the two inlets (data not shown). Besides, the trypan blue is found to be an excellent colorimetric indicator to track the concentration gradient as well as to detect any cell/embryo death events during the live zebrafish embryo test (i.e., trypan blue can only penetrate through dead cells).

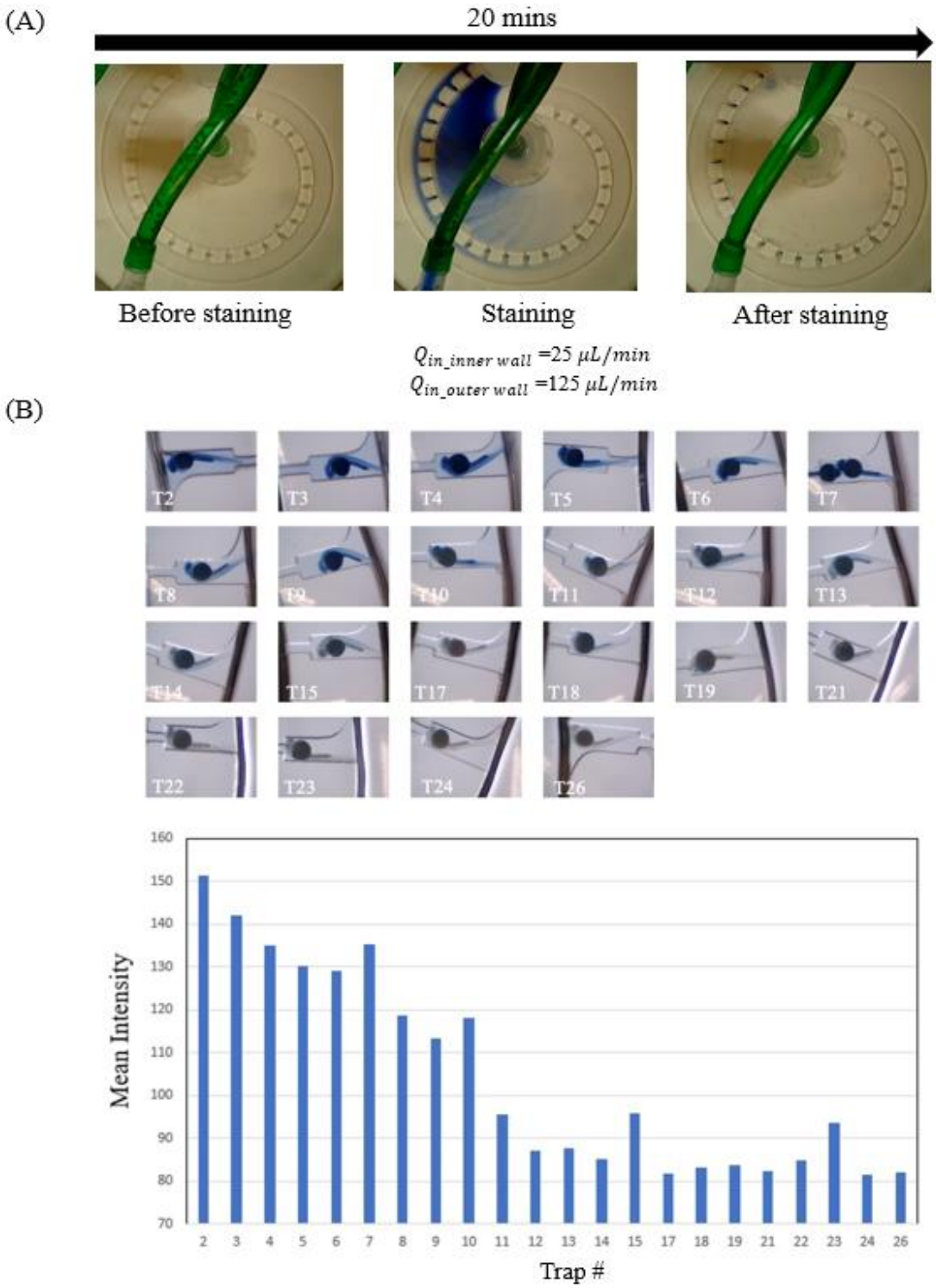

Figure 4.7. The quick validation experiment for concentration gradient generation. A) The representative images and experimental setups for the whole mount trypan blue staining. B) Top: microscopic images showing embryos with decreased trypan blue intensity along the main channel. Bottom: The measured mean trypan blue intensities of the embryos inside the traps.

One of the major concerns about using the CGG for the chemical toxicity test is the treatment time lag. This is because we employ a dynamic concentration gradient generation process in the CGG.[2,8] For instance, the zebrafish embryo in the first trap always has the longest treatment time compared to the zebrafish embryos in the downstream traps due to the earliest steady state concentration establishment (i.e., close to the inlets). Therefore, convective-based gradient generation ($P\acute{e} > 1$) is preferred for the acute chemical toxicity test as the treatment time differences can be minimized by quickly reaching the steady state concentration levels. In this study, 7 different flowrate combinations are selected to study the dynamic concentration gradient generation. Specifically, the outer wall inlet is perfused with E3 buffer, and the flowrate ($Q_{in\_outer\ wall}$) is maintained at 300 $\mu l/min$. The inner wall inlet is perfused with 0.04% Trypan blue/testing chemical (i.e., 2 mg/ml Caffeine in this study) mixture and the flowrates ($Q_{in\_inner\ wall}$) are set to be 10 $\mu l/min$, 30 $\mu l/min$, 50 $\mu l/min$, 60 $\mu l/min$, 75 $\mu l/min$, 100 $\mu l/min$, and 150 $\mu l/min$.

To check if the dynamic gradient generation is convective mass transfer dominant, the $P\acute{e}$ number (Eqn. 4.1) heatmap is generated using the CFD and mass transfer simulations. The heatmap showed that the $P\acute{e}$ number decreases along the spiral main channel before reaching the narrowed section. Since the level of $P\acute{e}$ number is dependent on the relative velocity between the two miscible streams, the lowest $P\acute{e}$ number should be found at the minimum relative velocity viz. $Q_{in\_inner\ wall}$ equals 150 $\mu l/min$ (Figure 4.8.A). When $Q_{in\_inner\ wall}$ is 150 $\mu l/min$, the lowest $P\acute{e}$ number found at the end of the main channel is around 550 indicating the selected flowrates can ensure a convective-based gradient generation in the CGG. Note the characteristic length of the main channel was used to calculate the $P\acute{e}$ numbers in the CGG. According to the time dependent mass transfer simulations as well as the validation experiments, a stable concentration level inside the traps can be reached in about 10 mins for all the chosen flowrates (Figure 4.8.B&C).

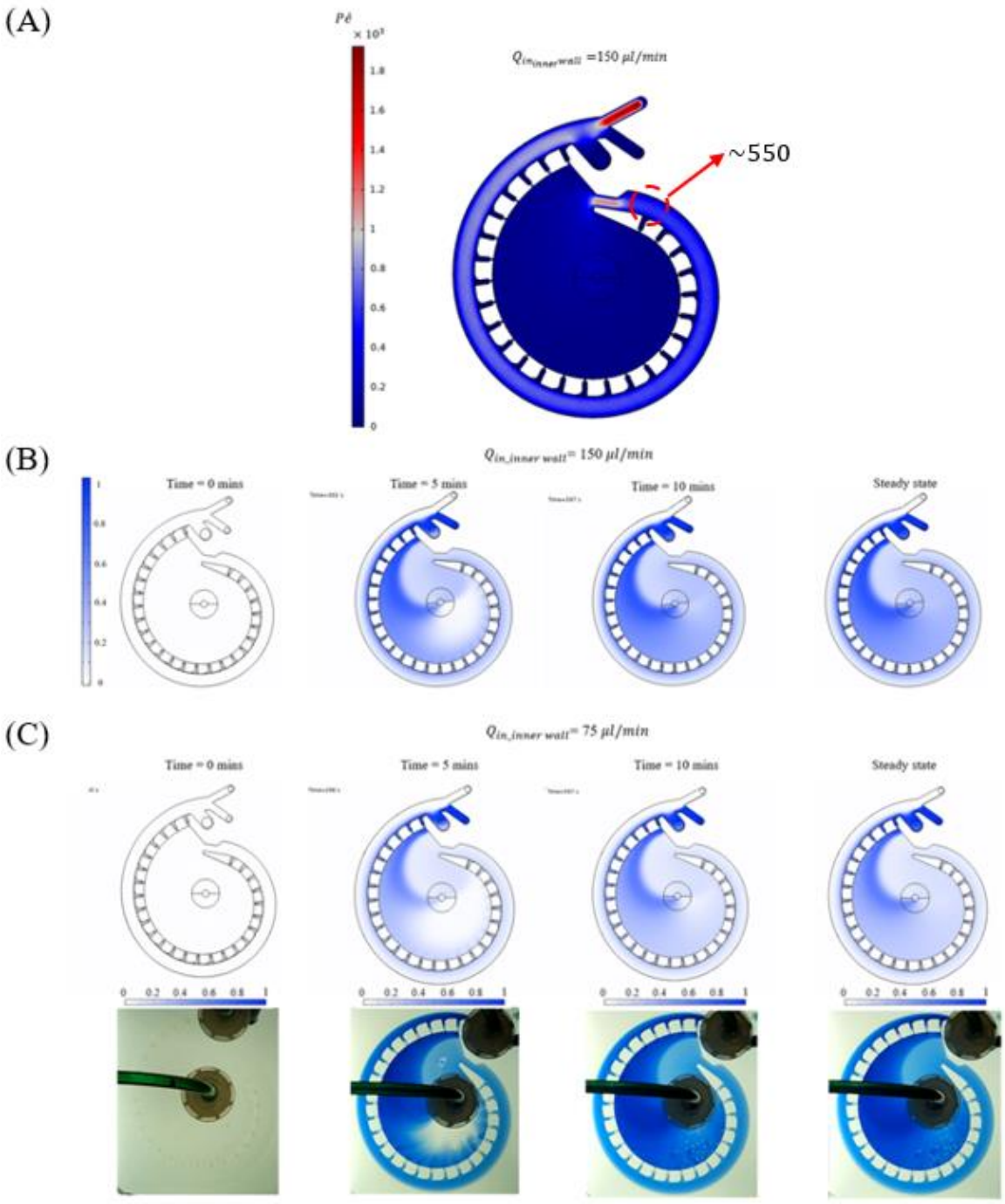

Figure 4.8. The convective-based dynamic concentration gradient generation. A) The $P\acute{e}$ number heatmap in CGG when $Q_{in\_inner\ wall}$ is 150 $\mu l/min$ (i.e., minimum relative velocity). The lowest $P\acute{e}$ number is about 550 (dash line circled area). B) Time-dependent mass transfer simulations showing the concentration gradient at each time point when $Q_{in\_inner\ wall}$ is 150 $\mu l/min$. C) Time-dependent mass transfer simulation as well as validation experiment showing the concentration gradient at each time point when $Q_{in\_inner\ wall}$ is 75 $\mu l/min$. The $Q_{in\_outer\ wall}$ is maintained at 300 $\mu l/min$.

The duration of the zebrafish embryo chemical toxicity tests is limited by both the temporal resolution of the pump and the zebrafish embryo growth rate. In this study, we employed a syringe pump that is compatible with 60 ml syringe. Therefore, the maximum testing window was around 3.33 hours when applying a constant $Q_{in\_outer\ wall}$ of 300 $\mu l/min$ for the dynamic concentration gradient generation. Also, since the dynamic concentration gradient generation is highly sensitive to changes in fluidic velocity fields, the size increase of the zebrafish embryo would increase the hydraulic resistance inside the traps and thus varies the fluidic velocity field. The 3.33-hour test window is considered suitable for the CGG-based acute FET test as the zebrafish embryo size increase is not that significant and the variations in concentration levels are expected to be minor.[9] According to the OECD's guideline for the acute FET tests (TG 236), the chemical exposure time for the zebrafish embryo needs to be 96 hours. We are aware that our CGG cannot fully meet the OECD's requirements for the acute FET. The acute zebrafish embryo chemical toxicity tests demonstrated in this study only focuses on some extreme cases where the sublethal endpoints (e.g., tail curvature, pericardial edema, yolk sac edema, etc.) can be developed after short period of chemical exposure (i.e., less than 3.33 hours).

For the live zebrafish embryo assays, the shear stress impact to the embryonic development is another factor that needs to be considered. Although some previously reported ZOCs and flow through systems have shown that the continuous flow is unlikely to cause morphonology changes or development abnormality on zebrafish embryos.[5,10] Other studies as well as our study in chapter 2 have demonstrated the shear stress exerted by fluidic flow can cause hatching delay and abnormal postures in the zebrafish embryos cultured in the flowthrough environments.[11] Based on the CFD simulations, the maximum shear stress is found on the upper surface of the embryo body inside the trap. When applying the highest overall flowrate (i.e., 300 $\mu l/min + 150\ \mu l/min = 450\ \mu l/min$) for concentration gradient generation, the maximum shear stress can reach approximately 0.021 Pa on the embryo in the first trap (Figure 4.9.A). Also, the maximum shear stress is about 0.0835 Pa on the embryos when applied 2 ml/min (i.e., the lowest flowrate for the peristaltic pump) for close loop perfusion (Figure 4.9.B). The maximum shear stress level for both operation modes are lower than the maximum shear stress of 0.088 Pa reported by Fuad et al. which is considered as a low shear stress environment for the zebrafish embryonic development and is expected not to cause development abnormalities for the zebrafish embryos.[5]

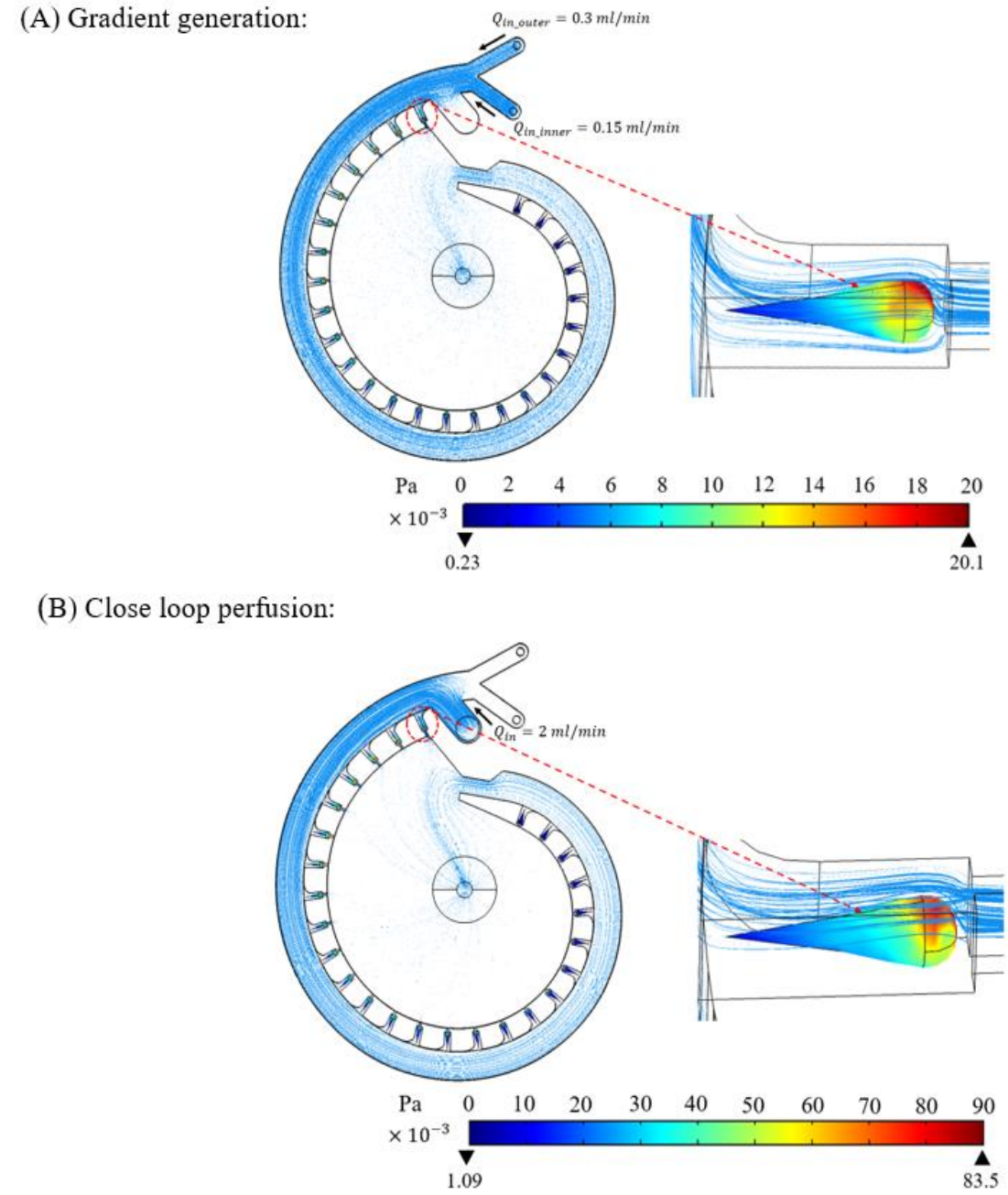

Figure 4.9. The zebrafish embryo body shear stress heatmap at different CGG perfusion modes. A) The zebrafish embryo body shear stress heatmap during concentration gradient generation using the maximum $Q_{in\_inner\ wall}$ and $Q_{in\_outer\ wall}$.B) The zebrafish embryo body shear stress heatmap during close loop perfusion at 2 ml/min. The zebrafish embryo at the first trap is selected for the maximum body shear stress demonstration.

The zebrafish embryos are exposed in the steady state concentration gradient for the acute FET test. Based on the mass transfer simulations and validation experiments, the interface of the two miscible streamlines is found to shift towards the inner wall traps along the spiral

main channel. This interface shifting is due to the hydrodynamic suction flows that pass through the traps. Besides, the degree of interface shifting is dependent on the flowrate ratios of the two inlets as the "thickness" of the inner wall streamline decreases when $Q_{in\_inner\ wall}/Q_{in\_out\ wall}$ decreases (Figure 4.10.). At steady state, the two streamlines form "Taichi-like" concentration gradient patterns in the CGG.

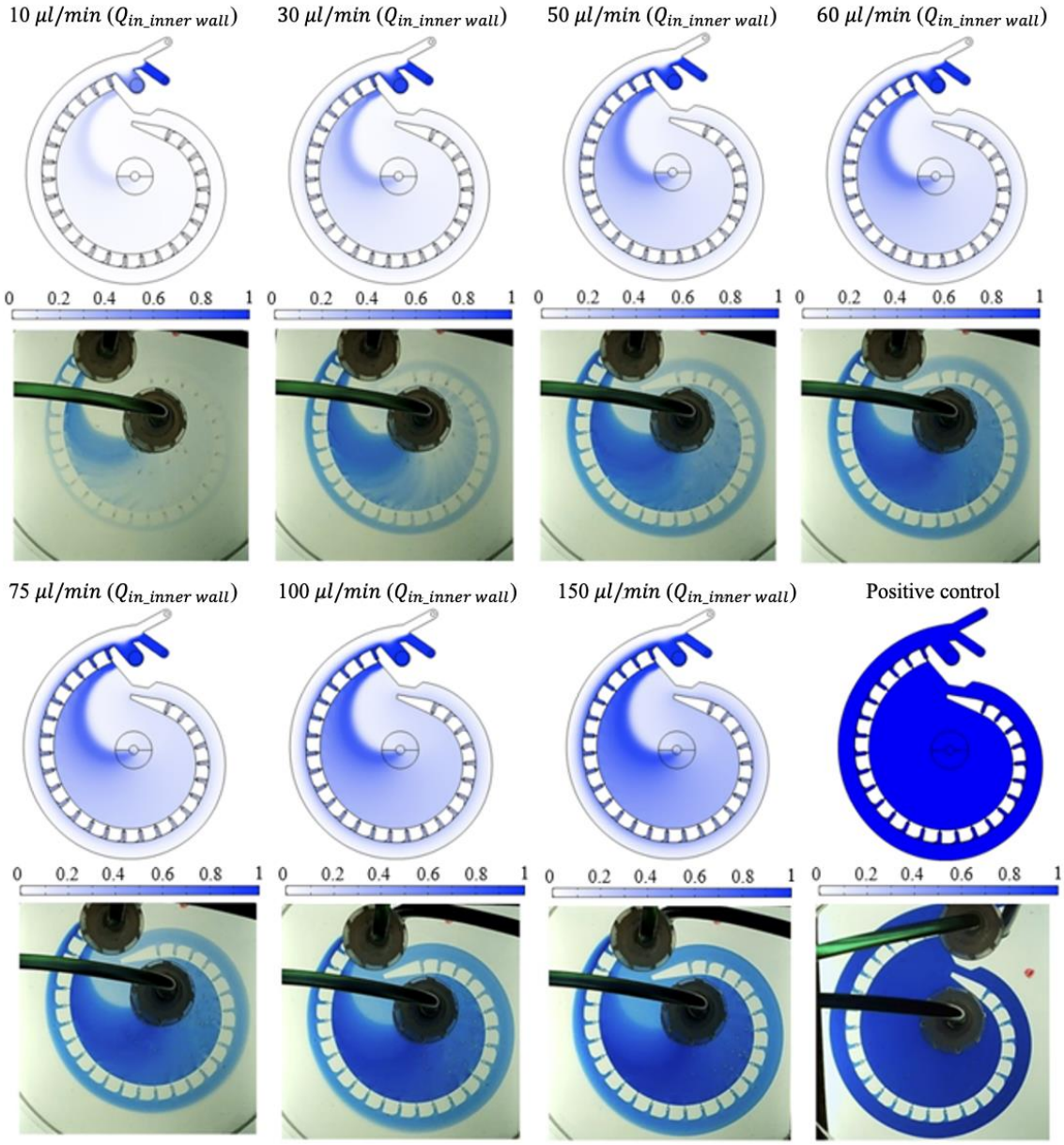

Figure 4.10. The steady state concentration gradients at different $Q_{in\_inner\ wall}$. The mass transfer simulation and validation results are paired at each row in the top panel and bottom panel, respectively.

The acute FET test demonstrated in the next section selects caffeine as the testing chemical. For the test, the outer wall inlet is perfused with E3 buffer at a constant flowrate of 300

$\mu l/min$ ($Q_{in\_outer\ wall}$).To track the caffeine concentration, 0.04% trypan blue/ 2 mg/ml caffeine mixture is perfused through the inner wall inlet. Five inner wall inlet flowrates ($Q_{in\_inner\ wall}$) viz. 10 $\mu l/min$, 30 $\mu l/min$, 75 $\mu l/min$, 100 $\mu l/min$, and 150 $\mu l/min$ are selected for steady state caffeine concentration simulations and measurements. Based on the mass transfer simulation, the concentration level and gradient range at steady state depend on the flowrate ratio between the inner wall inlet and outer wall inlet. The concentration level increases while the gradient range decreases when $Q_{in\_inner\ wall}/Q_{in\_outer\ wall}$ increases (Figure 4.11.). For instance, the concentration in the first trap can reach a minimum of 0.7 mg/ml when $Q_{in\_inner\ wall}$ is 10 $\mu l/min$ (i.e., $Q_{in\_inner\ wall}/Q_{in\_outer\ wall}=\frac{1}{30}$, the lowest ratio). Meanwhile, the concentration difference between the first and last trap reaches a maximum of 6.5 times.

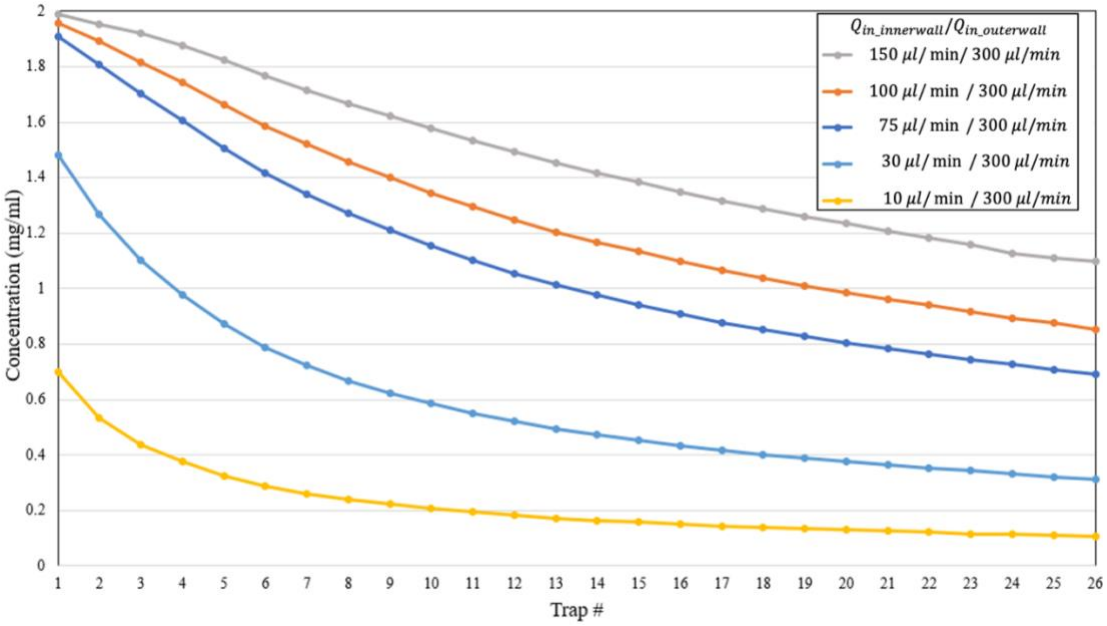

Figure 4.11. The simulated steady state caffeine concentration distribution in the traps of CGG.

For experimental measurements, the steady state concentration level at each individual trap was estimated by the trypan blue intensity. A MATLAB script was created to quickly obtain the trypan blue/caffeine mixture intensities at each individual trap (section 4.2.4). The experimental concentration measurements showed similar, yet trembling trends to the simulation results (Figure 4.12.). The trembling and varied experimental concentration measurements were due to the limitations of the imaging tools as well as the surrounding environment. In this study, we integrated the ZOC system with a USB microscope and an LED light source for imaging. We realized the CMOS digital camera used in the USB microscope has a poor light sensitivity for the intensity measurement and is susceptible to the noise (i.e., environment light). Moreover, the intensity on the LED light source was found not evenly distributed (data not shown). To ensure accurate concentration measurements in the future, additional image processing is necessary to increase the signal

to noise ratio. Also, image acquisition using a CCD camera, a stable light source, as well as, in a low noise environment may improve the overall concentration measurements.

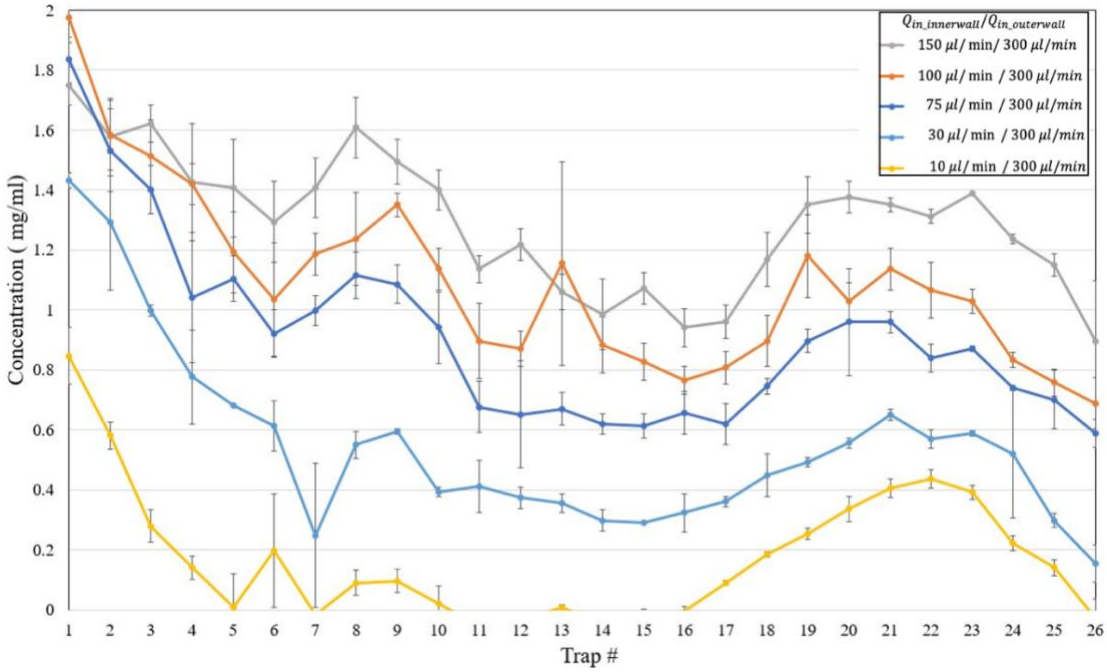

Figure 4.12. The measured steady state caffeine concentration distribution in the traps of CGG (N≥ 3, error bar:±SD).

4.3.4 Well plate-based Acute FET test for Caffeine Overdose Study

Caffeine is a natural psychoactive substance that is widely consumed by adults and children in the form of drinks, foods, or medicines.[12] When caffeine is consumed, it competes with adenosine, a nucleotide that has similar structure to caffeine and is important in regulating the physiological activities such as neural activity, heart rates, vasoconstriction/vasodilation, and energy metabolism.[12] According to the U.S. Food and Drug Administration, a moderate 400 mg daily caffeine consumption is generally considered safe for healthy adults.[13] However, the excessive caffeine consumption or caffeine overdose in some groups of people may cause adverse effects such as nausea, vomiting, regular heart, and even death.[14] There are numerous studies that have used zebrafish embryos to investigate the toxicity of caffeine.[15–17] In 2010, Rana et al. reported the study on the effect of caffeine on zebrafish embryo heart rate. They found the acute treatment with millimolar concentration of caffeine can decrease the heart rate in 48 hpf to 72 hpf zebrafish embryos in a dose-dependent manner and eventually stop the heart when keep increasing the dose.[17] Other secondary endpoints include cardiac arrhythmia and trunk/tail kinking were also reported after the acute caffeine treatments in Rana et al. 's study.[17] In 2015, Lantz-McPeak et al. used a high content screening technique to measure the acute toxicity of caffeine to the zebrafish embryo.[18] In their study, the 28 hpf zebrafish embryos were treated with caffeine for 24 hours and the embryos with over 0.5 mM (~ 0.1 mg/mL) caffeine treatment were found to have abnormal developments.[18]

Most caffeine acute toxicity studies followed the OECD guideline TG 236 to test the acute toxicity of caffeine. Despite it being a simple and robust method for assessing acute chemical toxicity, TG 236 has limitations to simulate complex chemical exposure scenarios. For instance, caffeine is usually used as a "morning awaking" or "later night boosting" chemical and is consumed intermittently throughout the day. The continuous caffeine exposure to zebrafish embryos for multiple day experiments may not be suitable for simulating the effect of daily caffeine consumption. In addition, the OCED guideline TG 236 for acute FET test determines the lethality by the 4 core endpoints viz. coagulation of fertilized eggs, lack of somite formation, lack of detachment from the yolk sac, and lack of heartbeat.[1] Because the focus is shifting toward the detection of lethal endpoints, the concentration-dependent sublethal endpoints are sometimes neglected in the acute FET tests which can be critical in understanding the toxic effects for certain chemicals.[19]

In this study, the objective is to investigate the instant effects of caffeine overdose as well as how these effects change during the recovery period. To restore a more realistic caffeine consumption scenario, a much shorter zebrafish embryo caffeine treatment time was used compared to the standard acute FET test procedure. Furthermore, most of the zebrafish embryos were exposed to an extensive amount of caffeine in this short period to simulate the caffeine overdose. Most importantly, to capture the instant effect of caffeine overdose, the temporal feature of the sublethal endpoint was considered in the screening and the sublethal endpoints are ranked by their timing of occurrence during the test. For the experiment setups, specifically, the zebrafish embryos were treated with caffeine for 2 hours following 24 hours recovery in E3 buffer (section 4.2.3). During the static experiments, the zebrafish embryos were treated with 6 caffeine concentrations, 2 mg/mL, 1 mg/mL, 0.5 mg/mL, 0.125 mg/mL, 0.0325 mg/mL, and 0 mg/mL (control) for the 2 hours in the 24-well plate (10 embryos per well, $N \geq 4$). The survival rate and sublethal endpoints were recorded after the 2-hour treatment and 24-hour recovery (Figure 4.13.). Note the caffeine was also mixed with 0.04% trypan blue for the later comparison with CGG-based caffeine overdose test.

Figure 4.13. The short-term well plate-based zebrafish embryo caffeine overdose study. Top: representative images for the zebrafish embryos after 2-hour caffeine treatment in well plate. Bottom: representative images for the zebrafish embryos after 24-hour recovery in well plate.

The zebrafish embryos showed a strong vitality in the 2-day experiment in which over 90% of zebrafish embryos can survive at the end of the experiment and no significant survival rate drop was observed in all caffeine concentrations (Figure 4.14.A). This indicated the selected caffeine concentrations were unable to trigger lethal endpoints in the zebrafish embryos within the experiment period. After the 2-hour caffeine treatment, the very first and most prominent sublethal endpoint found in the zebrafish embryos was the tail curvature (i.e., scoliosis) (Figure 4.14.B). The frequency of the zebrafish embryo tail curvature was found to be concentration dependent as the tail curvature event became more frequent as the caffeine concentration increased (Figure 4.14.C). The degree of embryo tail curvature was also seen to be concentration dependent as pig-tail-like tail curvatures were usually found at high caffeine concentrations. In addition, most of the zebrafish embryos with tail curvature were found to be recovered to normal after 24 hours culturing in E3 buffer. Because of the early timing of tail curvature development, it was marked as the primary sublethal endpoint for the zebrafish embryo caffeine overdose effect.

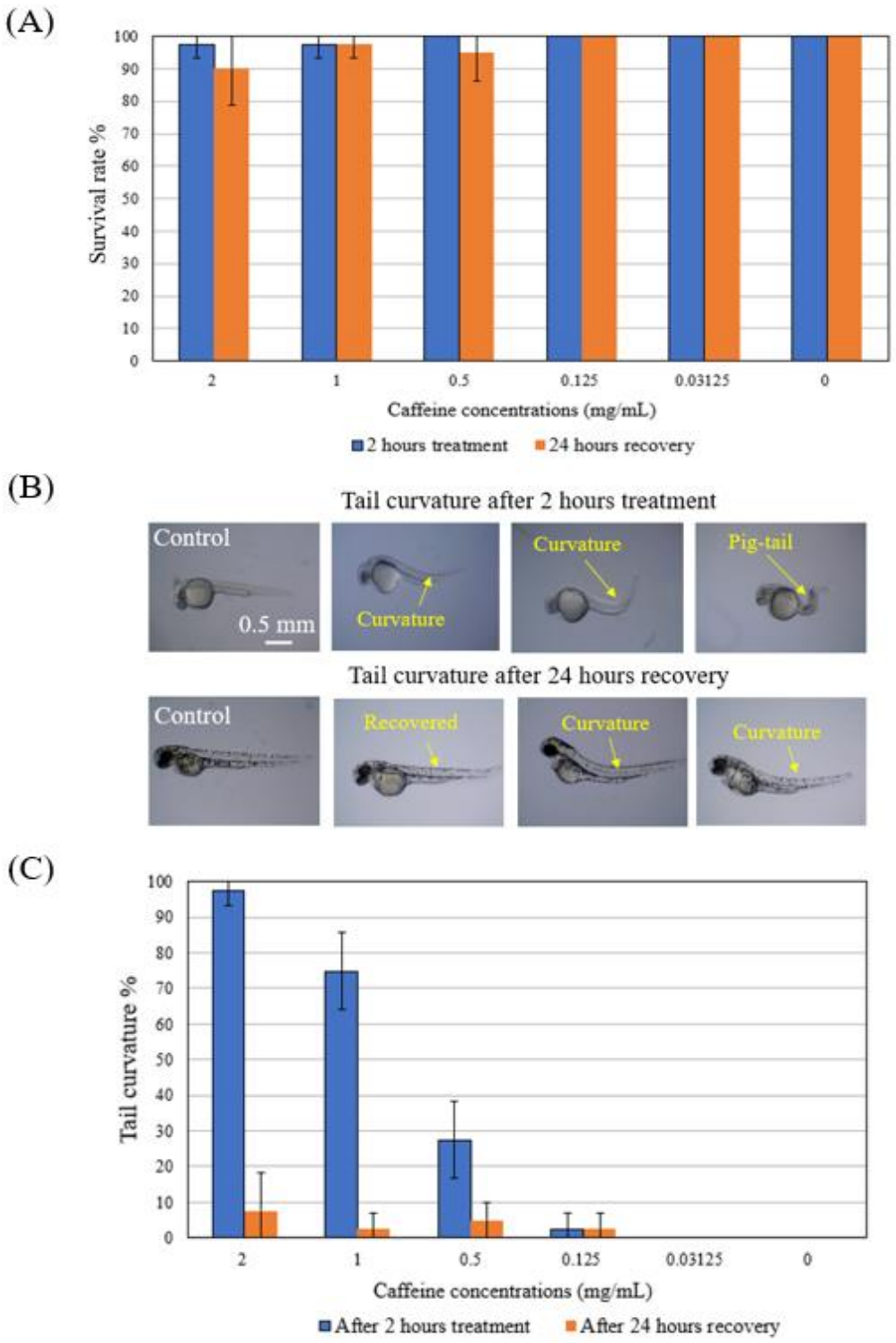

Figure 4.14. The zebrafish embryo endpoint screenings in 24-well plate. A) The zebrafish embryo survival rate after 2-hour caffeine treatment and 24-hour recovery in well plate. B) microscopy imaging showing tail curvature in the zebrafish embryo after 2-hour caffeine treatment (top) and 24-hour recovery (bottom). C) The tail curvature occurrence rate at different caffeine concentrations in day 1 and day 2 screening (N≥ 4, error bar:±SD).

Another phenotype that was detected after the 24-hour recovery is edema (Figure 4.15.A). Both yolk sac edema (YE) and pericardial edema (PE) were observed after 24 hours of recovery. However, the edema prevalence is low in the well plate and can only be found at the highest caffeine concentration, 2 mg/mL (Figure 4.15.B). Because of that, edema is considered as a secondary endpoint for the instant caffeine overdose treatment. Note YE and PE are not distinguished and were both classified as edema in this study.

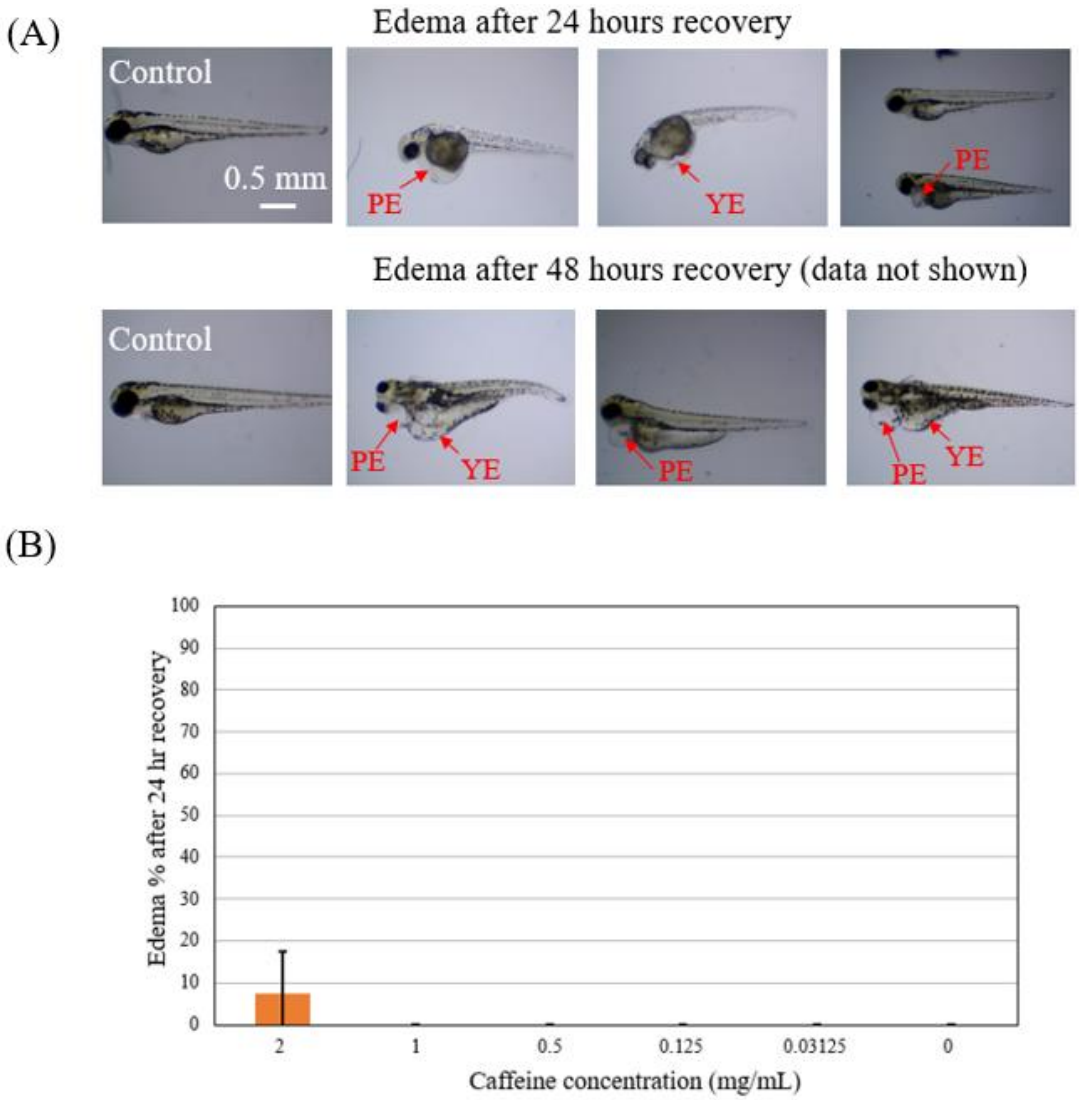

Figure 4.15. Edema detection after 24-hour recovery in 24-well plate. A) zebrafish embryo developed with edema after 24-hour recovery (top) and 48-hour recovery (bottom). B) The edema occurrence rate after 24-hour recovery at different caffeine concentration ($N \geq 4$, error bar:$\pm$SD).

Collectively, within the current experiment settings, the chosen caffeine concentrations were able to simulate the caffeine overdose scenarios in the zebrafish embryo. The tail curvature is identified as the primary sublethal endpoint for the zebrafish embryos after the

short-term caffeine treatment in the well plate and is expected to be detected in CGG-based caffeine overdose tests as well.

4.3.5 CGG-based Acute FET Test for Caffeine Overdose Study

The studies reported by Zhu et al. and Fraud et al. have shown the milli fluidic-based zebrafish embryo culture has the advantages in real time monitoring embryonic development and detecting sublethal endpoints.[20,21] In their studies, the acute FET tests were modified by integrating additional sublethal endpoints with the 4 lethal endpoints to form a new index, iFET (Sublethal Fish Embryo Toxicity Index), for acute chemical toxicity assessments.[20,21] Besides, the results of the acute FET test performed by their milli fluidic devices were strongly correlated with results generated by the well plate-based method in testing stable chemical and was found more dose-effective in testing unstable chemicals such as nicotine.[20,21] In this study, we used similar strategies as Zhu et al. and Fraud et al. in measuring the concentration related sublethal effect. Yet, due to the temporal features of the sublethal endpoints, the iFET which was used to pack a suite of endpoints for dose-response analysis was not used here. Instead, "the most instant sublethal endpoint" during/after the caffeine treatment was targeted for the dose-response analysis.

During the acute FET test in CGG, the zebrafish embryos were treated under 3 steady state caffeine concentration gradients for 2 hours. Specifically, the caffeine concentration gradients were generated by using 75 $\mu l/min$, 100 $\mu l/min$, and 150 $\mu l/min$ as the inner wall inlet flowrates ($Q_{in\_inner\ wall}$). As demonstrated in section 4.3.3, 2 mg/mL caffeine/0.04% trypan blue mixture was perfused through the inner wall inlet and mixed with E3 buffer loaded at the outer wall inlet for the dynamic concentration gradient generation (N ≥ 6). The outer wall flowrate ($Q_{in\_outer\ wall}$) was kept constant at 300 $\mu l/min$. For positive control, 150 $\mu l/min$ was used as inner wall inlet flowrate ($Q_{in\_inner\ wall}$) and both inner wall and outer wall inlets were perfused with 2 mg/mL caffeine/0.04% trypan blue mixture. The steady state caffeine concentration gradients for the 3 selected flowrates can cover a caffeine concentration range (i.e., from 0.69 mg/mL to 2 mg/mL) that is expected to induce abnormality in the zebrafish embryos during/after the 2-hour treatment. For the 24-hour recovery, the caffeine was first flushed out of the CGG by the E3 buffer after the 2-hour treatment. The E3 buffer then circulates in the CGG system at 2 mL/min for the 24-hour recovery.

In terms of embryo vitality, the zebrafish embryos cultured in the CGG had a survival rate that is close to the zebrafish embryo tested in the well plate throughout the experiment without any significant drop between the first day and second day monitoring (Figure 4.16.).

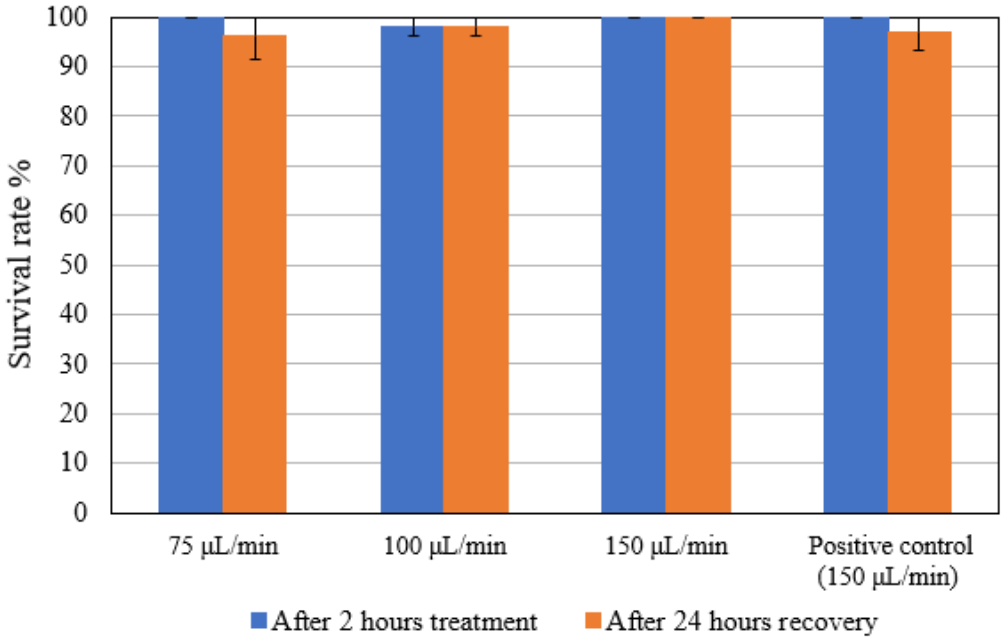

Figure. 4.16. The zebrafish embryo survival rate after 2-hour caffeine treatment and 24-hour recovery in CGG (N=6, error bar:±SD).

As expected, the tail curvature identified in the well plate was also observed in the zebrafish embryos tested in the CGG. The overall tail curvature events were found elevated when increased the flowrate at the inner wall inlet (Figure 4.17.). Besides, no significant difference in overall tail curvature rate was found between the CGG positive control and the highest caffeine concentration (i.e., 2 mg/mL) treatment group in well plate.

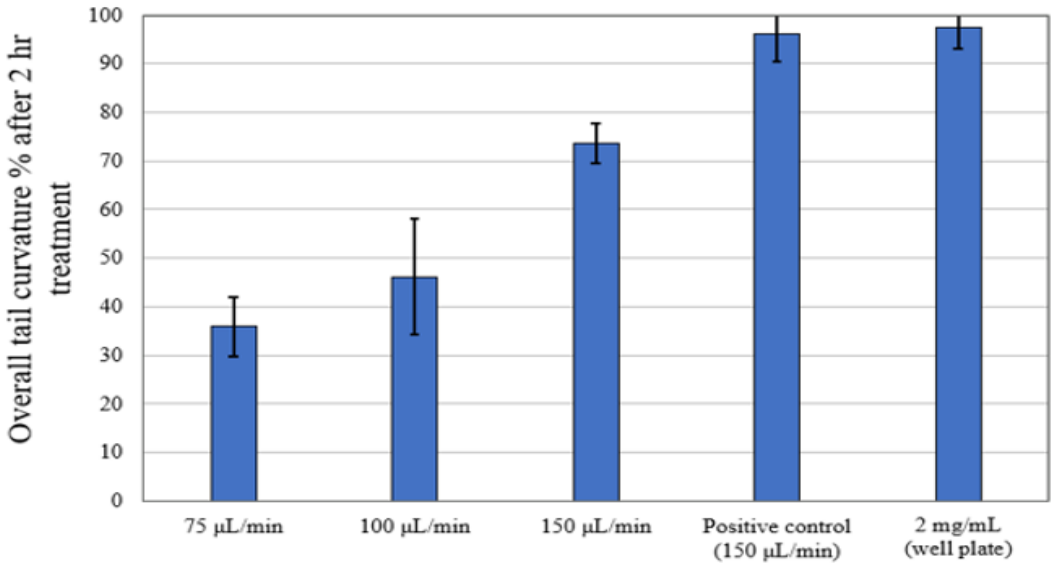

Figure 4.17. The overall tail curvature occurrence rate after 2-hour treatment at different steady state caffeine concentration gradients in CGG (N=6, error bar:±SD) and the 2 mg/mL caffeine treatment in well plate (N≥4, error bar:±SD).

The zebrafish embryo tail curvature frequency distribution in the CGG was found following the caffeine concentration gradient as the tail curvature events were more frequent in the upstream traps (Figure 4.18.A). Moreover, when the overall caffeine concentration is elevated by increasing the flowrate at the inner wall inlet, the tail curvature occurrences shift towards the downstream traps. Consistent with what was found in well plate-based tests (data not shown), the degree of zebrafish embryo tail curvature also seems to correlate with the caffeine concentration as the “severe tail curvatures" such as pig-tail were often found at the upstream traps (Figure 4.18.B).

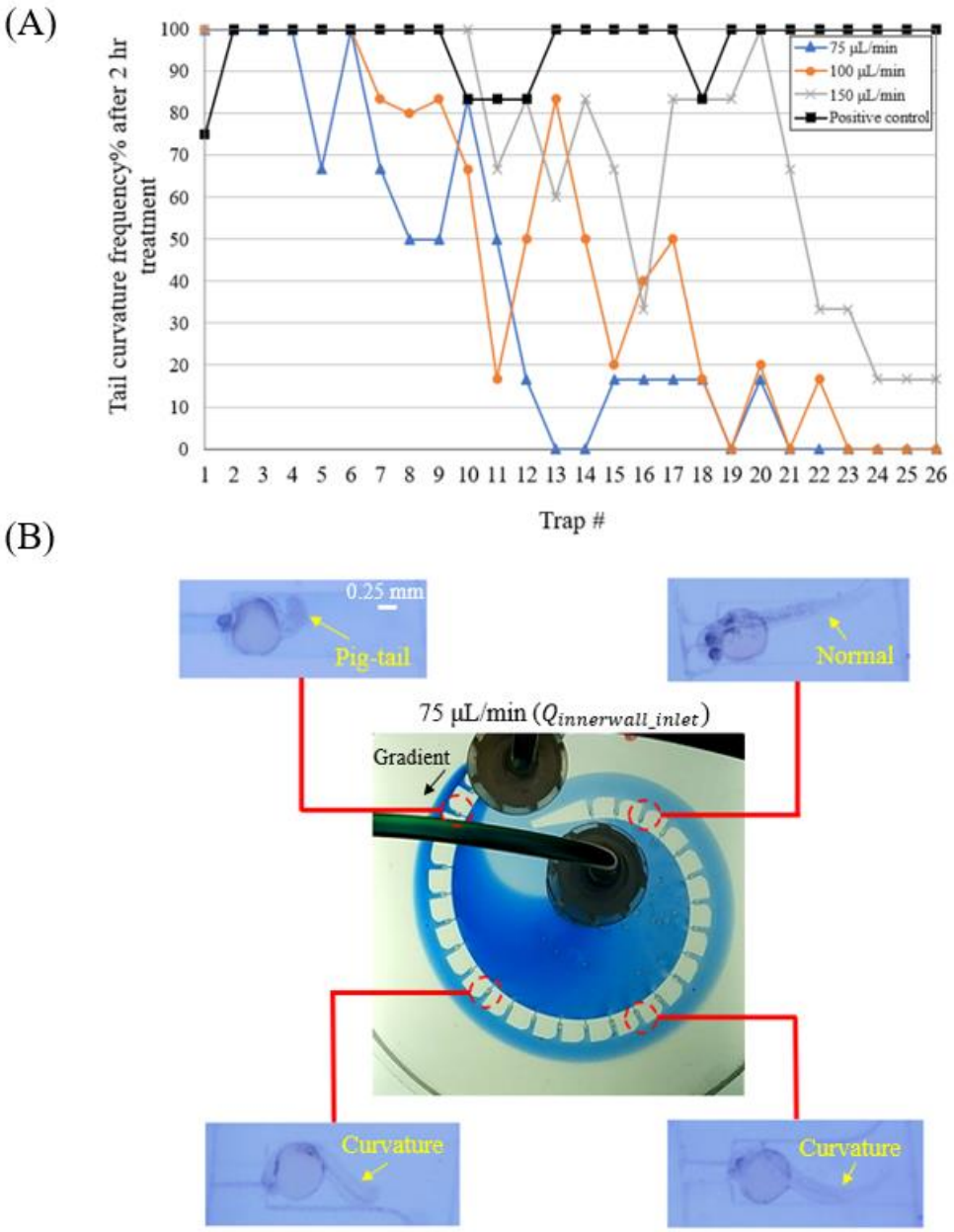

Figure.4.18. The zebrafish embryo endpoint screening in the CGG. A) Tail curvature frequency distribution in the traps of CGG at different steady state concentration gradients (N=6, error bar:±SD). B) Representative images showing a potential dosage dependent embryo tail curvature degree in the CGG.

Overall, the sublethal endpoint, tail curvature, can be easily detected and parallelly compared in the CGG during/after the 2-hour caffeine treatment. However, the embryos preserved with the tail curvature after 24-hour recovery were found difficult to identify. The folded body postures, which were reported in chapter 2, were also observed in the zebrafish embryos cultured in the CGG on day 2. The folded body postures were initially suspected to be caused by the crossflow and the high shear stress level used in chapter 2.

Here, we believe that the crossflow is more likely to be the main cause of the abnormal postures, as the shear stress has already been reduced to a level that is close to what has been previously reported as a low shear stress level.[20] In the current trap dimension, the zebrafish embryos would slightly outgrow the trap after 48 hpf and some of their body may be exposed to the flow at the main channel (i.e., continuously "hit" by the main channel flow) and trigger the abnormal postures (Figure 4.19). Due to the ambiguity of zebrafish embryo's tail postures, the attempts to quantify the embryos preserved with the tail curvature may cause false positive results after 24-hour recovery. Therefore, the measurements for zebrafish embryos with tail curvature were excluded in the CGG on day 2.

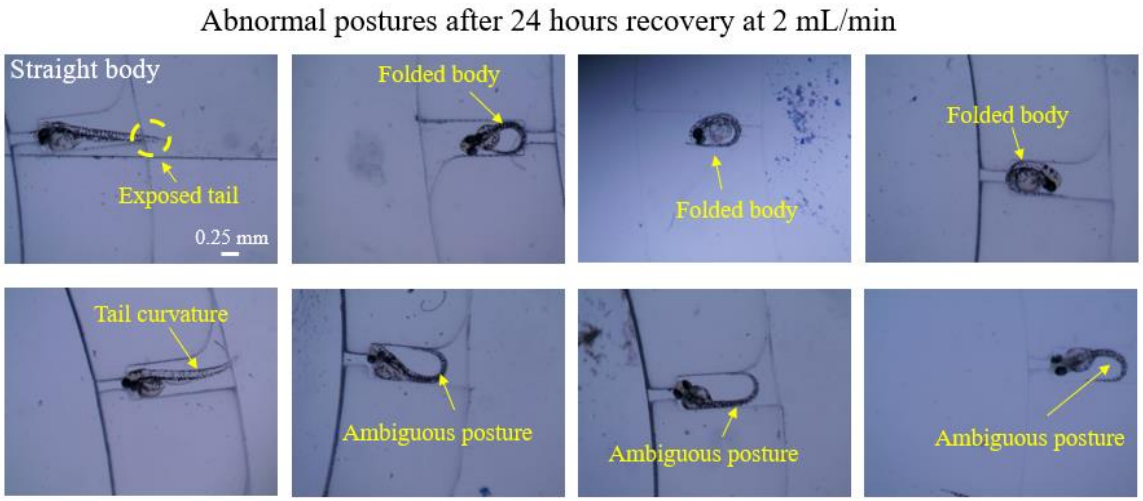

Figure 4.19. Ambiguous tail curvature detection after 24-hour recovery in CGG due to the zebrafish embryo abnormal postures.

In addition to the tail curvature, edema was found surprisingly prevalent in the zebrafish embryos cultured in the CGG after 24 hour-recovery (Figure 4.20.A). In contrast to the tail curvature, the development of edema in the zebrafish embryos seems more sensitive to the flowthrough environment as the overall frequency of edema occurrences was significantly higher in the CGG than in the well plate (Figure 4.20.B). The increased caffeine concentration level was also found to affect the edema development as the occurrence of edema increased when using higher inner wall inlet flowrates (i.e., more caffeine introduced). In this study, edema was not targeted as the primary sublethal endpoint for the instant caffeine overdose effect investigation. Therefore, the measurement for edema frequency distribution in the CGG was excluded in this study. The recovery effect and the occurrence time differences of the tail curvature and edema suggested that the FET and iFET-based endpoint packing methods may not be ideal for the evaluation of short-term chemical overdose effects as the iFET various overtime and may not contributed by same set of sublethal points. For future experiments using the CGG, it will be valuable to investigate the temporal features as well as the effect of flowthrough environment to the zebrafish embryo edema development.

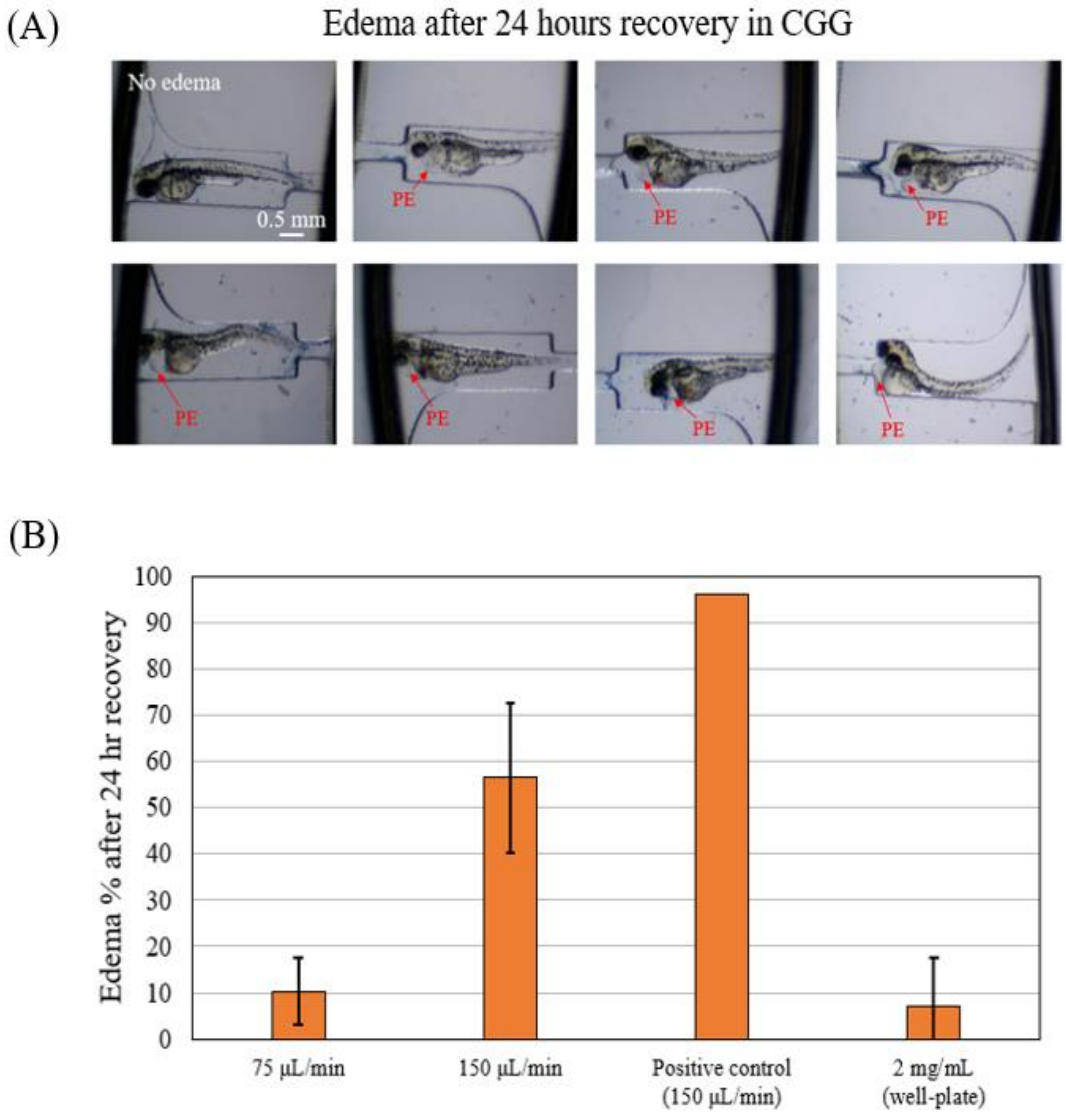

Figure 4.20. Zebrafish embryo edema screening after 24-hour recovery in the CGG. A) Microscopy images showing edema detection in the zebrafish embryo after 24-hour recovery in CGG. B) The edema occurrence rates after 24-hour recovery in CGG at different steady state caffeine concentration gradients (N=6, error bar: ±SD) and in 2 mg/mL well plate caffeine treatment (N=7, error bar:±SD) Note N=1, for CGG positive control.

As demonstrated above, during the 2-hour treatment, the zebrafish embryos can develop tail curvature as a response to the different caffeine concentrations. To analysis how the tail curvature is affected by the different caffeine concentrations during the 2-hour treatment window, the dose-response curves for the 3 steady state caffeine concentration gradients as well as the well plate-based caffeine toxicity test were generated for comparison. Due to the limitations in the experimental concentration measurements in the CGG, the concentrations from both simulation estimations (Figure 4.11) and experimental measurements (Figure 4.12) are employed in generating the dose-response curve for the 3

steady state caffeine concentration gradients. Note, for comparison, the top and bottom for all the dose-response curves are constrained as 100% and 0%, respectively.

The absolute EC50 (50% effective concentration) for the caffeine during the 2-hour well plate based acute toxicity test is found to be 0.6904 mg/mL. For the CGG-based test, when using the simulated concentrations, the absolute EC50 for the 3 caffeine concentration gradients were found to be 1.175 mg/mL, 1.220 mg/mL, and 1.208 mg/mL, from lowest to highest inner wall inlet flowrates (Figure 4.21.A). Similarly, the absolute EC50 values were found to be 0.9932 mg/mL, 1.080 mg/mL, and 0.9869 mg/mL, from lowest to highest inner wall inlet flowrates, for the 3 tested gradients when inputting the measured concentrations (Figure 4.21.B). All the absolute EC50 values found in the CGG are higher than the absolute EC50 value for the well plate-based method which indicates the caffeine is less effective to trigger the tail curvature endpoint in the CGG than in the well plate during the 2-hour treatment. In addition, the hillslope values for the dose-response curves generated by the CGG are greater than the hillslope of well plate-based dose-response curves. The steeper dose-curves in the CGG suggested the zebrafish embryo is more concentration sensitive to the caffeine in the CGG than in the well plate during the 2-hour treatment. Furthermore, the absolute EC50 values and hillslope values found in CGG are close to each other among the 3 tested caffeine concentration gradients which indicates an excellent consistency for CGG-based acute caffeine FET tests.

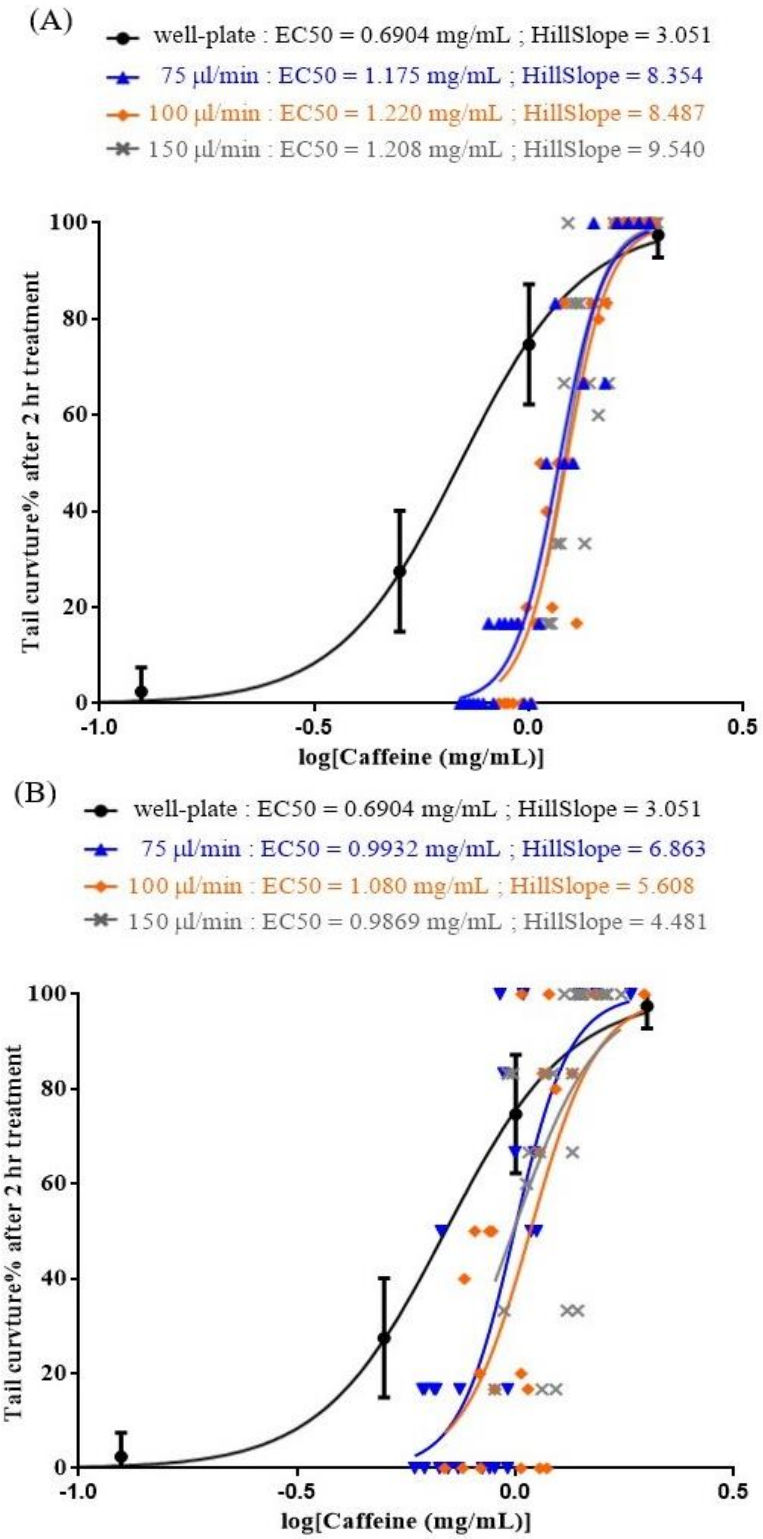

Figure 4.21. Dose-response curves for the caffeine concentration related zebrafish embryo tail curvature. A) The dose-response curve when using simulated concentrations. B) The dose-response curve when using measured concentrations.

In a nutshell, the CGG demonstrated in this work has proved to be feasible in performing short-term zebrafish embryo caffeine overdose study. The tail curvature, which was observed in the well plate-based test was also observed in the CGG and was identified as the primary sublethal endpoint for the acute caffeine overdose effect. In addition, the zebrafish embryos were found to have a changing response to the different caffeine concentrations in the CGG which is consistent with the observations in the well plate. The CGG was found to be an effective tool in real-time embryo monitoring, parallel phenotype comparison, as well as high resolution dose-response analysis. Moreover, the caffeine dose-response curves for the embryo tail curvature were able to be obtained by replicating the high-resolution acute FET tests in the CGG (i.e., 6 replicates per gradient). Interestingly, the comparisons between the caffeine dose-response curves generated by the CGG-based and well plate-based methods have shown that the zebrafish embryos have stronger caffeine tolerance (i.e., larger EC50), yet are more caffeine concentration sensitivity (i.e., larger hillslope) in the CGG than in the well plate. To our best knowledge this finding has not been reported by similar studies conducted in ZOC or well plate which can be useful in understanding the mechanism of caffeine overdose effects.

4.4 Conclusion and Discussion

In this study, we reported the development and application of the multifunctional CGG for zebrafish immobilization, and high-resolution dose-response screening. Both experimental and CFD simulation methods have been employed to estimate the microenvironments (i.e., flowrate, shear stress, and concentration) inside CGG when the zebrafish embryos are on board. The CGG has also been shown to be capable of generating various concentration gradients by adjusting the flowrates at the Y branch inlets. Furthermore, the concentration levels inside the CGG were able to be traced by trypan blue colorimetric methods or estimated by using mass transfer simulation. The proof-of-concept zebrafish embryo acute caffeine overdose study has shown that the CGG is effective in high-resolution dose-response analysis and the embryos tested in the CGG's flowthrough environment would have different dose-response level compared to the embryo tested in the static well plate. At last, the temporal characteristics of the sublethal endpoints found during the "caffeine overdose and recovery study" reveals the conventional FET and iFET toxicity index-based evaluation methods is not suitable to analysis the dose-response of specific "instant toxic effect" as well as to simulate realistic consumption scenarios of some chemicals.

The feature, "one embryo per trap" is the most significant advantage for the CGG-based phenotype screening, however it is also the major disadvantage for concentration dependent tests as one embryo only corresponds to one concentration. This lowers the throughput and leads to the binary results at each concentration level. The present work tested the 3 caffeine concentration gradients with 6 replicates per gradient in the CGGs which are still inadequate to draw a very decisive conclusion for the caffeine dose-response analysis. To address the sample size limitation, one way is to connect the multiple CGGs in parallel using flow splitters such as a 3-way valve (i.e., 2-way flow splitter). In this case, the sample size for each concentration is dependent on the capacity of the flow splitter and the number of flow splitters used. Besides another way is to integrate our ZOC with other concentration gradient generators (e.g., the Christmas tree-like CGG) and only let the ZOC

to be used for downstream zebrafish embryos immobilization purpose (i.e., give up the concentration gradient generation feature).[6]

In addition to the sample size, another limitation for our CGG is the concentration gradient range is not wide enough for individual ZOC in a single run. One potential solution for this is to connect the CGGs and flow splitters in a certain order, so that more concentration gradients can be generated at the downstream CGGs (Figure 4.22.).

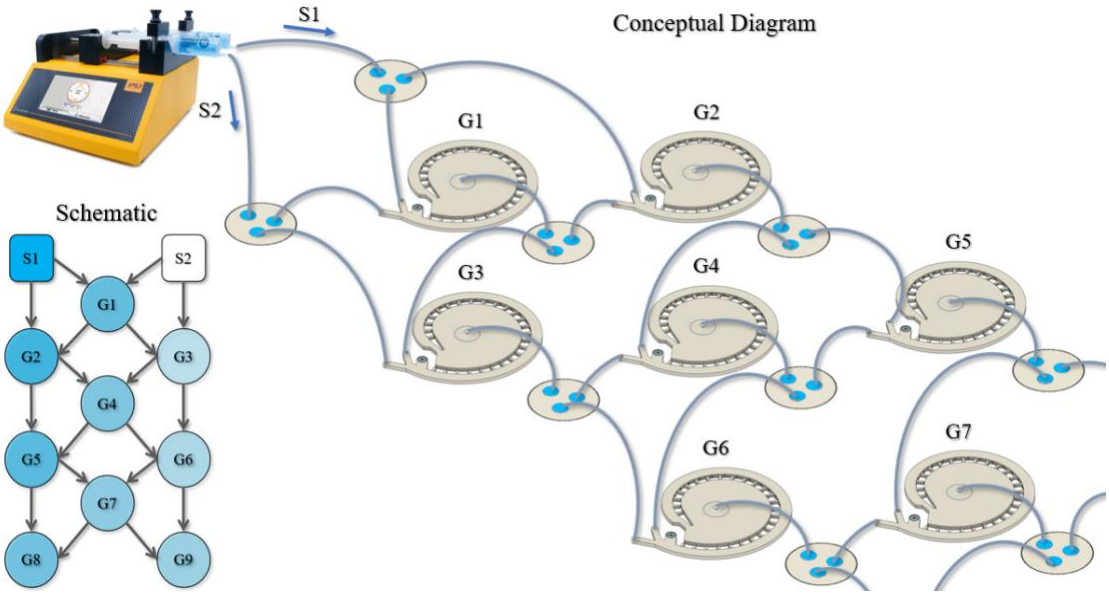

Figure 4.22. CGGs connection using 2-way flow splitters to create more concentration gradients.

Finally, due to the temporal resolution of the pumping system, the size increase impacts of the embryos, and the potential large reagent consumption for the dynamic concentration generation, the current CGG design is found only suitable for short-term zebrafish embryo chemical exposure tests and cannot meet the duration requirements of the OECD TG 236 guideline. To address these limitations, applying discontinuous dynamic concentration gradient generation as well as utilizing the feature of Laplace pressure-based droplet formation (section 2.3.4) would be a potential solution and are worth trying in the future.

In our current work, it is difficult to definitively conclude whether our CGG is more appropriate than the traditional well plate method for short-term zebrafish embryo chemical exposure test. This is because only caffeine has been tested so far, and both methods have yielded different results in the caffeine test. Despite this, some of the benefits of using CGG for acute FET tests have been demonstrated in this study and may be useful for chemical exposure studies of other substances. Hence, we hope our CGG design can be accepted by the research communities to encourage more people to use it for different chemical toxicity assessments.

4.5 References

1. OECD GUIDELINES FOR THE TESTING OF CHEMICALS: Fish Embryo Acute Toxicity (FET) Test. (2013).
2. Valle, N. M. E. *et al.* Advances in Concentration Gradient Generation Approaches in a Microfluidic Device for Toxicity Analysis. *Cells* **11**, 3101 (2022).
3. Yang, F., Gao, C., Wang, P., Zhang, G.-J. & Chen, Z. Fish-on-a-chip: microfluidics for zebrafish research. *Lab Chip* **16**, 1106–1125 (2016).
4. Frey, N., Sönmez, U. M., Minden, J. & LeDuc, P. Microfluidics for understanding model organisms. *Nat Commun* **13**, 3195 (2022).
5. Fuad, N. M., Kaslin, J. & Wlodkowic, D. Development of chorion-less zebrafish embryos in millifluidic living embryo arrays. *Biomicrofluidics* **11**, 051101 (2017).
6. Choudhury, D. *et al.* Fish and Chips: a microfluidic perfusion platform for monitoring zebrafish development. *Lab Chip* **12**, 892–900 (2012).
7. Inglesby, M. K. & Zeronian, S. H. Diffusion coefficients for direct dyes in aqueous and polar aprotic solvents by the NMR pulsed-field gradient technique. *Dyes and Pigments* **50**, 3–11 (2001).
8. Toh, A. G. G., Wang, Z. P., Yang, C. & Nguyen, N.-T. Engineering microfluidic concentration gradient generators for biological applications. *Microfluid Nanofluidics* **16**, 1–18 (2014).
9. Kimmel, C. B., Ballard, W. W., Kimmel, S. R., Ullmann, B. & Schilling, T. F. Stages of embryonic development of the zebrafish. *Developmental Dynamics* **203**, 253–310 (1995).
10. Wielhouwer, E. M. *et al.* Zebrafish embryo development in a microfluidic flow-through system. *Lab Chip* **11**, 1815 (2011).
11. Akagi, J. *et al.* Miniaturized Embryo Array for Automated Trapping, Immobilization and Microperfusion of Zebrafish Embryos. *PLoS One* **7**, e36630 (2012).
12. Temple, J. L. *et al.* The Safety of Ingested Caffeine: A Comprehensive Review. *Front Psychiatry* **8**, (2017).
13. Wikoff, D. *et al.* Systematic review of the potential adverse effects of caffeine consumption in healthy adults, pregnant women, adolescents, and children. *Food and Chemical Toxicology* **109**, 585–648 (2017).
14. De Sanctis, V. *et al.* Caffeinated energy drink consumption among adolescents and potential health consequences associated with their use: a significant public health hazard. *Acta Biomed* **88**, 222–231 (2017).
15. Basnet, R. M. *et al.* Caffeine inhibits direct and indirect angiogenesis in zebrafish embryos. *Int J Mol Sci* **22**, (2021).
16. Maeda, H., Hasumi, A. & Yoshida, K. ichi. Caffeine-induced bradycardia, death, and anxiety-like behavior in zebrafish larvae. *Forensic Toxicol* **39**, 427–436 (2021).
17. Rana, N. *et al.* Caffeine-Induced Effects on Heart Rate in Zebrafish Embryos and Possible Mechanisms of Action: An Effective System for Experiments in Chemical Biology. *Zebrafish* **7**, 69–81 (2010).
18. Lantz-McPeak, S. *et al.* Developmental toxicity assay using high content screening of zebrafish embryos. *Journal of Applied Toxicology* **35**, 261–272 (2015).
19. Hedgpeth, B. M. *et al.* Analysis of Sublethal Toxicity in Developing Zebrafish Embryos Exposed to a Range of Petroleum Substances. *Environ Toxicol Chem* **38**, 1302–1312 (2019).

20. Fuad, N. M., Kaslin, J. & Wlodkowic, D. Development of chorion-less zebrafish embryos in millifluidic living embryo arrays. *Biomicrofluidics* **11**, 051101 (2017).
21. Zhu, F. *et al.* Automated Lab-on-a-Chip Technology for Fish Embryo Toxicity Tests Performed under Continuous Microperfusion (μFET). *Environ Sci Technol* **49**, 14570–14578 (2015).

Chapter 5
Conclusion and Future Directions

5.1 Conclusion

The major achievement of this dissertation was the establishment of an automated, high-throughput, and multifunctional zebrafish testing platform including the development of novel zebrafish-on-a-chip (ZOC) milli fluidic systems and the demonstration of two applications using these systems for whole mount zebrafish antibody staining (ABS) and acute fish embryo toxicity (FET) test.

In that, the trapping ability of zebrafish embryo in the ZOC was systematically analyzed both theoretically and experimentally. The feasibility for ZOC-based zebrafish embryo culture was tested using both unhatched and dechorionated embryos. Trap geometry and shear stress were found to be the parameters affecting the zebrafish embryonic development and limiting the embryo culture duration. In addition, the ZOC's ability in streamlining and accelerating the zebrafish procedures was demonstrated by performing the whole mount zebrafish Caspase-3 antibody staining (ABS). The washing steps were targeted for optimization and were found to be accelerated by applying higher perfusion flowrates in ZOC. Also, the consistency and convenience of the procedure was improved using the ZOC. Moreover, the ZOC design's versatility was shown by modifying into a concentration gradient generator (CGG) and used for acute fish embryo toxicity (FET) test. The functionality of the CGG was examined by testing the zebrafish embryo caffeine overdose effects. The CGG was found to be excellent in high resolution dose-response screening (i.e., sublethal endpoints detection and parallel comparison), and concentration control. However, the throughput of the CGG-based acute FET test is low for individual concentration and can be further improved via parallel connection of CGGs. Besides, the CGG was found only suitable for short-term chemical exposure tests and cannot fully meet the OECD guideline for acute FET test, due to the temporal resolution of the syringe pump, embryo growth effects as well as the large reagent volume requirement for long-term test.

Overall, in this dissertation, the efforts in integrating lab-on-a-chip (LOC) technologies with zebrafish studies have shown promising outcomes in responding some of the needs in zebrafish research, yet limitations and room for improvements remain (Table 5.1). In addition, the applications of ZOC for zebrafish studies are still very low and are constrained in a small research community mainly due to the complexity and high cost for the ZOC development. My dissertation presents a complete pipeline for ZOC development and applications using economic prototyping techniques and simple design strategies (Figure 5.1). More robust ZOC systems with new functions and features can be iterated and developed to help the researchers in the zebrafish community.

Table 5.1. Advantages and limitations for the ZOC-based applications.

Applications	Advantages	Limitations
Zebrafish embryo culture	• Anesthetic-free automated embryo positioning • Microenvironment control • High throughput screening • Close-loop embryo culture • Real-time monitoring	• Embryo outgrow the trap • Abnormal embryo posture • Embryo escape after hatching (Deign I)
Whole mount zebrafish ABS	• Automated embryo positioning • Manual step reduction • Procedure acceleration • On-chip imaging	• Large reagent consumption • Bubbles occasionally entering the traps
CGG for Acute FET test	• Anesthetic-free automated embryo positioning • High resolution dose-response analysis • Parallel phenotype screening • Real-time monitoring	• Large reagent consumption • Short-term chemical exposure • Narrowed concentration range • Binary data (i.e., one embryo per one concentration)

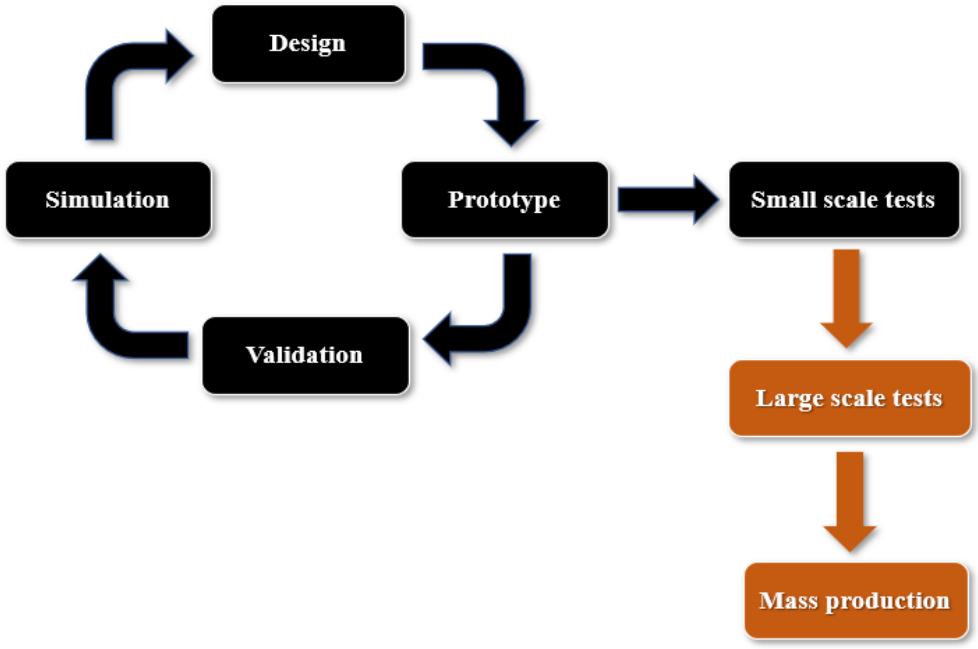

Figure 5.1. ZOC development and application pipeline. The black pipeline indicates the ZOC development and application process demonstrated in the dissertation. The orange steps are for the future productization.

I envision that the development and applications of ZOC will keep increasing in the zebrafish research. The user community for the ZOCs as well as other small animal LOCs will also continuously expand as the LOC and 3D printing technologies become more

accessible to the people from varies research fields. Additionally, to embrace the ongoing changes, both engineering and scientific expertise are needed for the researchers.[1] All in all, the advancements of ZOC and the increased level of laboratory automation will continue facilitate the new discoveries in zebrafish research with unprecedented speed and ways.

5.2 Future Directions

One of the primary goals for this Ph.D. training is to identify the areas for my personal development over the next 10 to 20 years. For all these years' training, I have witnessed the challenges that students and faculty face when manually conducting complex procedures, as well as experienced the painfulness of experiment failure due to lack of experimental automation in the laboratory. Improving laboratory automation will certainly be one of my striving goals in the future. In terms of ZOC, I believe this technology has a bright future in zebrafish research and has already made changes in the field. The continuous exploitation of ZOC's potential in zebrafish research applications as well as attempting for the complete procedure automation will be the present and future focus for the ZOC development. Some of the potential directions for the ZOC development are listed here.

5.2.1 ZOC for Whole Mount Zebrafish *in situ* Hybridization

The whole mount zebrafish *in situ* hybridization (ISH) is a common molecular staining procedure used in zebrafish research for gene localization information detection.[2] Like the whole mount zebrafish ABS demonstrated in chapter 3, the whole mount zebrafish *in situ* hybridization involves a series of washing and staining steps which are labor-intensive, time-consuming, and prone to human error (Figure 5.2). The development of highly integrated ZOC-based automated systems for whole mount zebrafish *in situ* hybridization can significantly reduce the burdens of researchers in performing the assay as well as accelerate the overall zebrafish studies.

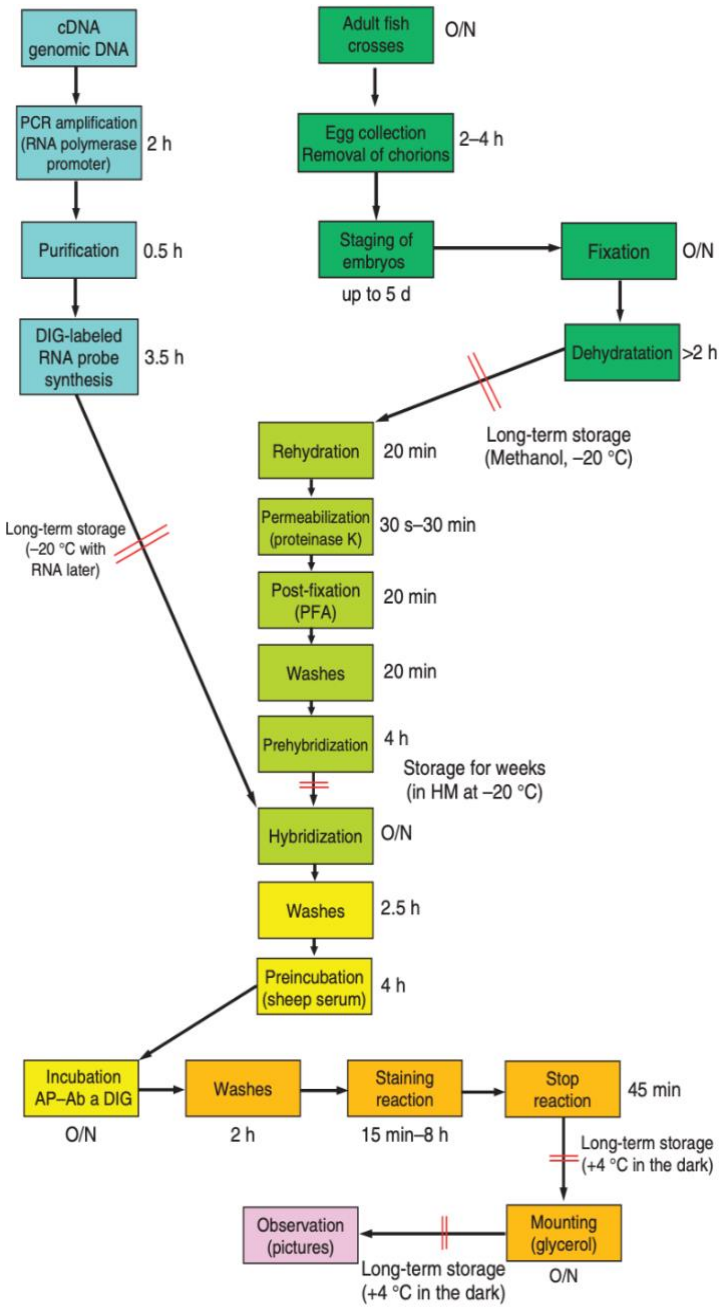

Figure 5.2. The workflow for the whole mount zebrafish ISH.[2]

5.2.2 "Sample-in-and-answer-out" Zebrafish Testing and Analysis System

In contrast to the conventional well plate and petri dish-based methods which rely on low-controlled assay conditions and bulk measurements, the ZOCs offer highly controlled experimental conditions for high-throughput and resolution analysis. This gives the ZOC advantages in assay standardization and automation. By far, most of ZOC systems only reached semi-automated or partially automated. The level of "sample-in-and-answer-out" is still distanced for the ZOC systems (Figure 5.3). The development of ZOC platforms for

fully automated zebrafish testing and analysis can significantly facilitate the zebrafish studies and revolutionize the drug discovery process. To achieve this goal, efforts from both academia and industry are needed.

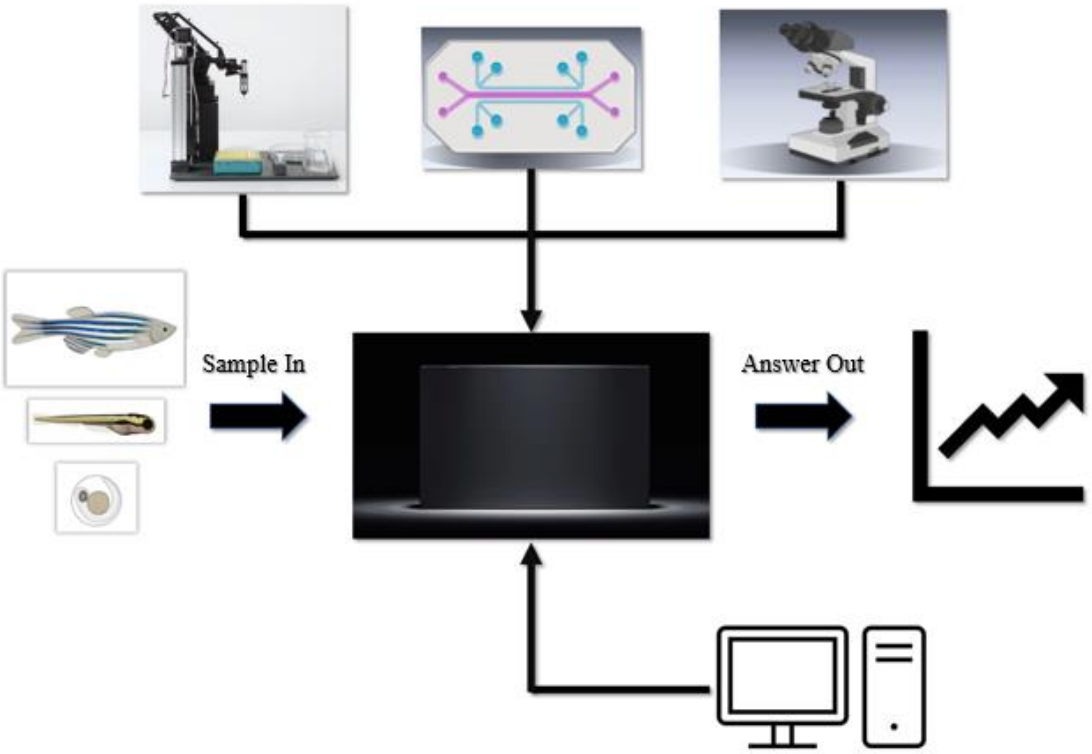

Figure 5.3. Conceptual diagram for the "sample-in-and-answer-out" zebrafish testing and analysis system.[3,4]

5.3 References

1. Holland, I. & Davies, J. A. Automation in the Life Science Research Laboratory. *Front Bioeng Biotechnol* **8**, (2020).
2. Thisse, B. & Thisse, C. In Situ Hybridization on Whole-Mount Zebrafish Embryos and Young Larvae. in 53–67 (2014). doi:10.1007/978-1-4939-1459-3_5.
3. Frey, N., Sönmez, U. M., Minden, J. & LeDuc, P. Microfluidics for understanding model organisms. *Nat Commun* **13**, 3195 (2022).
4. https://www.noldus.com/applications/zebrafish-video-tracking. Noldus.